CFD Research Corporation

3325 Triana Blvd. • Huntsville, Alabama 35805 • Tel.: (205) 536-6576 • FAX: (205) 536-6590

CFDRC

VIRTUAL PROTOTYPING TOOLS FOR SEMICONDUCTOR FABRICATION EQUIPMENT

A Phase II SBIR Final Report

by
A. Krishnan, S.A. Lowry, and V.J. Harrand

September 1995

Sponsored by
Advanced Research Projects Agency (DoD)
Defense Small Business Innovation Research Program
ARPA Order No. 6685
Issued by U.S. Army Missile Command Under
Contract # DAAH01-93-C-R140

Business Address: CFD Research Corporation
3325 Triana Blvd.
Huntsville, AL 35805

Effective Date of Contract: June 28, 1993
Contract Expiration Date: June 30, 1995
Reporting Period: June 28, 1993 - September 15, 1995

Principal Investigator: Dr. Anantha Krishnan, Group Leader
Phone Number: (205) 536-6576
Virtual Prototyping Tools

DISCLAIMER NOTICE

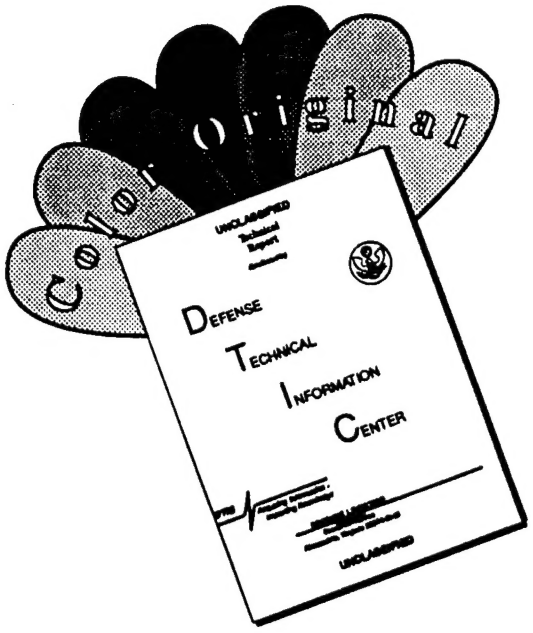

THIS DOCUMENT IS BEST QUALITY AVAILABLE. THE COPY FURNISHED TO DTIC CONTAINED A SIGNIFICANT NUMBER OF COLOR PAGES WHICH DO NOT REPRODUCE LEGIBLY ON BLACK AND WHITE MICROFICHE.

ADVANCED RESEARCH PROJECTS AGENCY
3701 NORTH FAIRFAX DRIVE
ARLINGTON, VA 22203-1714

NOV 29 1995

MEMORANDUM FOR DTIC-OCC
ATTENTION: (GOPALAKRISHNAN NAIR)

SUBJECT: Distribution Statements on Technical Documents

This is in response to your memorandum dated requesting a distribution statement for the document entitled "Virtual Prototyping Tools for Semiconductor Fabrication Equipment." All copies should carry the Distribution Statement "A" (Approved for Public Release, Distribution Unlimited).

Debra K. Amick
Technical Information Officer

Attachments

TABLE OF CONTENTS

		Page
ACKNOWLEDGEMENTS		vi
1.	INTRODUCTION	1
1.1	Need for Virtual Prototyping	1
1.2	Need for Integration	2
1.3	Proposed Phase II Objectives	4
1.4	Accomplishments of the Project	4
1.5	Organization of the Report	7
2.	DESCRIPTION OF PROCESS MODELS	8
2.1	Governing Equations	8
2.2	The Transport Model	10
2.3	Thermal Radiation Model	15
2.4	Gas/Surface Chemistry	16
2.5	Particle Transport Model	18
2.6	Model for Plasma Enhanced Chemistry	20
3.	DESCRIPTION OF THE VIRTUAL PROTOTYPING ENVIRONMENT	21
3.1	Introduction	21
3.2	Master VPE Graphical User Interface	21
3.2.1	Basic Operation	21
3.2.2	Information Files	22
3.2.3	File Protection	25
3.2.4	File Management	25
3.3	CFD-GEOM	29
3.3.1	CFD-GEOM Interface to the Virtual Prototyping Environment	31
3.3.2	Virtual Parts Library	31
3.4	CFD-ACE	33
3.5	CFD-VIEW	35
4.	DEMONSTRATION CASES	38
4.1	Bell Jar Reactor	38
4.2	Jipelec Reactor	49
4.3	Planetary Reactor	59
4.4	Wedge Reactor	67
4.5	Batch Reactor	73
4.6	Interface with TCAD	80
4.7	Demonstration of Particle Transport Model	81
4.8	Demonstration of Plasma Chemistry Model	81

TABLE OF CONTENTS (Continued)

		Page
5.	COMMERCIAL APPLICATIONS	85
6.	PLANS FOR FUTURE WORK	88
	6.1 Phase III Plans	88
	6.2 Future Development	88
7.	REFERENCES	91
APPENDIX A -	SEMATECH BENCHMARK CASES	A-1
APPENDIX B -	PUBLICATIONS AND EXHIBITIONS RESULTING FROM THE CURRENT PROJECT	B-1
APPENDIX C -	JOURNAL ADVERTISEMENTS AND MATERIALS BROCHURES	C-1

LIST OF ILLUSTRATIONS

		Page
Figure 1-1.	Flow Chart for the Integrated Environment	3
Figure 3-1.	Master VPE Graphical User Interface	23
Figure 3-2.	VPE Information Window	24
Figure 3-3.	Integrated Virtual Prototyping Environment	26
Figure 3-4.	VPE File Management Window	28
Figure 3-5.	CFD-GEOM: Conceptual Overview	30
Figure 3-6.	Illustration of Virtual Parts Library; the Generic Model, the Various Parts and the Resulting Models	32
Figure 4-1.	Schematic of Bell Jar CVD Reactor	38
Figure 4-2.	Illustration of Boundary Conditions for the Bell Jar Simulation	41
Figure 4-3.	Bell Jar Geometry (°45 Section) in CFD-GEOM	43
Figure 4-4.	Boundary Conditions for Bell Jar as Defined in CFD-GEOM	44
Figure 4-5.	Boundary Conditions Window in CFD-ACE GUI: Bell Jar Radiator Selected	46
Figure 4-6.	Bell Jar Simulation (°45 Section): Comparison of 1400°K Radiator versus 1000°K Radiator	47
Figure 4-7.	Full View of the Bell Jar Reactor	48
Figure 4-8a.	Side View of Model Geometry	50
Figure 4-8b.	Location of Views Shown in Figures 4-8c - 4-8e	50
Figure 4-8c.	Top View of Model Geometry at Section A-A	50
Figure 4-8d.	Top View of Model Geometry at Section B-B	51

LIST OF ILLUSTRATIONS (Continued)

	Page
Figure 4-8e. Top View of Model Geometry at Section C-C	51
Figure 4-9a. Chamber Geometry	52
Figure 4-9b. Complete Geometry of Chamber with Windows and Lamps	52
Figure 4-10. Geometry of Reactor Visualized in CFD-GEOM	54
Figure 4-11. Jipelec Reactor	55
Figure 4-12. Jipelec Reactor Simulations (No Radiation)	57
Figure 4-13. Jipelec Reactor Simulation (With Radiation)	58
Figure 4-14a. Cross Section of the Reaction Chamber through the Main Axis	60
Figure 4-14b. Top View of the Substrate Holder	60
Figure 4-15. Geometry of Planetary Reactor in CFD-GEOM	62
Figure 4-16. Visualization of the Planetary Reactor in CFD-VIEW	63
Figure 4-17. Boundary Condition Specification in the CFD-ACE GUI	65
Figure 4-18. Results from the Planetary Reactor Simulations	66
Figure 4-19. Schematic of the Wedge Reactor	67
Figure 4-20. Geometry of the Wedge Reactor Visualized in CFD-GEOM	69
Figure 4-21. Reactor and Substrate Geometry Visualized in CFD-VIEW	70
Figure 4-22a. Results for Reactor Pressure of 0.1 atm.	72
Figure 4-22b. Results for Reactor Pressure of 1 atm.	70
Figure 4-23. Schematic of the Batch Reactor	73
Figure 4-24. Geometry of the Batch Reactor Visualized in CFD-GEOM	75

LIST OF ILLUSTRATIONS (Continued)

	Page
Figure 4-25. Computational Grid for the Batch Reactor	76
Figure 4-26. Boundary Condition Specification in CFD-GEOM	77
Figure 4-27a. Results for Pitch Size of 0.3"	79
Figure 4-27b. Results for Pitch Size of 0.6"	79
Figure 4-28. Predictions of Oxide Thickness Using TMA-SUPREM (with data from CFD-ACE)	82
Figure 4-29. Analysis of High Velocity Oxygen-Fuel (HVOF) Thermal Spray Torch	83
Figure 4-30. Plasma Enhanced Chemistry in a Multi-Wafer CVD Reactor	84

ACKNOWLEDGEMENTS

This project was a Phase II SBIR study (of 2 year duration) sponsored by ARPA-ESTO. The authors would like to thank Dr. Nick Naclerio, the project monitor, for his enthusiastic support and guidance during the course of this work.

Dr. Andrzej Przekwas, Vice President/Research and Dr. Ashok Singhal, President & Technical Director of CFDRC, provided valuable in-house guidance on this project. Mr. Fritz Owens, Mr. Milind Talpallikar and Mr. Lyle Johnson were instrumental in adapting the commercial CFD code, CFD-ACE, for microelectronic applications. Dr. Ning Zhou's assistance with the implementation of the energy and species equations for multi-component transport and stiff chemistry is greatly appreciated. The radiation model was developed and implemented by Dr. M. Giridharan. The framework for the VPE was developed by Mr. Jayesh Patel. The authors would like to thank Ms. J. Swann for preparation of this report.

The authors would also like to acknowledge the cooperation received from representatives of SEMATECH and its member companies during this project. In particular, the authors would like to thank Mr. Roger Hill and Dr. Franz Geyling of SEMATECH for undertaking the benchmarking of CFD-ACE. And last but not least, the authors express their appreciation for the support and critical feedback received from the microelectronic industry which made it possible to improve and extend the capabilities of the model.

1. INTRODUCTION

This report documents the creation of a Virtual Prototyping software package under a Phase II SBIR study titled "Virtual Prototyping Tools for Semiconductor Fabrication Equipment". The project successfully developed and integrated software tools from a variety of disciplines (such as CAD/CAM, Fluid Dynamics, Graphics and Database Management Systems) to form a design environment for semiconductor fabrication processes/equipment. The resulting virtual prototyping environment provides the semiconductor industry with a tool for optimizing the design and operation of fabrication equipment to meet the rapidly increasing demands of the industry.

1.1 Need for Virtual Prototyping

The rapid growth in the use of semiconductors for microelectronic devices has led to the need for better and faster material processing and fabrication techniques. Significant progress has been made in recent years in developing new device structures and higher levels of integration. As the feature size of these devices continues to shrink and their level of integration and complexity continues to increase, the material processing industry is faced with the constant challenge of mass production of high quality devices at minimum cost. In addition, the industry has to be well prepared to find solutions to future problems that are sure to be encountered in a continuously evolving field such as microelectronics.

In order to keep pace with the development in the field and to commercialize new and advanced concepts quickly, it is necessary to be able to simulate the entire fabrication process. Direct experimentation with hardware is time consuming and prohibitively expensive. Reliable computational models have to be developed to simulate each of the individual operations in order to optimize the process. Some of the advantages of using computer simulations versus physical testing are listed below.

a. Different reactor designs can be tested easily to study the efficiency of the process. The simulation can be done very quickly and at a fraction of the cost involved with hardware experimentation.

b. After a particular design is selected, the model can be used to conduct parametric studies to determine optimum operating conditions that would maximize the production efficiency.

c. The results of the model simulations can be easily displayed on a monitor and it would be possible to focus in on any one of the operations in the process. Instantaneous visualization of the entire sequence enhances understanding and thus enables better control of the fabrication process.

d. New and improved design requirements can be studied easily with the model. The cost of developing new manufacturing tools can be greatly reduced.

In addition, advanced models of the equipment/process can also be used for real time, on-line control of fabrication processes.

1.2 Need for Integration

Although significant progress has been made in modeling specific processes such as CVD, etching, *etc.*, no attempts have been made to integrate these models to form a design tool. Furthermore, CAD/CAM software is used routinely in the aerospace and automobile industry for the design of engine components. However, these tools have yet to be utilized for the design of semi-conductor fabrication equipment. A complete simulation environment requires the integration of the following components:

a. A software package to analyze design features and requirements of the fabrication equipment/process and to translate this information into a virtual prototype;

b. An advanced CAD package to design components for the virtual prototype based on design conditions, and perform the grid generation;

c. An advanced process analysis tool with capabilities of modeling the flow field, the transport process and the chemistry in the reactor;

d. A complementary solid mechanical/structural model to analyze the reactor material and geometry based on the results of the process model analysis; and

e. Advanced visualization tools for display of the simulation results on monitors.

All of the above information needs to be processed iteratively in a loop until a satisfactory design is obtained. This process is illustrated by the flowchart in Figure 1-1. The information can then be passed on for a physical prototyping of the process. The results of the equipment analysis should be used to provide the boundary conditions for the Technology CAD (TCAD) design of device structures. The interfacing of the integrated tool with the TCAD framework is illustrated in Figure 1-1.

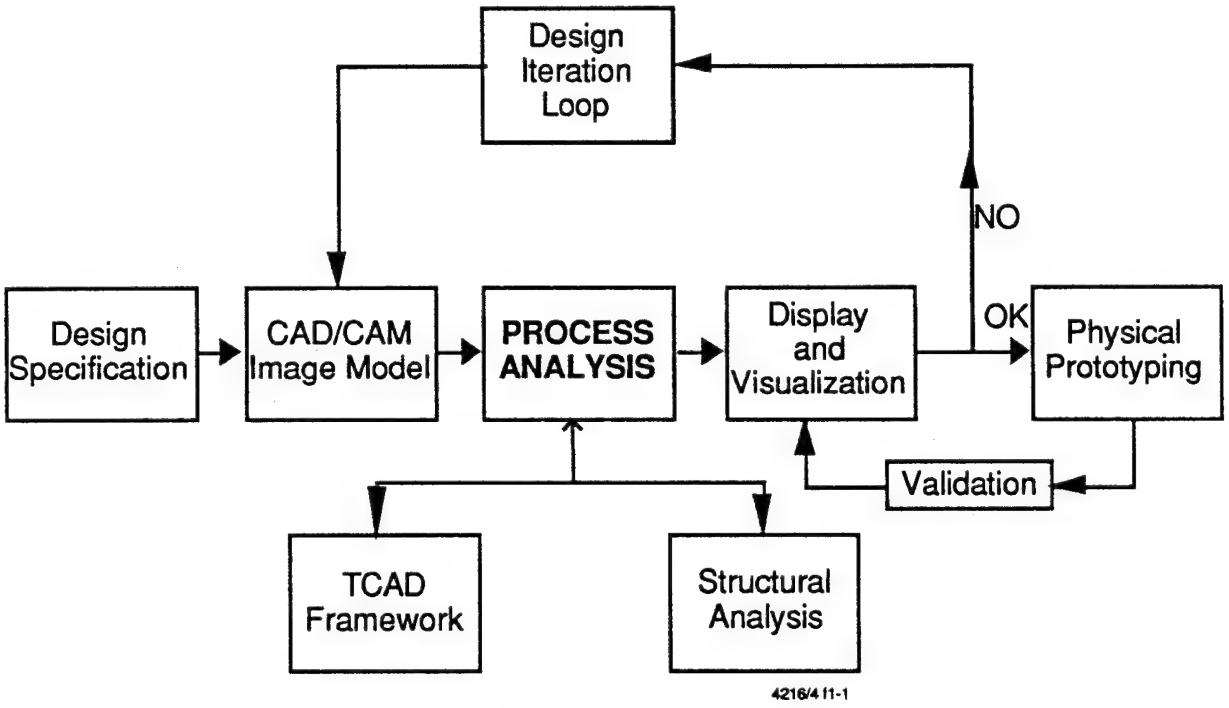

Figure 1-1. Flow Chart for the Integrated Environment

The complete simulation process requires the integration of information from various disciplines such as CAD/CAM, Solid/Structural Analysis, CFD, Graphics, Database Management, *etc.* Although significant advances have been made in developing modeling tools in each one of these fields, a compatible integration of all these models has not been done.

1.3 Proposed Phase II Objectives

The objectives of the Phase II study were:

1. Development of Interfaces with Commercial Technology Computer Aided Design (TCAD) device models.

2. Refinement of the process models to account for particle transport, plasma effects, and incorporation of multi-block capability to model complex reactor geometries efficiently.

3. Development of interfaces between modules that conform to established standards.

4. Application and testing of the integrated environment.

5. Customization and commercialization of the tool for use by the industry.

6. Implementation of a database management system for the efficient and optimal use of the tool.

1.4 Accomplishments of the Project

The major accomplishments of the project are as follows:

(1) Refinements to the Process Model: The following refinements were made to an existing commercial Computational Fluid Dynamics (CFD) code, CFD-ACE, developed and marketed by CFDRC:

a. **Multi-Component Transport Model**: Implementation of a comprehensive multi-component transport model (based on the kinetic theory of gases) to compute viscosities, conductivities, diffusivities and thermodiffusion (Soret) coefficients as functions of local pressure, temperature and mixture composition.

b. **Homogeneous/Heterogeneous Chemistry Model**: Incorporation of a general purpose model for homogeneous gas phase and heterogeneous surface chemistry involving multi-step, finite rate reactions. Special algorithms such as the Jacobian Linearization method were implemented to treat stiff systems. Plasma enhanced dissociation in the gas phase is modeled by using a Druyvesteyn distribution for the electron energy. The surface chemistry was extended to model processes such as deposition and etching by doing a detailed diffusion-reaction balance at the surface.

c. **Thermal Radiation Model**: A discrete-ordinate thermal radiation model was implemented to simulate radiation transport in processes such as RTP. The model is based on the gray-diffuse approximation and can handle semi-transparent, participating media with spatially varying properties. The radiation model is fully coupled with the fluid flow, heat transfer and chemistry models.

d. **Particle Transport Model**: A Lagrangian particle transport model was incorporated into the Eulerian fluid flow model to simulate the motion of particles in a reactor. Processes such as melting and vaporization of particles are also considered in the model.

e. **Multi-Block Capability**: All of the above models have been implemented in the framework of a structured, multi-block gridding environment. The models have been demonstrated on highly non-orthogonal, body-fitted-coordinate (BFC) grids for three-dimensional applications.

(2) <u>Development of Interfaces and Integration of Modules</u>: All of the software modules in the virtual prototyping environment (VPE) are accessed through Graphical User Interfaces (GUIs). Furthermore, additional interfaces were developed to communicate information between the modules. For example,

a. CFD-GEOM, the geometry and grid generation software, accepts input from external CAD programs through IGES files and generates grid and

boundary condition information that is transmitted to CFD-ACE, the process model.

b. CFD-ACE performs the simulations and the results are output in PLOT3D standard that can be imported by CFD-VIEW and other commercial visualization packages for visual inspection of the data.

All the modules share information on grids, boundary conditions, blocked/solid regions and block interfaces.

(3) Interfacing with TCAD Models: TMA-SUPREM, a TCAD software marketed by TMA, Inc. of California was interfaced with the VPE. Values of pressure, temperature and composition computed by CFD-ACE were communicated to SUPREM (a zero-dimensional model) which then computes the local oxide thickness, junction depths and sheet resistance. The output of SUPREM was modified to accommodate the PLOT3D standard so that the results can be viewed using CFD-VIEW.

(4) Application and Demonstration of the Integrated Model: The integrated model was applied to simulate a number of fabrication systems currently used by the microelectronic industry. This work was done in collaboration with SEMATECH and a number of organizations such as FSI International, LAM Research Corporation, Silicon Valley Group (SVG) Thermco, Motorola, Sandia Labs, Lawrence Livermore Labs, Semitool Inc., IBM, etc. The model was applied to a number of systems such as wafer cleaning equipment, RTP systems, low pressure etching reactors, MOCVD reactors, crystal growth systems, etc. A workshop was organized at SEMATECH in June 1994 to demonstrate the tool to member companies and potential clients.

(5) Incorporation of a Database Management System: A database management system was developed to allow the user to create, modify, visualize and store simulations of a diverse set of hardware types/processes. Access to the management system is via a Graphical User Interface that allows direct control of the integrated software packages. The geometries and models of different designs and processes are stored in a tree structure that allows quick retrieval, copying, visualization and

execution of existing cases. The database management system thus serves both as a Master GUI for the integrated package and as a database for analyzing existing designs or creating a new one.

1.5 Organization of the Report

Section 2 describes the governing equations, the multi-component transport model, the particle model, the thermal radiation model and the plasma model. The integrated virtual prototyping environment (VPE) is described in Section 3. Section 4 describes the application of the VPE to several demonstration cases. The commercial applications of this tool are summarized in Section 5. The conclusions and plans for future work are presented in Section 6.

2. DESCRIPTION OF PROCESS MODELS

This section describes the formulation of the models for multi-component transport, thermal radiation, gas/surface chemistry, particle motion and plasma enhancements.

2.1 Governing Equations

The mass conservation for the flow can be represented by the continuity equation. This formulation accounts for a variable density flowfield:

$$\frac{\partial \rho}{\partial t} + \nabla \cdot \rho u = 0.0 \tag{2.1}$$

where ρ is the density of the fluid and u is the velocity vector. The mass conservation for each individual specie may be written as:

$$\frac{\partial \rho Y_i}{\partial t} + \nabla \cdot \rho u Y_i = \nabla \cdot j_i + w_i \tag{2.2}$$

where Y_i is the mass fraction of specie, j_i is the total diffusive flux and W_i is a source term consisting of reaction rate expressions (see Equation 2.47). The total diffusive mass flux j_i for specie i is composed of fluxes due to concentration gradients as well as those due to thermal gradients (thermodiffusion or the Soret effect):

$$\mathbf{j}_i = \mathbf{j}_i^c + \mathbf{j}_i^T \tag{2.3}$$

The diffusive flux due to the concentration gradients is expressed as:

$$\mathbf{j}_i^c = D_i \nabla Y_i \tag{2.4}$$

where D_i is the mass diffusion coefficient of specie i. The diffusive flux due to the Soret effect is given by:

$$j_i^T = D_i^T \nabla(\ln T) \tag{2.5}$$

where D_i^T is the thermo diffusion coefficient for specie i and T is the local fluid temperature.

The momentum conservation equation for the flow is written as:

$$\frac{\partial \rho u}{\partial t} + \nabla \cdot \rho uu = -\nabla p + \nabla \cdot \tau + \rho g \tag{2.6}$$

where p is the local pressure. The shear stress tensor τ is given as:

$$\tau = \mu(\nabla \mathbf{u} + \nabla \mathbf{u}^T) - \left(\frac{2}{3}\mu\right)(\nabla \cdot \mathbf{u})\mathbf{I} \tag{2.7}$$

where μ is the dynamic viscosity g is the gravity vector, and I is the unit tensor. It is assumed that the gas behaves as a Newtonian fluid. The energy conservation equation for the system is given by:

$$\frac{\partial \rho h}{\partial t} + \nabla \cdot \rho uh = \nabla \cdot \left[(\lambda \nabla T) + \sum_i h_i j_i\right] + \tau : \nabla u + \frac{\mathrm{dp}}{\mathrm{dt}} \tag{2.8}$$

where h is the static enthalpy of the mixture and h_i is the enthalpy of specie i, and λ is the mixture conductivity. The equation of state is written as:

$$\rho = \frac{pM}{RT} \tag{2.9}$$

where R is the universal gas constant. The mixture molecular weight, M, is given by:

$$M = \sum_{i=1}^{N} x_i M_i \tag{2.10}$$

where x_i is the mole fraction. The mixture specific heat is computed as:

$$C_p = \sum_{i=1}^{N} Y_i C_{pi} \tag{2.11}$$

The C_{pi} for individual species are obtained from JANNAF data. In some cases, C_{pi} is also expressed as:

$$C_{pi} = C_0 + C_1 T + C_2 T^2 + C_3 T^3 \tag{2.12}$$

The Dufour effect (diffusion of heat due to a concentration gradient) is neglected in this formulation.

2.2 The Transport Model

The single component viscosities for the individual species are calculated using the following expression from kinetic theory[1]:

$$\mu_i = 2.6693 \, x \, 10^{-6} \frac{\sqrt{M_i T}}{\sigma_i^2 \, \Omega_\mu} \tag{2.13}$$

where μ_i is in kg/m-sec, M_i is the molecular weight of the species, T is the temperature in Kelvin, σ_i is the Lennard Jones collision diameter of the molecule (in Angstrom units) and Ω_μ is the collision integral which is a function of the dimensionless temperature given by kT/ϵ. ϵ is a characteristic energy of interaction between the molecules and k is the Boltzmann constant. The quantity ϵ/k is a constant for each specie. The collision integral Ω_μ is obtained as[2]:

$$\Omega_\mu = \left[A(T^*)^{-B}\right] + C[exp\,(-DT^*)] + E[exp\,(-FT^*)] \tag{2.14}$$

where

$T^* = kT/\epsilon$, $A = 1.16145$, $B = 0.14874$, $C = 0.52487$,
$D = 0.77320$, $E = 2.16178$ *and* $F = 2.43787$

Viscosity may also be evaluated as a function of temperature according to:

$$\mu_i = A_0 + A_1 T + A_2 T^2 + A_3 T^3 \tag{2.15}$$

For a multi-component mixture consisting of various species, the mixture viscosity is obtained using the Wilke's approximation[1]:

$$\mu = \sum_{i=1}^{N} \frac{x_i \mu_i}{\sum_{j=1}^{N} x_j \phi_{ij}} \tag{2.16}$$

where

$$\phi_{ij} = \frac{1}{\sqrt{8}} \left(1 + \frac{M_i}{M_j}\right)^{-\frac{1}{2}} \left[1 + \left(\frac{\mu_i}{\mu_j}\right)^{\frac{1}{2}} \left(\frac{M_j}{M_i}\right)^{\frac{1}{4}}\right]^2 \tag{2.17}$$

x_i is the mole fraction of species i.

The thermal conductivity for each individual species is obtained by using Eucken's formula for polyatomic gases[1]:

$$\lambda_i = \left(C_{pi} + \frac{5}{4}\frac{R}{M_i}\right) \mu_i \tag{2.18}$$

where C_{pi} is the specific heat at constant pressure for the specie i and R is the universal gas constant. Conductivity may also be evaluated as:

$$\lambda_i = B_0 + B_1 T + B_2 T^2 + B_3 T^3 \tag{2.19}$$

The thermal conductivity of the mixture is given by:

$$\lambda = \sum_{i=1}^{N} \frac{x_i \lambda_i}{\sum_{j=1}^{N} x_j \phi_{ij}} \tag{2.20}$$

The binary mass diffusion coefficient for a gas pair *i-j* is given as[1]:

$$D_{ij} = 1.8583 \times 10^{-2} \frac{\sqrt{T^3 \left(\frac{1}{M_i} + \frac{1}{M_j}\right)}}{p \sigma_{ij}^2 \Omega_D} \tag{2.21}$$

where D_{ij} is in m^2/sec, σ_{ij} is the collisional diameter for the gas pair in Angstrom units, p is the pressure in Pascals and Ω_D is the collision integral for the gas pair.

Ω_D is given as[2]:

$$\begin{aligned} \Omega_D = &\left[A(T^*)^{-B}\right] + C[exp(-DT^*)] \\ &+ E[exp(-FT^*)] + G[exp(-HT^*)] \end{aligned} \tag{2.22}$$

where

$$T^* = kT/\epsilon_{ij},\ A = 1.06036,\ B = 0.15610,\ C = 0.1930,$$
$$D = 0.47635,\ E = 1.03587,\ F = 1.52996,$$
$$G = 1.76474 \text{ and } H = 3.89411$$

The values of σ_{ij} and ϵ_{ij} are obtained from the individual species as:

$$\sigma_{ij} = \frac{1}{2}(\sigma_i + \sigma_j) \tag{2.23}$$

and

$$\epsilon_{ij} = \sqrt{\epsilon_i \epsilon_j} \tag{2.24}$$

The diffusion coefficient of specie i in a multi-component mixture is then calculated as:

$$D_i = \frac{\rho \sum_{j \neq i}^{N} x_j M_j}{M \sum_{j \neq i}^{N} \frac{x_j}{D_{ij}}} \tag{2.25}$$

where M is the mixture molecular weight.

For a binary system (i.e., N = 2), in order to satisfy the constraint $D_i = D_j$, the diffusion coefficient is calculated as:

$$D_i = \rho \left[\sum_{j \neq i}^{N} \frac{x_j}{D_{ij}} \right]^{-1} \tag{2.26}$$

Thermodiffusion (or the Soret Effect) is the diffusion of mass under a temperature gradient and is extremely important in CVD processes. The thermodiffusion coefficient is calculated as:

$$D_i^T = \sum_{j \neq i}^{N} \frac{\rho M_i M_j}{M^2} k_{ij} D_{ij} \tag{2.27}$$

where D_{ij} is the binary mass diffusion coefficient and k_{ij} is the thermodiffusion ratio. The thermodiffusion ratio is obtained as[3]:

$$k_{ij} = \frac{x_i x_j}{6\lambda_{ij}} \frac{S^i x_i - S^j x_j}{x_\lambda + y_\lambda} (6C^* - 5) \tag{2.28}$$

where x_i and x_j are the mole fraction of species i and j respectively. λ_{ij} is the binary thermal diffusion coefficient and C^* is a collision integral to be estimated from the tables as a function of the Lennard Jones parameters.

$$S^i = \frac{M_i + M_j}{2M_j}\frac{\lambda_{ij}}{\lambda_i} - \frac{15}{4A^*}\left(\frac{M_j - M_i}{2M_j}\right) - 1 \tag{2.29}$$

and

$$S^j = \frac{M_j + M_i}{2M_i}\frac{\lambda_{ij}}{\lambda_j} - \frac{15}{4A^*}\left(\frac{M_i - M_j}{2M_j}\right) - 1 \tag{2.30}$$

λ_i and λ_j are the individual thermal conductivities and A^* is a collision integral similar to C^*. x_λ and y_λ are calculated as:

$$x_\lambda = \frac{x_i^2}{\lambda_i} + \frac{2x_i x_j}{\lambda_{ij}} + \frac{x_j^2}{\lambda_j} \tag{2.31}$$

and

$$y_\lambda = \frac{x_i^2}{\lambda_i}U^i + \frac{2x_i x_j}{\lambda_{ij}}U^y + \frac{x_j^2}{\lambda_j}U^j \tag{2.32}$$

where

$$U^i = \frac{4}{15}A^* - \frac{1}{12}\left(\frac{12}{5}B^* + 1\right)\frac{M_i}{M_j} + \frac{1}{2}\frac{(M_j - M_i)^2}{M_i M_j} \tag{2.33}$$

and

$$U^y = \frac{4}{15}A^*\left[\frac{(M_i + M_j)^2}{4M_i M_j}\right]\frac{\lambda_{ij}^2}{\lambda_i \lambda_j} - \frac{1}{12}\left(\frac{12}{5}B^* + 1\right) - \frac{5}{32A^*}\left(\frac{12}{5}B^* - 5\right)\left[\frac{(M - M_i)^2}{M_i M_j}\right] \tag{2.34}$$

and

$$U^j = \frac{4}{15}A^* - \frac{1}{12}\left(\frac{12}{5}B^* + 1\right)\frac{M_j}{M_i} + \frac{1}{2}\frac{(M_j - M_i)^2}{M_i M_j} \tag{2.35}$$

B^* is another collision integral similar to A^* and C^*. The values for A^*, B^* and C^* are functions of the dimensionless temperature and have values very close to unity. In order to avoid time consuming interpolations from the tables, average values

were assumed for the three quantities. The values used were $A^*=1.11$, $B^*=1.15$ and $C^*=0.86$.

2.3 Thermal Radiation Model

The integro-differential radiative heat transfer equation for an emitting-absorbing and scattering gray medium can be written as[4]:

$$(\Omega \cdot \nabla) I(r, \Omega) = -(k+\sigma) I(r, \Omega) + k I_b(r) + \frac{\sigma}{4\Pi} \int_{\Omega'=4\Pi} I(r, \Omega') \phi(\Omega' \rightarrow \Omega) d\Omega' , \quad \Omega' = 4\pi \tag{2.36}$$

where Ω is the direction of propagation of the radiation beam, I is the radiation intensity, which is a function of both position (r) and direction (Ω), k and σ are the absorption and scattering coefficients respectively. Note that the absorption and scattering coefficients have units of 1/m. I_b is the intensity of black body radiation at the temperature of the medium given by:

$$I_b(r) = \frac{\sigma T^4(r)}{\pi} \tag{2.37}$$

ϕ is the phase function of the energy transfer from the incoming Ω' direction to the outgoing direction Ω. The term on the left hand side represents the gradient of the intensity in the specified direction Ω. The three terms on the right hand side represent the changes in intensity due to absorption and out-scattering, emission and in-scattering respectively.

The boundary condition for solving the above equation may be written as:

$$I(r, \Omega) = \varepsilon I_b(r) + \frac{\rho}{\pi} \int_{n \cdot \Omega' < 0} |n \cdot \Omega'| I(r, \Omega') d\Omega' \tag{2.38}$$

where I is the intensity of radiant energy, leaving a surface at a boundary location, ε is the surface emissivity, ρ is the surface reflectivity, and n is the unit normal vector at the boundary location.

In the discrete-ordinate method, Equations (2.35) and (2.37) are replaced by a discrete set of equations for a finite number of ordinate directions. The integral terms on the right hand side of the above equations are approximated by summation over each ordinate. The discrete-ordinate equations may then be written as:

$$\mu_m \frac{\partial I_m}{\partial x} + \xi_m \frac{\partial I_m}{\partial y} + \eta_m \frac{\partial I_m}{\partial z} = -(k+\sigma) I_m + k I_b + \frac{\sigma}{4\Pi} \sum_{m'} w_{m'} \phi_{m'm} I_{m'} \; ; m = 1, \ldots M \tag{2.39}$$

For cylindrical polar geometries, the discrete-ordinate equation may be written as:

$$\mu_m \frac{\partial I_m}{\partial x} + \frac{\xi_m}{r} \frac{\partial (r I_m)}{\partial r} - \frac{1}{r} \frac{\partial (\eta_m I_m)}{\partial \phi} = -(k+\sigma) I_m + k I_b + \frac{\sigma}{4\Pi} \sum_{m'} w_{m'} \phi_{m'm} I_{m'} \; ; m = 1, \ldots M \tag{2.40}$$

where the second term on the left hand side represents the angular intensity redistribution. It accounts for the change in the direction cosines as a beam travels in a straight line in the Ω direction.

2.4 Gas/Surface Chemistry

A generalized multi-step gas phase reaction mechanism can be written as[5]:

$$\sum_{i=1}^{N_{sp}} \nu'_{ij} \Lambda_i + M \Leftrightarrow \sum_{i=1}^{N_{sp}} \nu''_{ij} \Lambda_i + M \qquad j=1, \ldots, N_{st} \tag{2.41}$$

and the reaction rate can be expressed in the form:

$$\omega_j = \left\{ \sum_{i=1}^{N_{sp}} c_{ij} [\Lambda_i]^{b_{ij}} \right\} \left\{ K_{f,j} \prod_{i=1}^{N_{sp}} [\Lambda_i]^{a'_{ij}} - K_{b,j} \prod_{i=1}^{N_{sp}} [\Lambda_i]^{a''_{ij}} \right\} \tag{2.42}$$

where ν'_{ij}, ν''_{ij}, Λ_i, $[\Lambda_i]$ are forward and reverse stoichiometric coefficients, molecular symbol and concentration of i^{th} -species, respectively. N_{st} is the number of reactions

steps, N_{sp} is the number of species and M is a third body. c_{ij}, b_{ij} are coefficients of 3rd -body efficiency. $K_{f,j}$, $K_{b,j}$, a'_{ij}, a''_{ij} are rate constants and concentration exponents of reaction rate, and the $K_{f,j}$ (or $K_{b,j}$) can be expressed in Arrhenius form:

$$K_{f,j} = A_j T^{n_i} exp\left(-\frac{E_{a,j}}{R_u T}\right) \tag{2.43}$$

For a reaction rate obeying mass action law:

$$\begin{aligned} b_{ij} &= 1 \\ a'_{ij} &= \nu'_{ij} \\ a''_{ij} &= \nu''_{ij} \end{aligned} \tag{2.44}$$

and reverse rate constant is derived from:

$$K_{b,j} = \frac{K_{f,j}}{K_{eq,j}} \tag{2.45}$$

with equilibrium constant

$$K_{eq,j} = \left(\frac{p_o}{R_u T}\right)^{\sum_{i=1}^{N_{sp}} \left(\nu''_{ij} - \nu'_{ij}\right)} exp\left\{-\frac{\sum_{i=1}^{N_{sp}} \left(\nu''_{ij} - \nu'_{ij}\right) g_i}{RT}\right\} \tag{2.46}$$

where p_o is 1 atm and Gibbs free energy $g_i = h_i - T s_i$.

The final form of production rate for ith-species is obtained as

$$\dot{w}_i = M_i \sum_{j=1}^{N_{sj}} \left(\nu''_{ij} - \nu'_{ij}\right) \omega_j \tag{2.47}$$

Surface reactions are expressed as:

$$A \xrightarrow{\gamma} B(s) + C\uparrow \tag{2.48}$$

where A is the reactant, B is the solid deposit, and C is the gaseous product. The source/sink terms for the surface reaction is given by:

$$S_A = \gamma_A \sqrt{\frac{RT_w}{2\pi M_A}} \left(\rho Y_A\right)_w \tag{2.49}$$

The subscript 'w' refers to conditions at the wall or the surface. γ_A is a surface reaction probability of the form:

$$\gamma_A = A_p T_w^n exp\left(-E_a/RT_w\right) \tag{2.50}$$

$(\rho Y_A)_w$ is evaluated at the surface or the wall and is obtained by doing a diffusion-reaction balance at the surface, i.e,

$$\left(j_A^C + j_A^T\right)_w = \gamma_A \sqrt{\frac{RT_w}{2\pi M_A}} \left(\rho Y_A\right)_w \tag{2.51}$$

The implementation of surface reaction capability enables the simulation of processes such as deposition or etching occuring at the surface.

2.5 Particle Transport Model

The equation of motion for the particle is written as:

$$m_p \frac{dV}{dt} = C_D \rho (u - V) |u - V| \frac{A_p}{2} - V_p \nabla p + m_p g \tag{2.52}$$

where m_p is the mass of the particle and $V = u_p i + v_p j + w_p k$ its velocity vector; u_p,

v_p and w_p are the Cartesian velocity components; C_D is the drag coefficient; ρ, u and p are the density, velocity and pressure of the surrounding gas, respectively; A_p is the particle surface area and V_p is the particle volume. For a spherical particle, $A_p = \pi d^2$ and $V_p = \pi d^3/6$ where d is the particle diameter. The gravity vector is represented by g. Equation (2.52) accounts for the acceleration/deceleration of the particle due to combined effects of drag with gas, local pressure gradients and body forces such as gravity.

The drag coefficient, C_D, for the particle is a function of the local Reynolds number, which is evaluated as:

$$Re = \frac{\rho |\boldsymbol{u} - \boldsymbol{V}| d}{\mu} \tag{2.53}$$

where μ is the dynamic viscosity of the gas. The following correlations have been found to be valid for different ranges of Reynolds numbers:

$$\begin{aligned} C_D &= \frac{24}{Re} && \text{for } Re < 1 \\ C_D &= \frac{24}{Re}\left[1 + 0.15Re^{0.687}\right] && \text{for } 1 < Re < 10^3 \\ C_D &= 0.44 && \text{for } Re > 10^3 \end{aligned} \tag{2.54}$$

Substituting for C_D into Equation (2.52),

$$\frac{d\boldsymbol{V}}{dt} = \frac{18\mu f}{\rho_p d^2}(\boldsymbol{u} - \boldsymbol{V}) - \frac{\nabla p}{\rho_p} + g \tag{2.55}$$

where ρ_p is the particle mass density and $f = C_D Re/24$. The particle locations are determined from the velocities by numerically integrating the velocity-defining equation:

$$\frac{d\boldsymbol{r}}{dt} = \boldsymbol{V} \tag{2.56}$$

where r is the position vector of the particle.

2.6 Model for Plasma Enhanced Chemistry

The most important parameters in the plasma model are the electron energy and the electron number density and their respective distributions. As the ratio of the electron number density to the number density of gas molecules increases, the electron energy approaches a Maxwellian distribution. However, for most realistic situations, a Druvesteyn distribution is used. The normalized Druvesteyn distribution is given by[6]:

$$f(\varepsilon) = 1.04 \langle\varepsilon\rangle^{-\frac{3}{2}} \varepsilon^{\frac{1}{2}} exp\left[\frac{-0.55\,\varepsilon^2}{\langle\varepsilon\rangle^2}\right] \tag{2.57}$$

where ε is the electron energy and <ε> is the mean electron energy. The mean electron energy is function of the applied electric field and the gas pressure. The electron number density (n) is a function of the degree of ionization. The rate constant for the plasma enhanced decomposition process is calculated as:

$$k_p = n \int_0^{\infty} \left(\frac{2\varepsilon}{m}\right)^{1/2} \sigma_i(\varepsilon) f(\varepsilon)\, d\varepsilon \tag{2.58}$$

where m is the electron mass, σ_i is the dissociation cross-section for the specie i and n is the electron number density. For example, the dissociation cross-section for silane can be represented by the following relationship over a range of electron energy levels:

$$\begin{aligned} \sigma &= 0\ cm^2 \text{ for } \varepsilon < 8eV \\ \sigma &= 3.75 \times 10^{-17} (\varepsilon - 8)\ cm^2 \text{ for } 8 < \varepsilon < 40\ eV \\ \sigma &= 1.2 \times 10^{-15}\ cm^2 \text{ for } \varepsilon > 40\ eV \end{aligned} \tag{2.59}$$

The plasma source term has a finite value only between the electrodes and is zero elsewhere in the domain. Therefore, the creation of active radicals due to the plasma takes place only between the electrodes.

3. DESCRIPTION OF THE VIRTUAL PROTOTYPING ENVIRONMENT

3.1 Introduction

This section presents a description of the integrated virtual prototyping environment (VPE) for semi-conductor fabrication equipment. The complete process of designing and evaluating a prototype requires defining the geometry, creating a numerical grid, selecting the operating conditions, simulating the process, and analyzing and archiving the results. The performance of such diverse tasks requires the use of five diverse software codes. These codes have been developed and tested at CFDRC. They are designed such that they can be linked into a "seamless" package controlled by a single graphical user interface. The five codes and their respective functions are as follows:

a.	CFD-GEOM:	Create/modify geometries and grids
b.	CFD-ACE GUI:	Define boundary conditions and simulation parameters
c.	CFD-ACE Pre-processor:	Translate the input deck from the CFD-ACE GUI for input into the analysis code, CFD-ACE
d.	CFD-ACE:	Simulate the Process
e.	CFD-VIEW:	Visualize the predicted data.

The VPE links these codes into a unified environment and provides a master Graphical User Interface (GUI) for their application. The capabilities and features of the individual software packages as well as the Master GUI are described below.

3.2 Master VPE Graphical User Interface

3.2.1 Basic Operation

The master Graphical User Interface is the primary point of contact for the design engineer. All other software can be invoked via this interface by using a "mouse" and clicking on the appropriate button. In addition, the master GUI provides a tree-structure for creating a database of simulations.

Figure 3-1 shows an example of this interface. The first column lists the broad categories of existing simulations. New categories can be created by selecting the [CREATE] button. In this example, the existing category of "Jipelec " has been selected.

With "Jipelec" selected, column two displays the Jipelec designs that have been created for that class of reactor, i.e., "Reactor.1" and "Reactor.2". These two sub-categories each correspond to a specific geometry/numerical grid representing a Jipelec reactor design. If the operator wanted to add, modify, or display a given reactor design, he or she would select the [NEW], [EDIT], or [VISUALIZE] button respectively. The first two of these buttons invoke the geometry/grid package CFD-GEOM for the selected geometry. The third automatically starts the graphics program CFD-VIEW to provide an interactive 3-D view of the grid.

The last column in the master GUI contains the specific simulation cases performed for a given hardware design from column two. The files stored in this column contain both the input files required to run the simulation, and the corresponding results. The example indicates that four simulations have been performed for "Jipelec/Reactor_1". As with the geometries, each simulation case can be modified and/or visualized from the GUI using the [EDIT] and/or [VISUALIZE] button (Figure 3-1). This column also contains a [RUN] button for running a simulation with the analysis code, CFD-ACE. These simulations may either be continuation runs, using previous results, or a new run, starting from scratch.

3.2.2 Information Files

Each simulation case and geometry has an associated information file that is accessed by double clicking on the case/geometry name. This file can be edited by an authorized user to record information specific to a simulation. Figure 3-2 shows a sample information window.

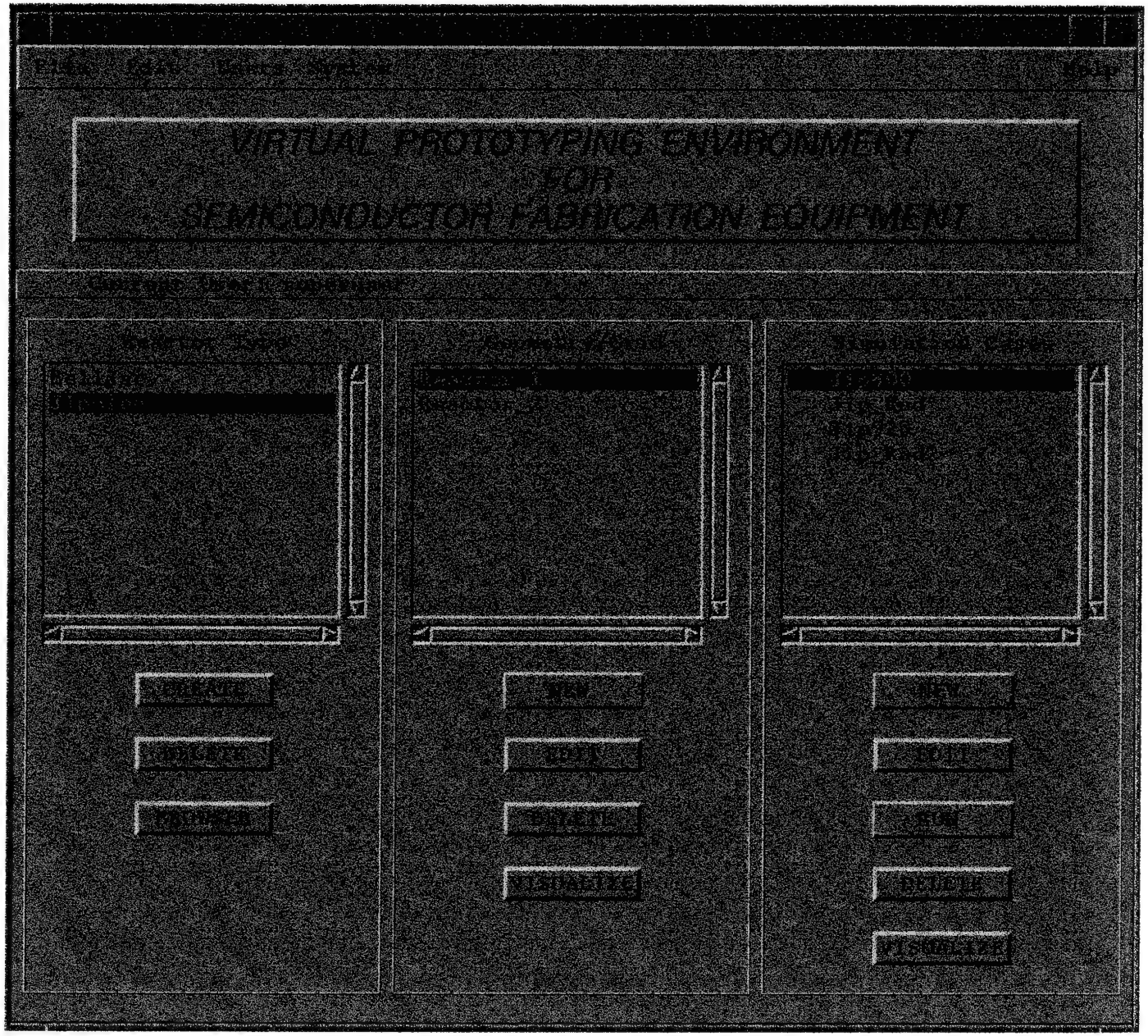

Figure 3-1. Master VPE Graphical User Interface

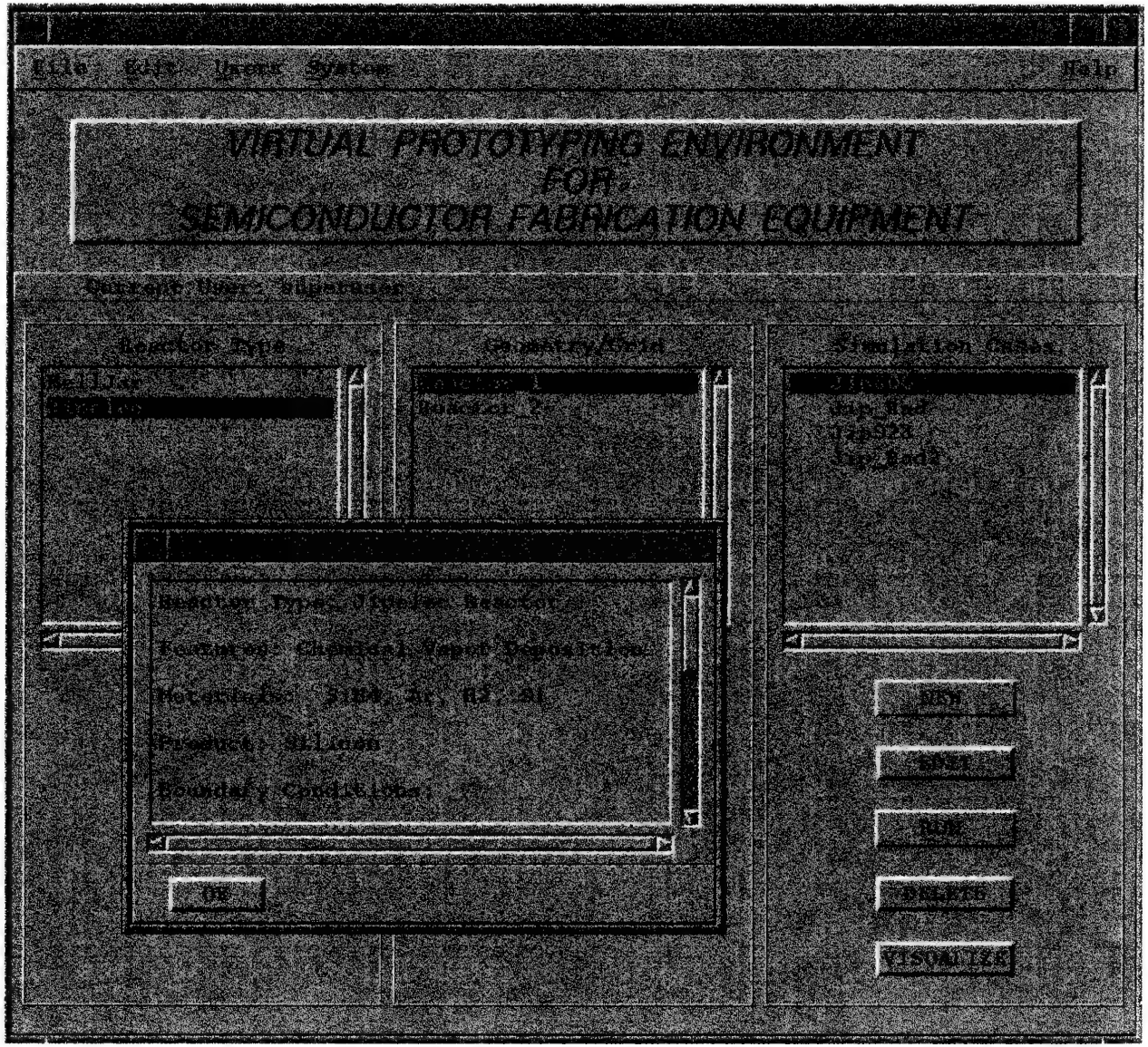

Figure 3-2. VPE Information Window

3.2.3 File Protection

The VPE has three levels of priority access to control and protect the files. These levels are:

a. Superuser;
b. Designer; and
c. Guest.

The first level, superuser, has the authority to create, view, and delete all files. The superuser can also set up accounts within the VPE. The next level, Designer, can view all unprotected files, and view, create or modify all files in his or her own account. The lowest level of priority is the Guest who can only view files created by other users.

3.2.4 File Management

As might be expected, a large number of computer files are generated in the process of creating and simulating a semiconductor reactor prototype. The VPE is designed to automatically manage these files with a minimum of input effort on the part of the user. The right-hand column in Figure 3-3 shows the total number of files that may be created in the course of a simulation.

In general, these files can be classified as either 1) restart files for restarting a code from previous conditions, 2) interface files, for transferring information between software packages, or 3) data files. The arrows linking the programs with the output files indicate the flow of information between codes. For the most part, these files are never seen by the user since the master GUI performs the link between the individual software package and automatically archives/retrieves all geometries, models and data files.

The interaction required by the user is indicated on the left-hand side of Figure 3-3. The user typically starts by using CFD-GEOM (via the Master GUI) to create the model geometry and grid. This can be done by 1) modifying an existing CFD-GEOM geometry, 2) creating a completely new geometry interactively, or 3) reusing a geometry/grid using a restart file from another geometry software package that uses the IGES standard. Once the grid is created, it is stored in file model.PFG for use in

the analysis code. A restart file model.GGD is also stored to serve as input for CFD-GEOM. This allows the designer to create a modified design starting with an existing geometry or grid. When the geometry/grid is constructed, the user has the option to specify the types and locations of the system boundaries, such as the position of an inlet or outlet. This information is automatically stored in file "model.IBC" and is passed on to the CFD-ACE GUI to facilitate the definition of the model boundary conditions.

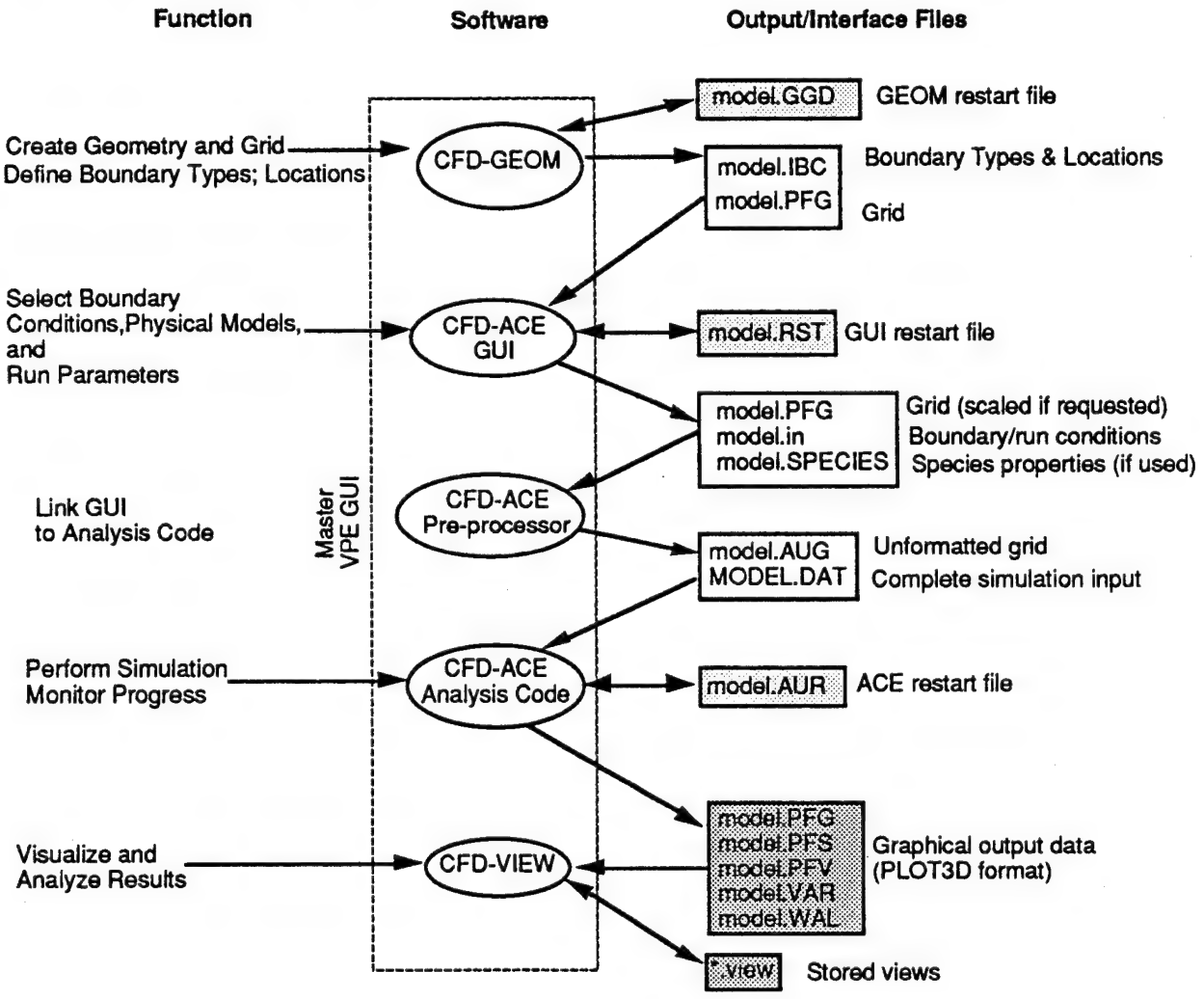

Figure 3-3. Integrated Virtual Prototyping Environment

Once the geometry and grid have been defined, the user interactively defines and selects the materials, physical models and boundary conditions for the current

simulation. This is accomplished by using the CFD-ACE graphical user interface, which is initiated from the Master GUI. The CFD-ACE GUI provides menus and windows for selecting and entering model information. The selected boundary conditions and run parameters are then stored in a user-readable, ASCII format input file "model.in." Prior to the development of the GUI, this input file served as the only means of defining a problem for the analysis code, CFD-ACE. Now, with the GUI, "model.in" serves as an invisible transfer file linking the GUI with the CFD-ACE pre-processor. Having created a set of run conditions, the user can submit a simulated run, monitor its progress, and view the results all in the framework of the CFD-ACE GUI. CFD-ACE GUI also creates a restart file, model.RST, which saves all the model settings and can be used as the starting point for a subsequent simulation.

The data files created during the course of a simulation are in the form of full field scalar/vector data (e.g. model.PFG, model.PFS, model.PFV). These data are either two-dimensional or three-dimensional and graphical in nature. They are viewed with the interactive graphics package CFD-VIEW, which may be initiated directly from the Master VPE GUI or via the subordinate CFD-ACE GUI. The result files required as input for data analysis are shaded in Figure 3-3. These files are the minimum data that must be stored in a data base in order to archive the results of a given simulation. This data base allows for the comparison of one set of results with another.

The files shown on the right-hand side of Figure 3-3 are the minimum files required for simulation and analysis of the reactors. However, the user has the option to create copies of these files using the file management button in the upper left hand corner of the Master VPE. This opens a window, such as displayed in Figure 3-4, that allows the user to operate on the individual files stored in either the "Geometry/Grid" column or the "Simulation Cases" column. For an authorized user, these operations include compressing, uncompressing, copying, renaming (move), and deleting. In addition, the VPE provides the option of backing up the essential model.* files in a subdirectory, as protection against inadvertent deletion of key files.

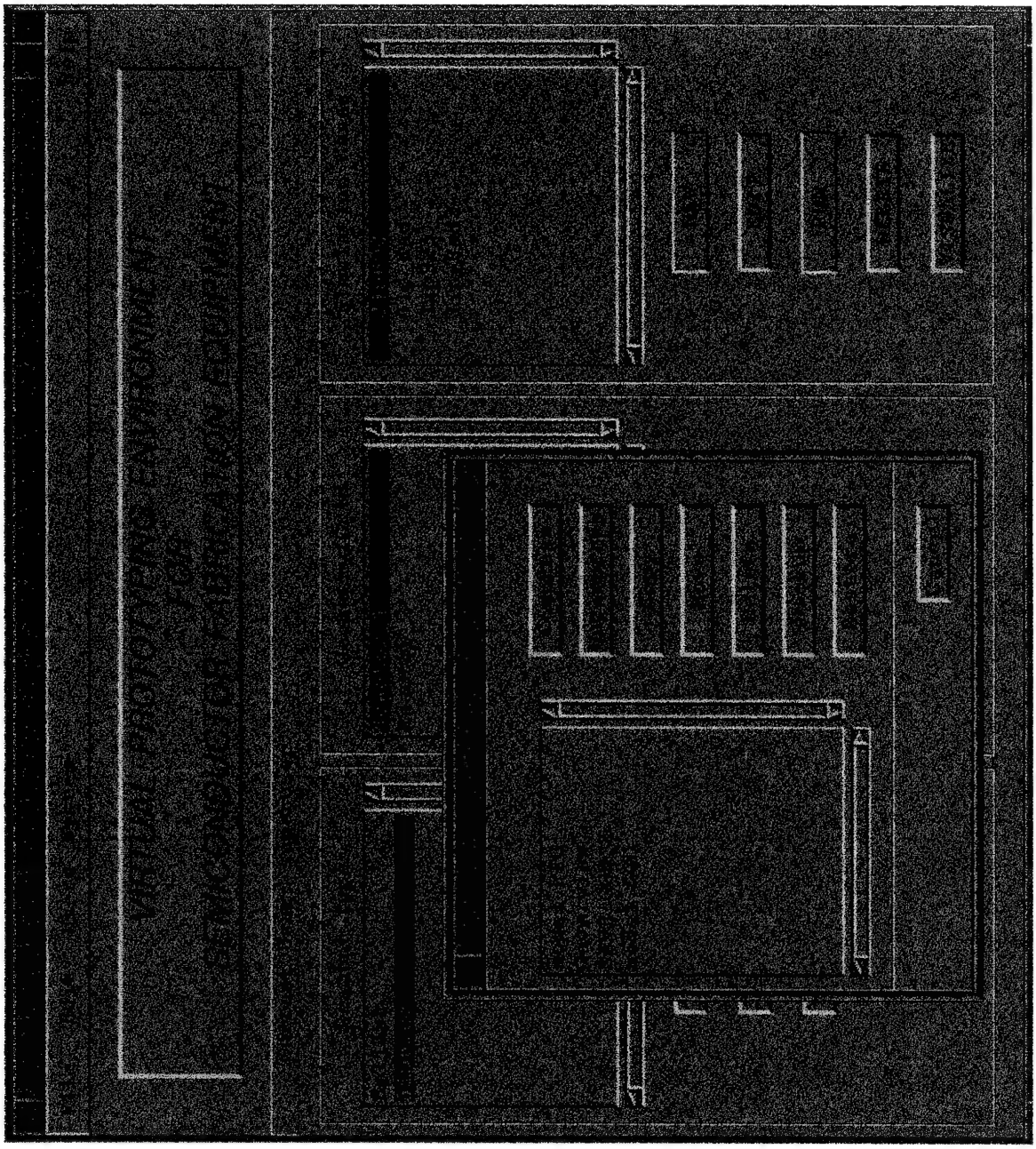

Figure 3-4. VPE File Management Window

3.3 CFD-GEOM

CFD-GEOM, developed and marketed by CFDRC, is an interactive program for geometry modeling and structured grid generation. The easy-to-use point-and-click graphical user interface, as well as the built-in orientation towards CFD applications (high level of integration between geometry and structured grid, assignment of boundary conditions, etc.) make it an ideal choice for this environment. In addition, the following features are important for this virtual prototyping environment:

- generation of boundary condition data and, if appropriate, cell type and domain interface data,
- virtual parts library.

CFD-GEOM is an interactive geometric modeling software package with fully integrated multi-block structured and unstructured grid generation capabilities. CFD-GEOM is targeted towards the CFD end-user; the main goal is to enable a non-expert user (in geometry modeling and grid generation) to interactively create a moderately complex model relatively easily.

The traditional grid generation process is often tedious and complex, due to the following reasons:

- the software is difficult to use or learn for non-expert users,
- the tools are inadequate for CFD applications (developed specifically for CAD/CAM or Finite Element Analysis),
- there is a lack of integration among the geometry and grid generation modules.

To facilitate the aforementioned goals, CFD-GEOM has the following characteristics:

- intuitive graphical user interface based on X-Windows and Motif,
- complete integration between geometry modeling and grid generation modules:
  - automatic update of relevant data structures after modifications in geometry, topology, or grid parameters (forward propagation),

- decoupling of geometric definition and topology information,
- virtual parts library,
- extensive geometry and grid editing capabilities with automatic update of entire model,
- complete integration with other software packages in the virtual prototyping environment,
  - same look-and-feel of graphical user interface,
  - boundary condition, cell types, and domain interfaces are communicated to the ACE flow solver,
- importing of grids for geometric modeling and regridding purposes,
- importing of existing geometries from third party CAD systems through the IGES data format.

A conceptual overview of the CFD-GEOM software structure is given in Figure 3-5.

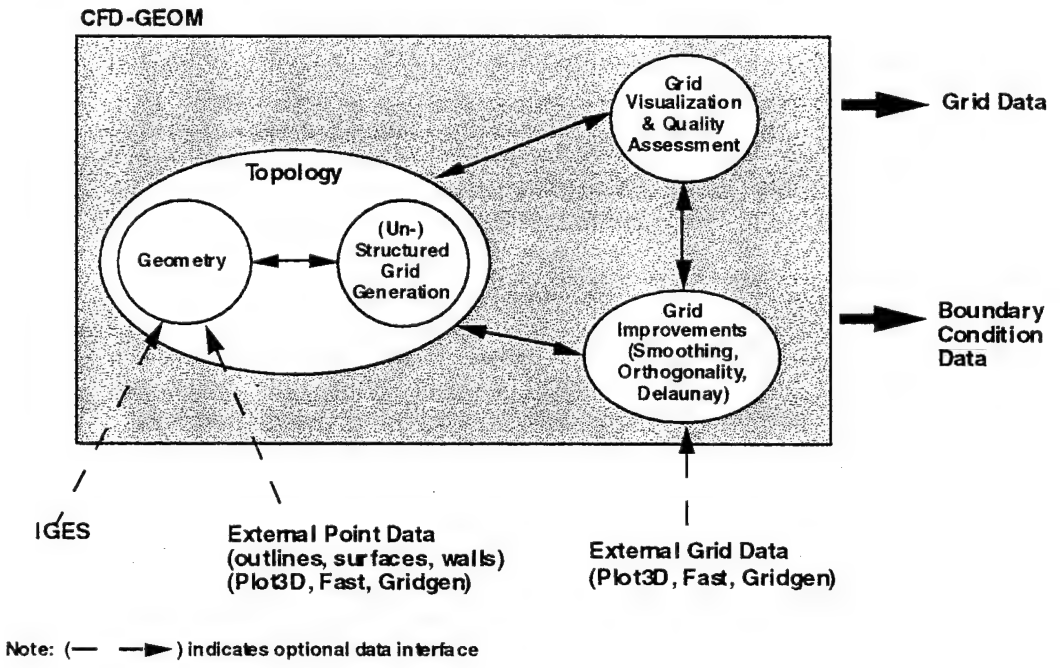

Figure 3-5. CFD-GEOM: Conceptual Overview

The CFD-GEOM software consists of several tightly integrated modules, a geometry module, a topology module, a structured grid generation module, an unstructured grid generation module, a grids smoothing module, and a module for interactive

visual grid quality assessment. As mentioned before, the full integration of the various modules is a very important characteristic to the user; e.g. it allows the user (after the entire grid has been generated) to modify the geometry and/or the grid parameters.

3.3.1 CFD-GEOM Interface to the Virtual Prototyping Environment

An interfacing mechanism, which is transparent to the user, among the various modules within the virtual prototyping environment is essential. Besides generating a grid file, CFD-GEOM generates a boundary condition and domain interface file (*.IBC) as well. This file contains information about all boundary condition types within the model (which can be given a symbolic name, e.g. 'inlet1' or 'lower-exit'), cell types (solid or blocked regions), and domain interface data in case of multi-domain simulations. The user specifies the boundary condition types and the regions while the domain interface data is automatically generated by CFD-GEOM as a result of the grid generation process.

As a result, the user does not have to specify all the boundary conditions by hand in the GUI for the ACE flow solver. More importantly, within CFD-GEOM all boundary conditions types and regions are specified on the geometry itself (instead of specifying grid regions in the ACE graphical user interface). This grid independent specification is a major step towards a user-friendly CFD analysis process in which grid densities may often change.

3.3.2 Virtual Parts Library

An important feature of CFD-GEOM, developed especially for the virtual prototyping environment, is the virtual parts library. It allows the user to compose models from a predefined set of sub-assemblies. For this purpose, CFD-GEOM has the layer concept. Entire models, parts, or sub-assemblies can be created per layer. The models or parts can be built up to an arbitrary degree of completeness, i.e. containing just geometric information, or topology and grid information up to a certain level (edges, faces, blocks) as well. The user can assemble full models by merging several layers into another layer. Either entire layers or subsets of layers can be merged (see Figure 3-6). This merging is a very complex process, in which duplicate geometry and topology information, as a result of this merging process, needs to be eliminated.

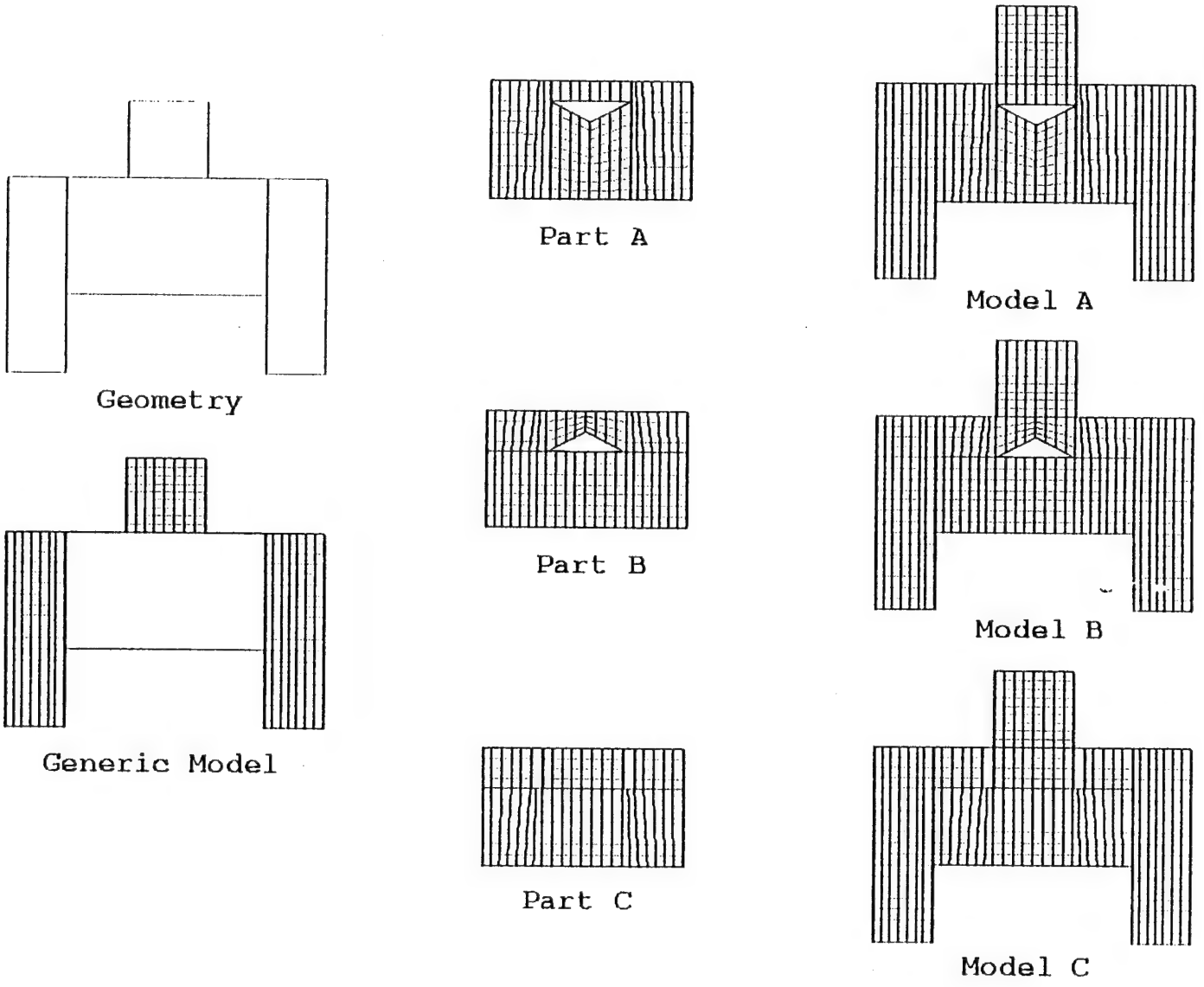

Figure 3-6. Illustration of Virtual Parts Library; the Generic Model, the Various Parts and the Resulting Models

The user can create an arbitrary number of layers, go from one layer to the other, delete layers, and merge layers. A set of layers, comprising a set of complete models, sub-assemblies, and/or parts for a certain CVD reactor design, can be stored in one file, this is called a virtual parts library (*.VPL default file extension). Each layer can be created and manipulated independently of all the other layers, and is stored in a regular *.GGD file (Geometry Grid Definition). Technical information about a certain layer can be obtained from CFD-GEOM (number of lines, curves, surfaces, grid points, grid blocks, etc.), as well as a short description of what model/part is contained in the layer.

The virtual parts library can be populated with entire models, parts, and sub-assemblies specifically for the design of microelectronic fabrication equipment. The idea here is to reduce the effort which is necessary to generate geometries and/or grids. The user can either use entire existing models as is, modify the grids and/or geometry of these predefined models, compose another reactor from predefined parts, create new parts and incorporate them into existing models, or just use the provided parts library as a set of documented examples.

In addition to the virtual parts library concept, CFD-GEOM has extensive capabilities to manipulate and modify geometries and grids with automatic updates of the entire model. Points, lines, and curves can be repositioned, the shape of curve and surfaces can be interactively modified. Grid density and distribution can be modified. Sets of curves and lines which specify one edge may be substituted by another set of lines and curves (edge substitution). Specific edge densities and distributions can be propagated throughout the model (edge linking). Multiple-block models can be combined into one block (if possible).

3.4 CFD-ACE

CFD-ACE is a general purpose commercial Computational Fluid Dynamics (CFD) code developed and marketed by CFDRC. It is capable of modeling fluid flow, heat/mass transfer and chemistry in engineering systems. The standard features of CFD-ACE include:

a. Solution of two and three dimensional Navier-Stokes equations for incompressible and compressible flows;
b. Non-orthogonal body-fitted-coordinates, moving and sliding grids;
c. Multi-domain simulations with implicit treatment of interfaces;
d. Fully implicit and conservative formulation;
e. k-ε turbulence model, multi-scale turbulence model, low Reynolds number k-ε model, and the Baldwin-Lomax mixing length model;
6. Chemical Equilibrium package based on the element potential method;
7. Gaseous combustion model with multi-step reactions and finite rate Arrhenius chemistry;
8. Spray Combustion model with two-liquid capability;
9. Second order central differencing scheme with damping terms;
10. Symmetric whole field solver; and
11. Pressure based solution algorithm.

In addition, the following capabilities were incorporated into CFD-ACE during the Phase II study:

a. A three-dimensional multi-component transport model based on kinetic theory of gases to estimate transport properties such as dynamic viscosity, thermal conductivity, diffusivity, and thermodiffusion (Soret) coefficients.

b. Capability for the user to input optional polynomial (up to fifth order) fits for transport properties such as viscosity, conductivity, and specific heat for individual species in the mixture.

c. A multi-step, finite rate, reversible/irreversible chemistry package that can handle up to 20 species and reactions with and without third body effects. The Arrhenius parameters are supplied as input by the user. The reverse reaction rate is either calculated from the equilibrium constant or can be specified explicitly by the user. A novel Jacobian Linearization method is available to handle extremely stiff systems of

equations.

d. A multi-step, irreversible surface chemistry model to simulate deposition processes such as Chemical Vapor Deposition (CVD), Physical Vapor Deposition (PVD) and Physical Vapor Transport (PVT). Capabilities to model etching processes are also available in the code.

e. A 3-dimensional thermal radiation model based on the discrete ordinate method. The model can simulate energy transfer by radiation through semi-transparent, participating media in conjunction with fluid flow, conductive/convective heat transfer and chemical reactions. A conjugate heat transfer model to simulate heat conduction through dissimilar materials is also available in the code.

f. A Lagrangian particle transport model accounting for effects of gas phase drag, pressure and gravitational forces on particle motion. Sub-models are available to simulate heat transfer with particles and melting/vaporization of particles.

All of the above models have been implemented in a generalized, non-orthogonal, Body-Fitted-Coordinates (BFC) system with multi-block capability. This facilitates the simulation of processing phenomena in complex reactor geometries.

3.5 CFD-VIEW

CFD-VIEW is a software package for interactive visualization and analysis of volumetric data (developed and marketed by CFDRC). The data can be any scalar and or vector field defined over a multi-domain structured, unstructured, or hybrid grid. Surface based visualization has been fully exploited to visualize the data; the user can display one or more computational planes, cutting planes, walls, and/or shaded iso-value surfaces within the volume.

Several basic visualization methods are possible to visualize surfaces within the volume. A surface can be either a computational plane, a cutting plane, an iso-value surface, an unstructured surface, the computational domain geometry, or a wall. A

surface can be displayed with grids, shading, surface plots, outline, hidden surface plot, contours, flooded contours, or vectors. Optionally, these basic visualization methods can be combined to create a **complex surface type**, e.g. flooded contours in combination with contour lines and grids.

A flow field can be visualized by showing arrow plots in one or more planes. The user can interactively modify any of the arrow characteristics, for example displayed vector length, arrow head size, and spacing of the arrows in a plane. Stream lines can be used to visualize a vector field as well. An arbitrary number of stream lines can be generated and displayed on the screen. The user has the option to restrict the stream lines to a certain computational plane, for example to show the vector field as oil streaks. All stream lines are truly multi-domain and the user does not have to specify explicitly where domain interfaces occur. Furthermore, flow fields can be characterized in terms of critical points using Topological Flow Visualization. Critical points are points in the flow field where the velocity field is zero. Particle traces can be released from those critical points; the set of critical points and particle traces form the topological flow map. The Point Probe facility built into CFD-VIEW allows the user to display the numerical values of the dataset at any point within the computational domain. The Line Probe allows the user to select a line within the domain and plot one or more variables (XY-plot) along that line.

An extensive color selection and interactive colormap editor mechanism has been built into CFD-VIEW. Several standard color maps are provided as well. CFD-VIEW allows the user to create image files from the screen. Two image formats are supported: Silicon Graphics RGB format and PostScript™. The RGB format allows extensive editing of these images on SGI machines. The PostScript™ format allows the creation of very high resolution images for printing. Furthermore, the user has several utilities at his/her disposal:

- show local coordinate system axes;
- interactive selection of center of rotation;
- reset viewing orientation;
- save and retrieve the visualization to or from permanent file;
- display information about the computational model;
- a built-in calculator; and

- data mirroring and duplication.

The graphical user interface is based on X-Windows and Motif, and provides a context-sensitive on-line help function. A general introduction to Motif graphical user interfaces is given in the next section.

4. DEMONSTRATION CASES

This section describes a series of demonstration cases performed using the VPE. The reactors considered in this study are industrial systems currently used for semiconductor wafer processing. All models are three-dimensional and involve the use of non-orthogonal body-fitted-coordinates (BFC) to account for the geometric complexity. Full coupling is maintained between all the physical models used in the study.

4.1 Bell Jar Reactor

A schematic of the Bell Jar CVD reactor is shown in Figure 4-1[7]. The susceptor is in the form of a frustum of an octagonal prism. The wafers to be processed are placed along the sides of the susceptor. The susceptor is heated either by induction coils placed around the bell jar or by direct radiation (through the transparent quartz wall of the bell jar) from an external source. The reactants enter through the top end of the reactor and flow around the susceptor and out of the reactor through the exit located at the bottom. The susceptor is usually rotated to enhance uniformity. The quartz wall of the reactor is air cooled.

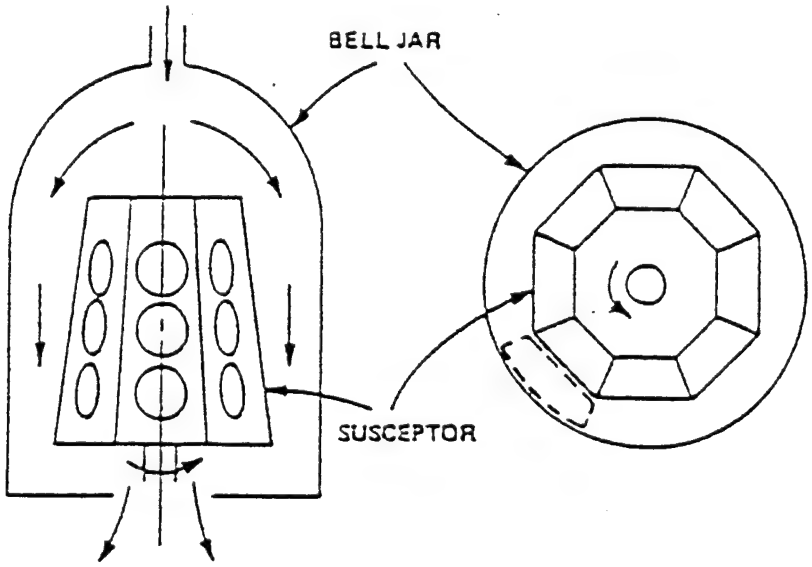

Figure 4-1. Schematic of Bell Jar CVD Reactor

Due to the shape of the susceptor, the flow area decreases along the flow path. This in intended to produce a favorable pressure gradient (due to flow acceleration) which would maintain a more or less uniform boundary layer thickness along the susceptor. The key issues in the operation of the reactor are the uniformity of temperature, flow and species distributions on the susceptor surface.

Operating Conditions: The reactant mixture consists of 11% silane and 89% hydrogen by mass. The deposited material is solid silicon. The inlet velocity and temperature of the reactants are 20 m/sec and 300°K respectively. The reactor pressure is 10 Torr. The susceptor is assumed to be heated by a radiator (located outside the reactor) at a high temperature. The emissivities of the radiator and the susceptor are assumed to be 1.0 and 0.8 respectively. The quartz wall of the bell jar is assumed to be a semi-transparent, absorbing material. The conjugate heat transfer through the susceptor block is modeled. The bottom end of the rod supporting the susceptor (near the flow exit) is maintained at 300°K. A 2-D schematic of this problem is provided in Figure 4-2. The gas phase and surface reactions for the problem are described below[8]:

Table 1. Reaction Mechanism for the 3-D Bell Jar CVD Reactor Case

Gas Phase	Reactions	$SiH_4(g) \xrightarrow{k_{f_1}} SiH_2(g) + H_2(g)$
		$Si_2H_6(g) \xrightarrow{k_{f_2}} SiH_4(g) + SiH_2(g)$
	Kinetics	$k_{f_1} = 2.438 \times 10^{16} \exp\left[\frac{-2.054 \times 10^8}{RT}\right]$
		$k_{f_2} = 1.584 \times 10^{12} \exp\left[\frac{-1.668 \times 10^8}{RT}\right]$
Surface	Reactions	$SiH_4(g) \xrightarrow{k_{s_1}} Si(B) + 2H_2(g)$
		$Si_2H_6(g) \xrightarrow{k_{s_2}} 2Si(B) + 3H_2(g)$
		$SiH_2(g) \xrightarrow{k_{s_3}} Si(B) + H_2(g)$
	Kinetics	$k_{s_1} = \gamma_{SiH_4} \sqrt{RT / 2\pi M_{SiH_4}}$ $\gamma_{SiH_4} = 1.08 \times 10^8 \, T^{-0.8822} \exp\left[-1.584 \times 10^8 / RT\right]$
		$k_{s_2} = \gamma_{Si_2H_6} \sqrt{RT / 2\pi M_{Si_2H_6}}$ $\gamma_{Si_2H_6} = 4.96 \times 10^{16} \, T^{-3.253} \exp\left[-1.681 \times 10^8 / RT\right]$
		$k_{s_3} = \gamma_{SiH_2} \sqrt{RT / 2\pi M_{SiH_2}}$ $\gamma_{SiH_2} = 1.0$

Parametric Study: Two demonstration cases were performed for the Bell Jar. The first was for a radiator temperature of 1000°K, the second for a temperature of 1400°K. The results of these cases are discussed in the section on computational results.

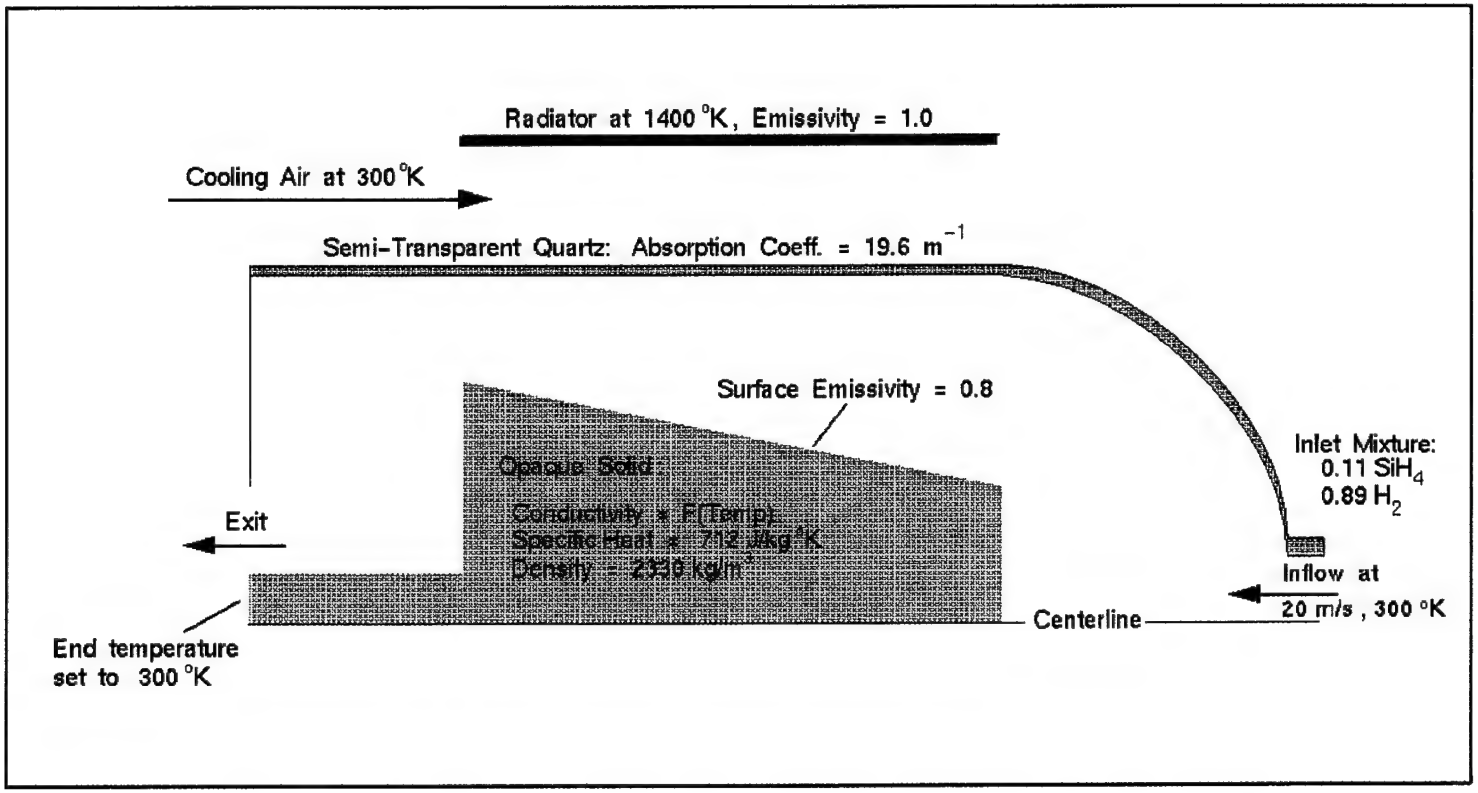

Figure 4-2. Illustration of Boundary Conditions for the Bell Jar Simulation

Computational Geometry and Grid: The simulation of the Bell Jar Reactor takes advantage of the octagonal symmetry of the susceptor/reactor and models a 45 degree "pie" sector of the geometry, with cyclic planes at $\theta = 0°$ and $\theta = 45°$. This approach saves computational time and allows for finer grid resolution.

The first step in the simulation was to construct a 45° slice of the Bell Jar reactor using CFD-GEOM. Figure 4-3 shows this geometry (and a grid plane at $\theta = 45°$) in the context of the CFD-GEOM window. The heavier lines represent the boundaries of individual geometrical feature such as the susceptor, the quartz wall and the radiator. Not all geometric features are evident, however, since some such as the stem of the susceptor, were created later in the CFD-ACE GUI by filling in grid cells with solid material. [As an aside, this procedure of making geometrical features dependent on the grid is not recommended, since it inhibits grid refinement. It is recommended, instead, that all geometries be explicitly defined in CFD-GEOM. Then, the user can manipulate the grid without disturbing the shape of the hardware.]

In addition to the geometry and grid, some of the boundaries were specified in CFD-GEOM, as shown in Figure 4-4, for automatic incorporation into the CFD-ACE model. For example, the light blue lines, in Figure 4-4 correspond to walls of fixed temperature corresponding to the end wall of the quartz and the external radiator. The yellow boundaries indicate inlets, one for flow into the reactor and one for cooling flow between the radiator and the quartz. The light green lines indicate an exit. The remaining faces are left unspecified, as indicated by the default color of olive drab. These default boundaries may still be defined subsequently in CFD-ACE.

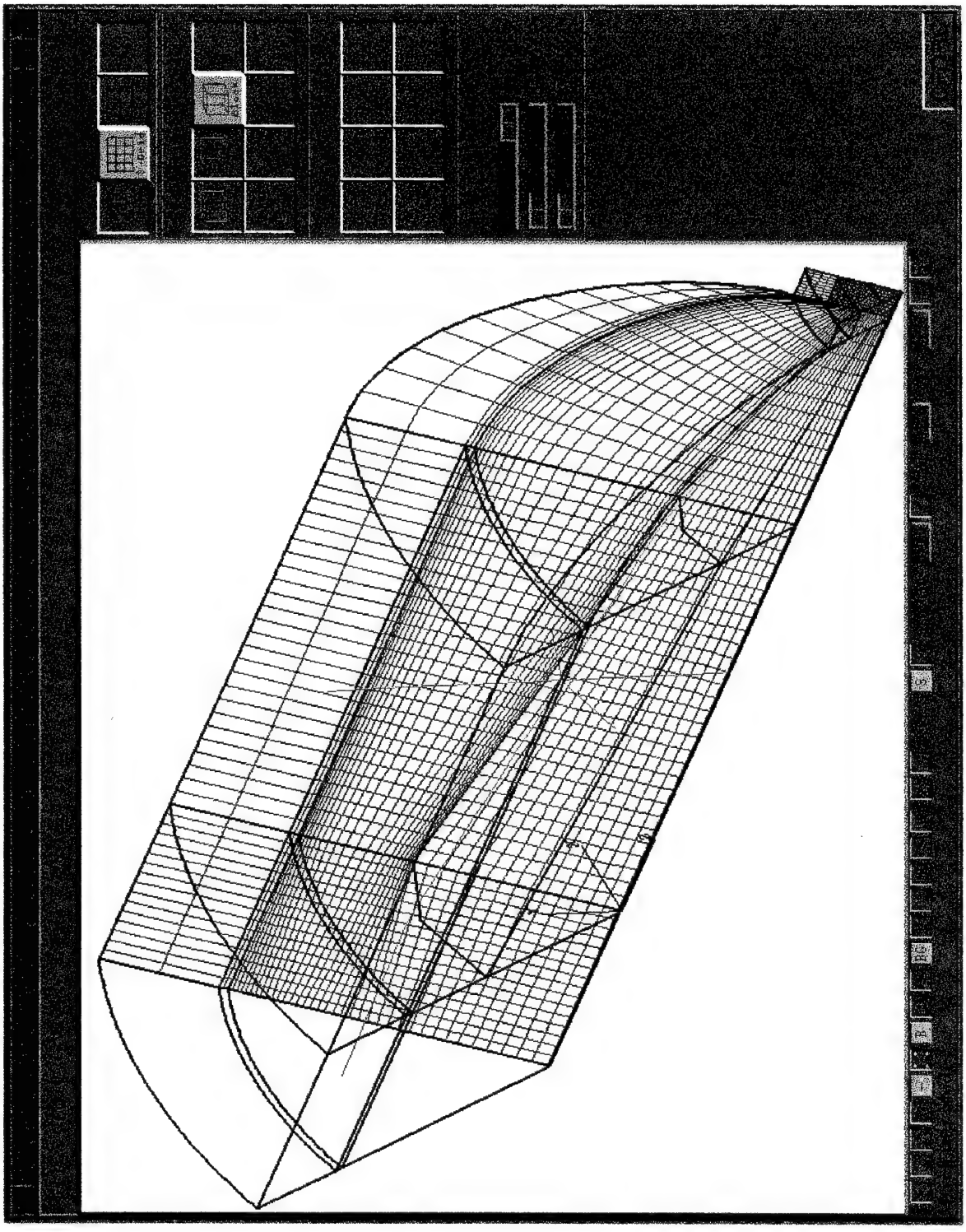

Figure 4-3. Bell Jar Geometry (45° Section) in CFD-GEOM

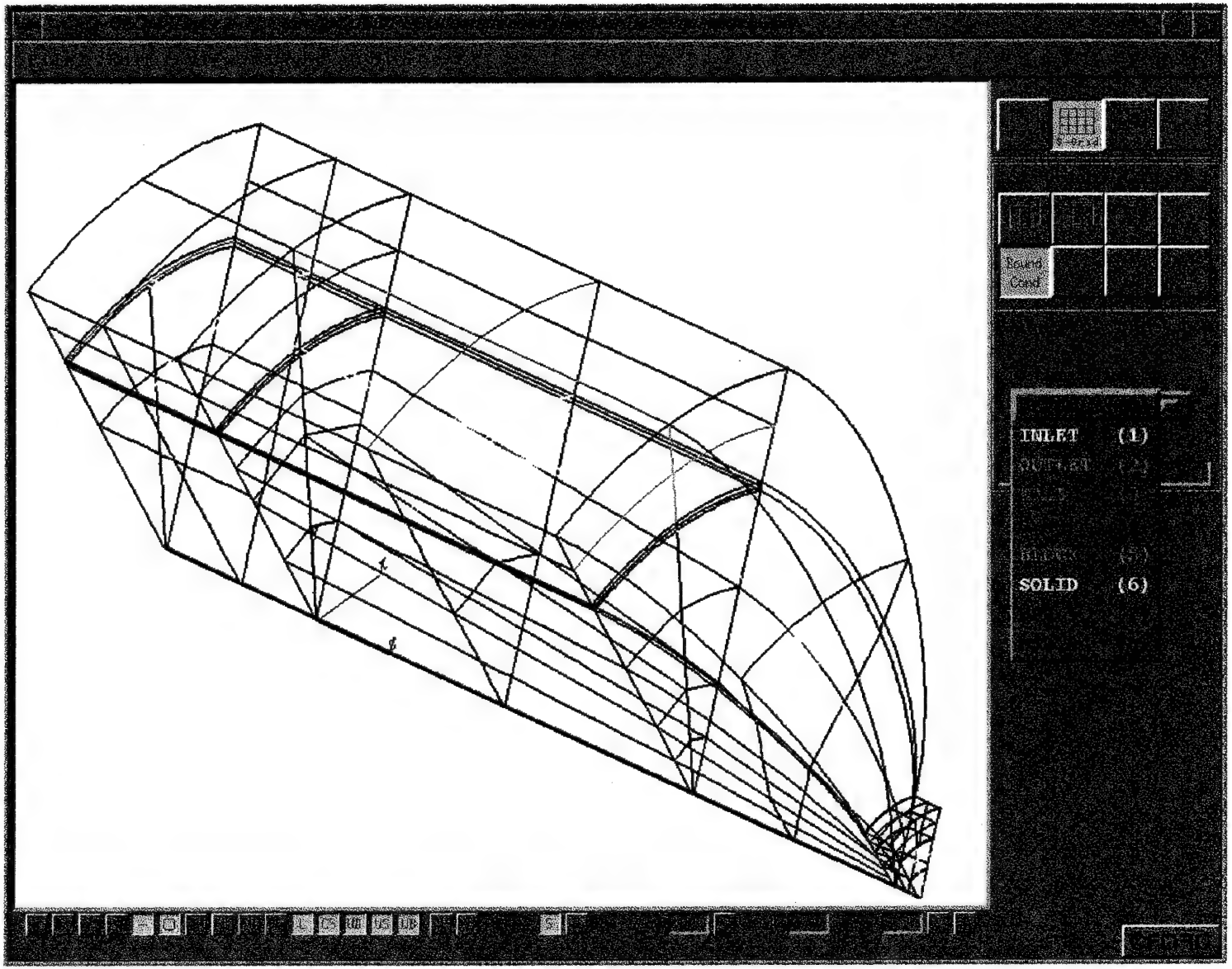

Figure 4-4. Boundary Conditions for Bell Jar as Defined in CFD-GEOM

Model Setup: The grid, shown in Figure 4-3, and the boundary conditions, shown in Figure 4-4, are loaded into files model.PFG and model.IBC, respectively. This information is then used by the graphical user interface (GUI) for CFD-ACE in the model setup definition. Within the CFD-ACE GUI (invoked via the Master GUI from column III) the boundaries, e.g., inlets, fixed temperature walls, exits, etc., are fully defined. Figure 4-5 displays the boundary condition windows in the CFD-ACE GUI. For this example, the radiator, defined as a wall in CFD-GEOM, is further designated as an isothermal wall, with no reaction, no velocity, a temperature of 1400°K, and an emissivity of 1.0. To run a parametric study, the user needs only to revise the boundary condition in this window, e.g., change 1400°K to 1000°K, and rerun the simulation. The results for such a parametric study are discussed below.

Computational Results: A demonstration parametric study was performed for the Bell Jar using a radiator temperature of 1000°K and 1400°K. All other operating conditions were as described in the section on operating conditions and illustrated in Figure 4-2. The results of the simulation are compared in Figure 4-6. The colors indicate the temperatures of the radiator, quartz, susceptor interior, and gas mixture, (using radial cutting planes through the geometry). The gray scale indicates the silicon deposition rate in kg/m^2-sec on the susceptor surface. The predictions indicate that an increase in radiator temperature has a strong effect on the deposition rate, increasing it by over an order of magnitude. Results also indicate that the uniformity of deposition can be significantly enhanced by increasing the susceptor temperature. Figure 4-7 shows a full 3-D view of the results for the 1400°K case.

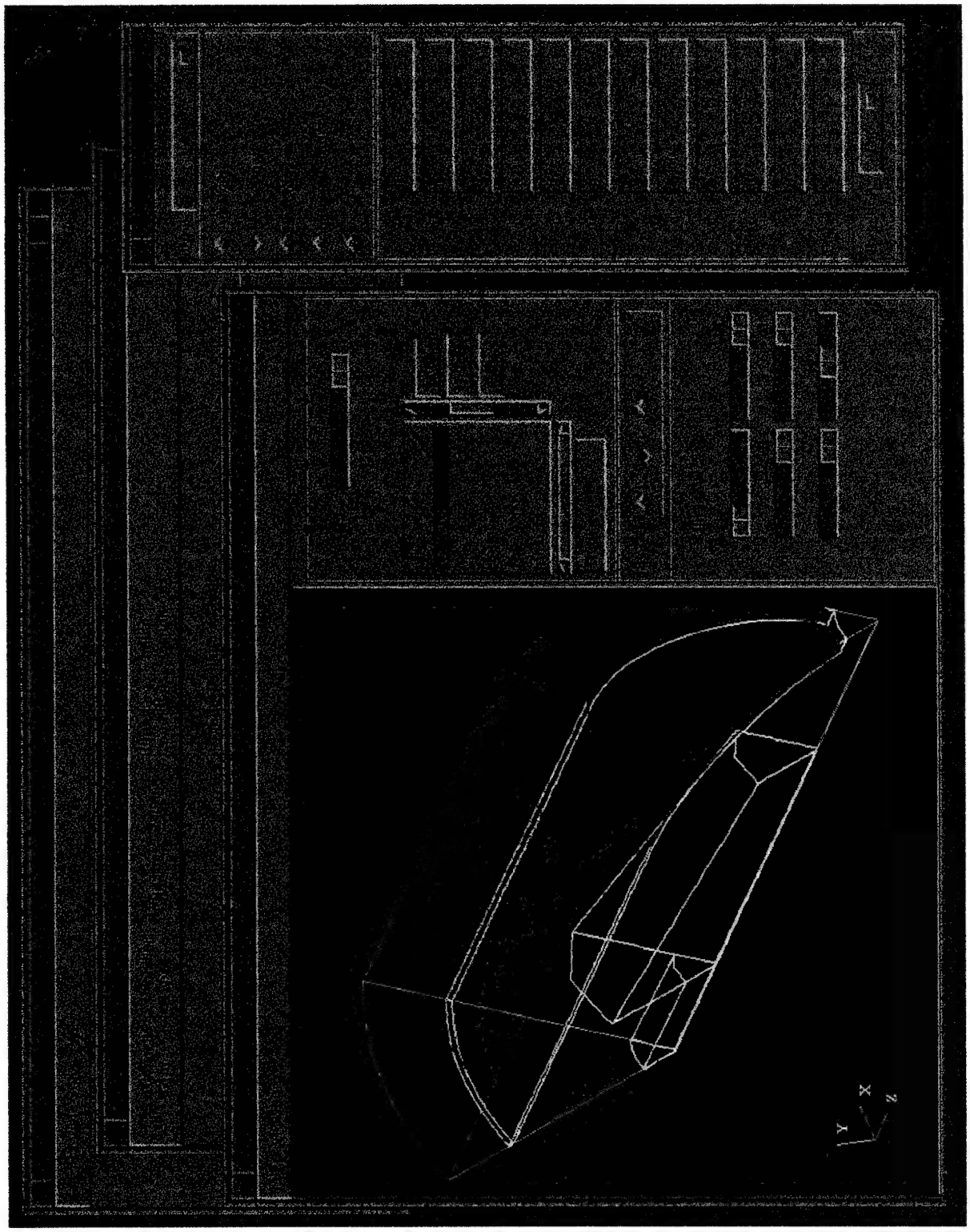

Figure 4-5. Boundary Conditions Window in CFD-ACE GUI: Bell Jar Radiator Selected

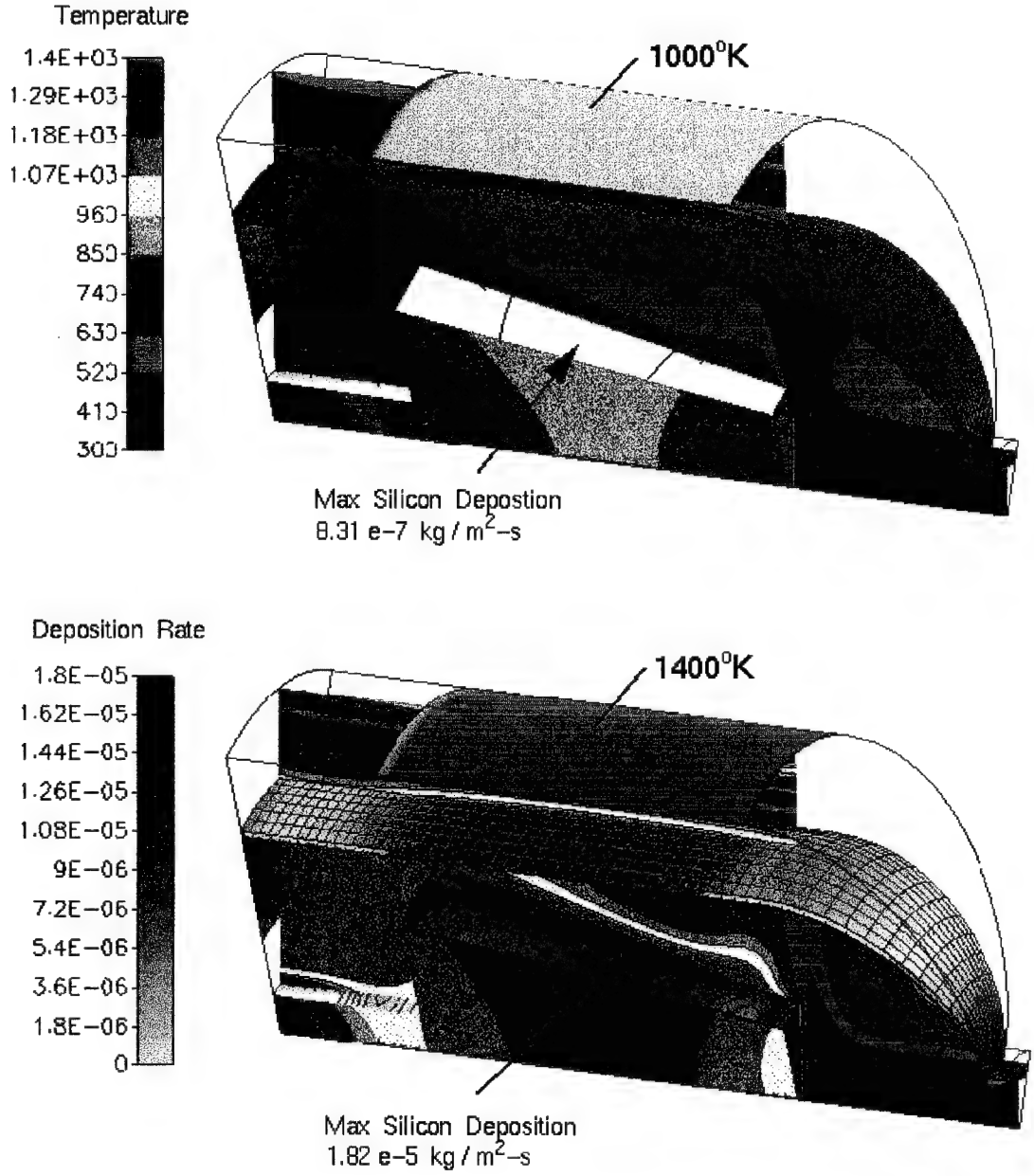

Figure 4-6. Bell Jar Simulation (45° Section): Comparison of 1400°K Radiator versus 1000°K Radiator

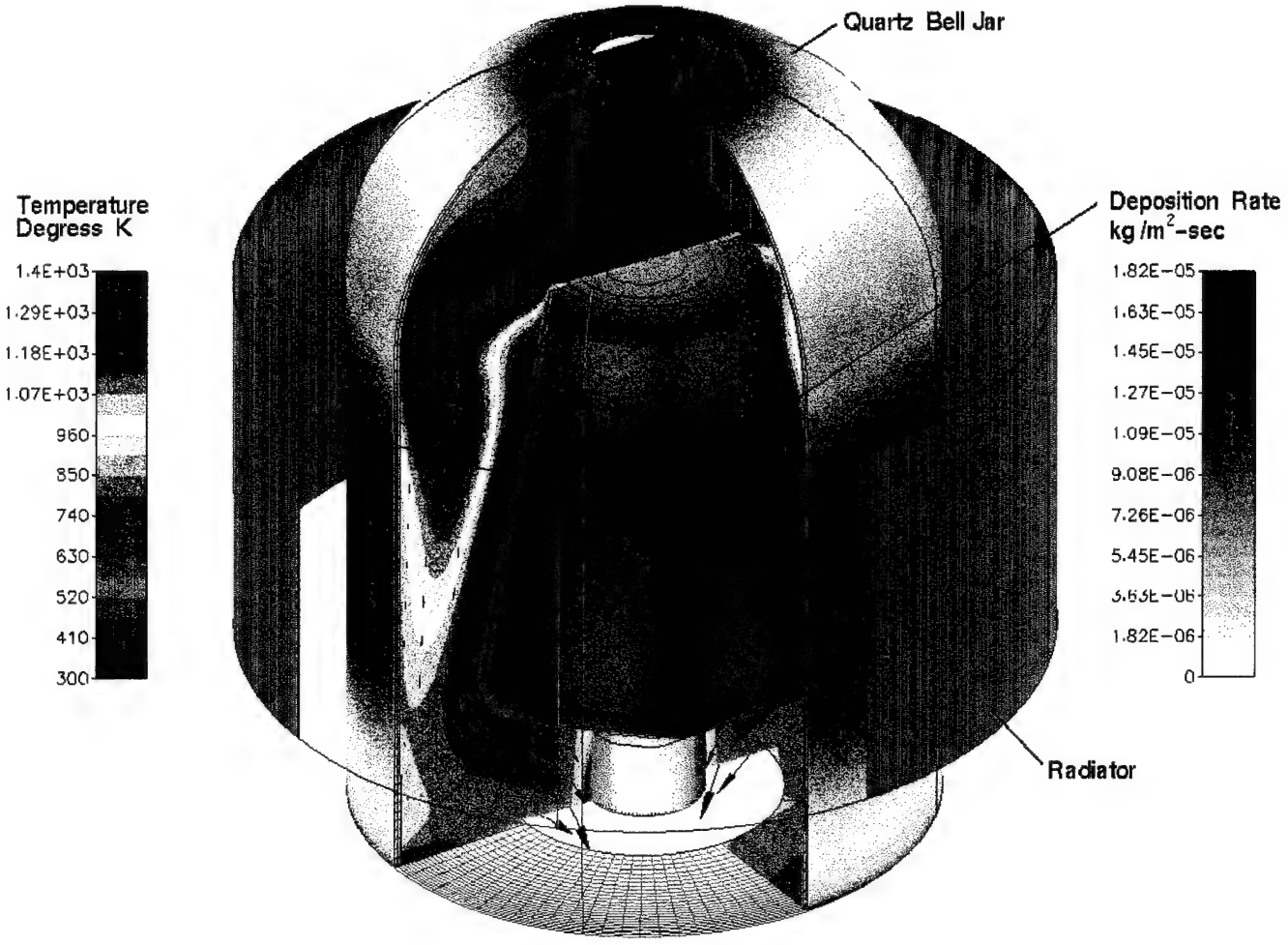

Figure 4-7. Full View of the Bell Jar Reactor

4.2 Jipelec Reactor

The second category of reactor in the data base is the Jipelec. As with the Bell Jar reactor it is used to grow silicon from silane using CVD. Figure 4-8 shows the different views of the Jipelec reactor[8]. The wafer is heated by radiation (from external lamps) through the semi-transparent window at the bottom. The reactants enter the chamber through the inlet located at the top. There are two circumferential outlets from the wafer chamber (Figure 4-9). The flow then exits to the main chamber and leaves the reactor through the outlet located on the right-hand-side of the reactor. The flow in the wafer chamber is almost (two-dimensional) axisymmetric while the flow in the main chamber is three-dimensional. Detailed simulations of a number of benchmark cases for the Jipelec reactor are presented in Appendix A.

The key issue in this system is the uniformity of temperature distribution on the top surface of the wafer. Although the chamber flow is more or less two-dimensional (axisymmetric), it is not clear if three-dimensional effects from the main chamber feed back to the wafer chamber.

Operating Conditions: The reactant flow consists of 3.8% silane and 96.2% argon by mass. The inlet flow rates are 2000 sccm of argon and 100 sccm of silane at a temperature of 300°K. The chamber pressure is 10 Torr. Conjugate heat transfer through the wafer holder is modeled. A single surface reaction is assumed to occur at the wafer surface[8]:

$$SiH_4\,(g) \xrightarrow{\gamma_s} Si(s) + 2H_2\,(g)$$

$$\gamma_s = 0.0402\, exp\,(-5021/T)$$

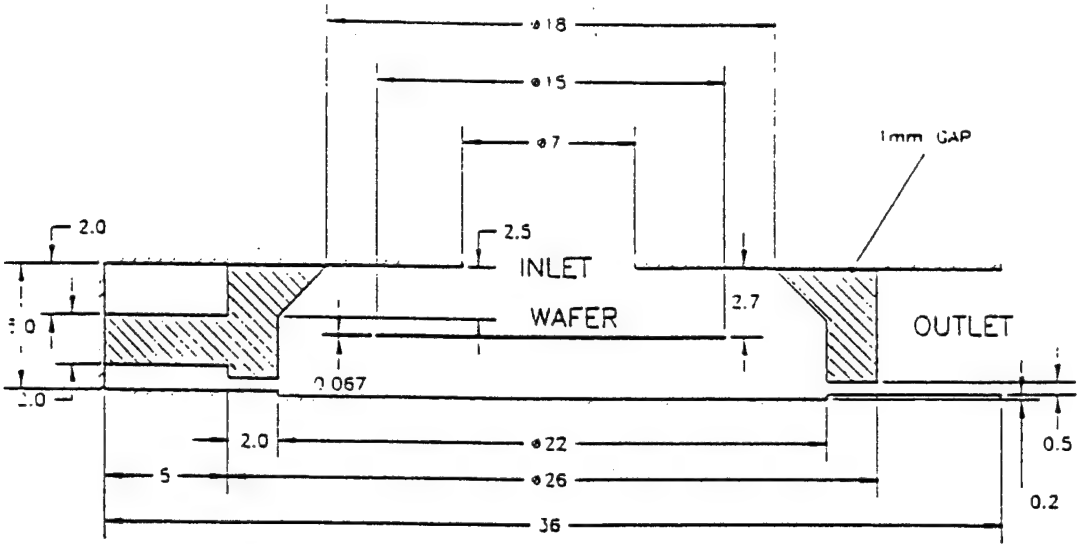

Figure 4-8a. Side View of Model Geometry (all dimensions are in centimeters)

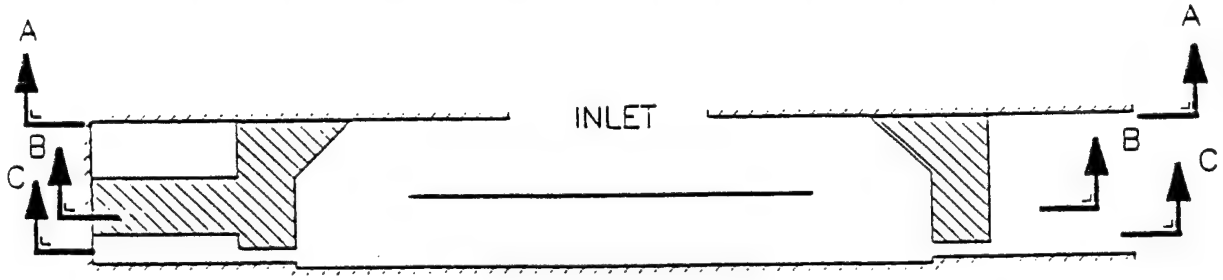

Figure 4-8b. Location of Section Views Shown in Figures 4-8c - 4-8e

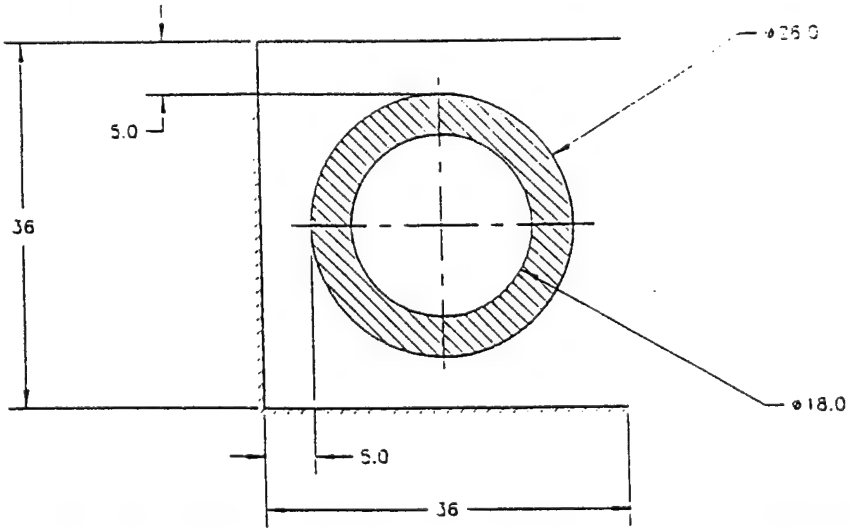

Figure 4-8c. Top View of Model Geometry at Section A-A (all dimensions are in centimeters)

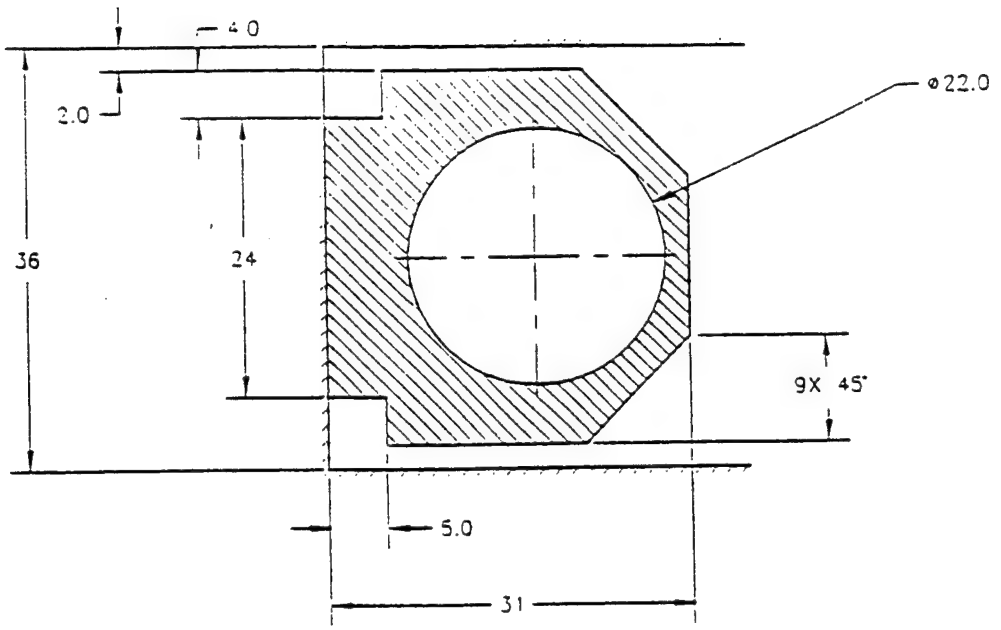

Figure 4-8d. Top View of Model Geometry at Section B-B (all dimensions are in centimeters)

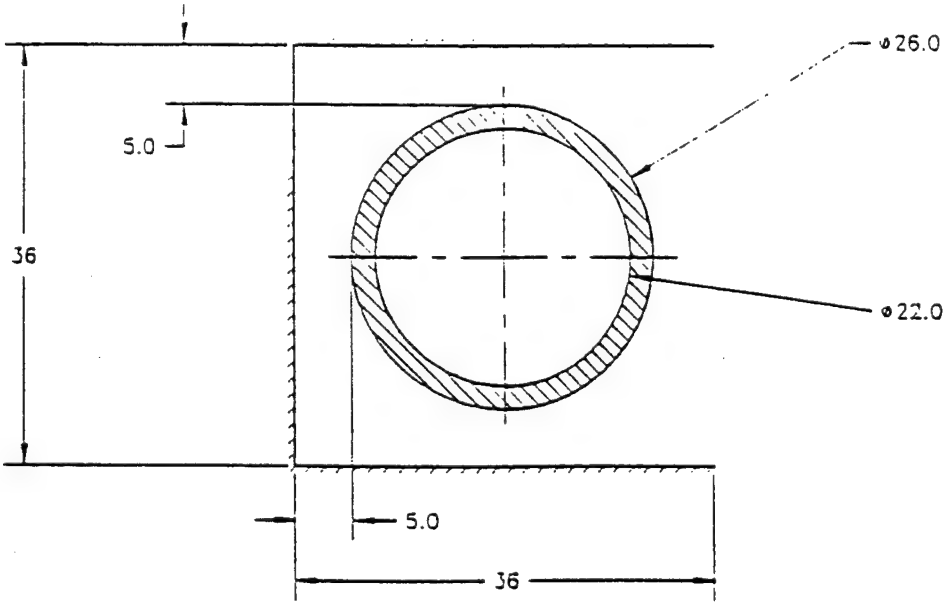

Figure 4-8e. Top View of Model Geometry at Section C-C (all dimensions are in centimeters)

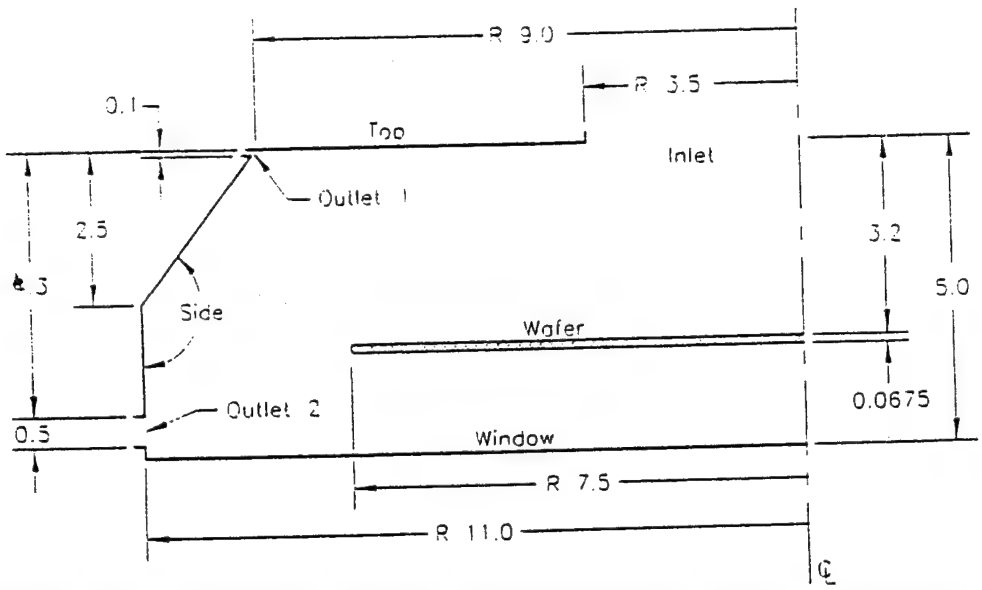

Figure 4-9a. Chamber Geometry (all dimensions are in centimeters)

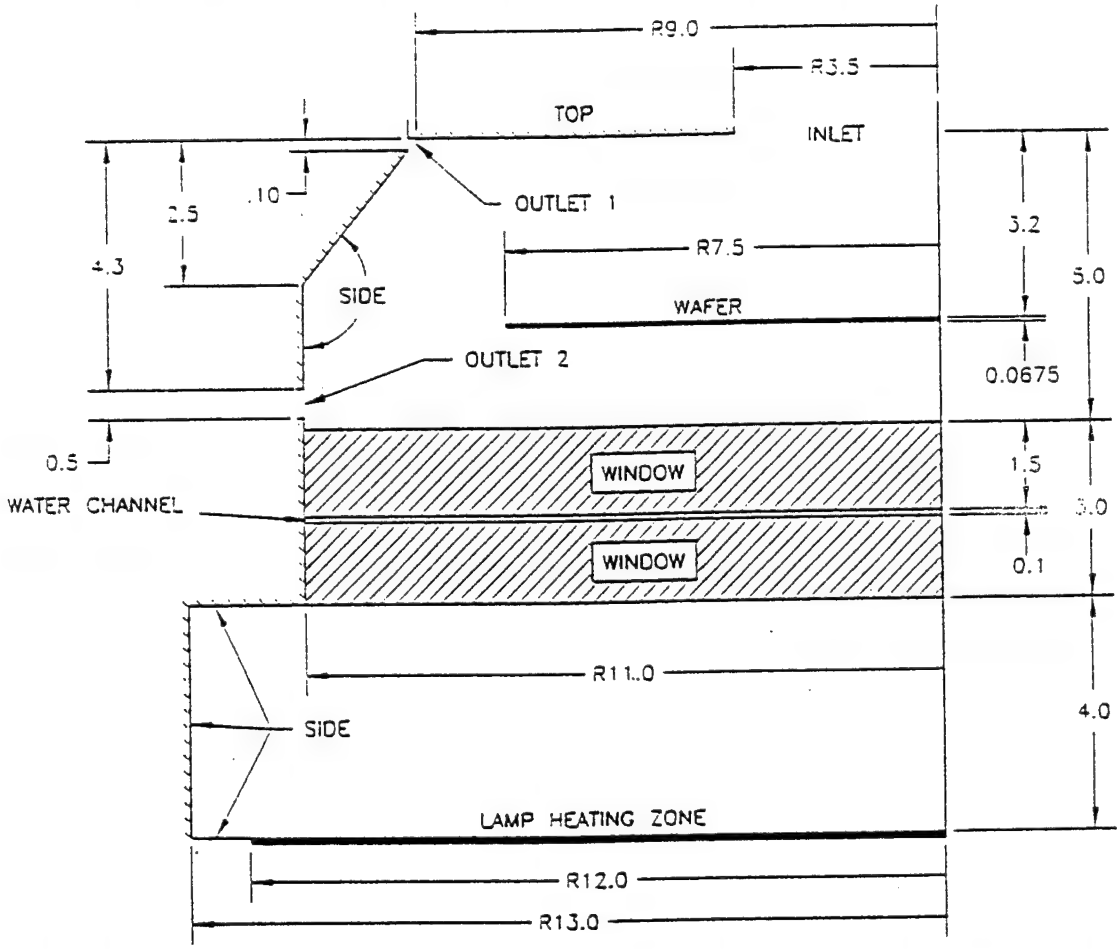

Figure 4-9b. Complete Geometry of Chamber with Windows and Lamps (all dimensions are in centimeters)

Parametric Study: Three demonstration cases were performed for this reactor. The first two cases ignore radiative heat transfer and analyze the deposition process for two wafer temperatures of 923°K and 800°K respectively. The window temperature for both cases was maintained at 600°K. A third case was simulated taking into account the effects of radiation. A fixed radiation intensity (of I= 5.e4 w/m^2) is specified at the window and the wafer is assumed to be an opaque conducting solid. The wafer temperature distribution is then obtained from the solution. The deposition patterns for all cases are compared.

Computational Geometry and Grid: The Jipelec reactor is symmetrical about its centerline (y = 0). Accordingly, the computational model only needs to simulate one half of the domain. However, due to the variety of shapes in the reactor, a single domain grid is infeasible. Instead, the half geometry is divided into seven domains. A grid is then superimposed on each domain. Figure 4-10 displays these seven domains, as constructed in CFD-GEOM, with sample grid planes at j=1. Once created in CFD-GEOM, the seven domains are composited into a multi-domain grid of 26,000 cells.

Model Setup: The reactor geometry and grid defined by CFD-GEOM serve as the starting point in the construction of the reactor model in CFD-ACE. The first step is to activate the appropriate model capabilities. In this case, the model is setup to solve for convective and conductive heat transfer in a flowing incompressible mixture. (For some of the parametric studies, radiation heat transfer is also activated.) The next step is to select the materials and define their properties. For all cases the fluid is specified as a variable gas mixture of Silane, Argon, Hydrogen and Silicon with an inlet composition of 3.8% Silane and 96.2% Argon. The density of the gas is specified as proportional to the inverse of temperature and the specific heat is computed using JANNAF data. The conductivity, diffusivity and viscosity are computed based on the kinetic theory of gases. The solid is specified as an opaque material with constant conductivity, specific heat and density. Having defined the materials, the next step is to define the surface reaction. This is done in accordance with the description of the surface reaction in the sub-section on operating conditions. Then the boundary conditions are specified. For all cases discussed here the inlet flow is set at 0.691 m/sec at 300°K.

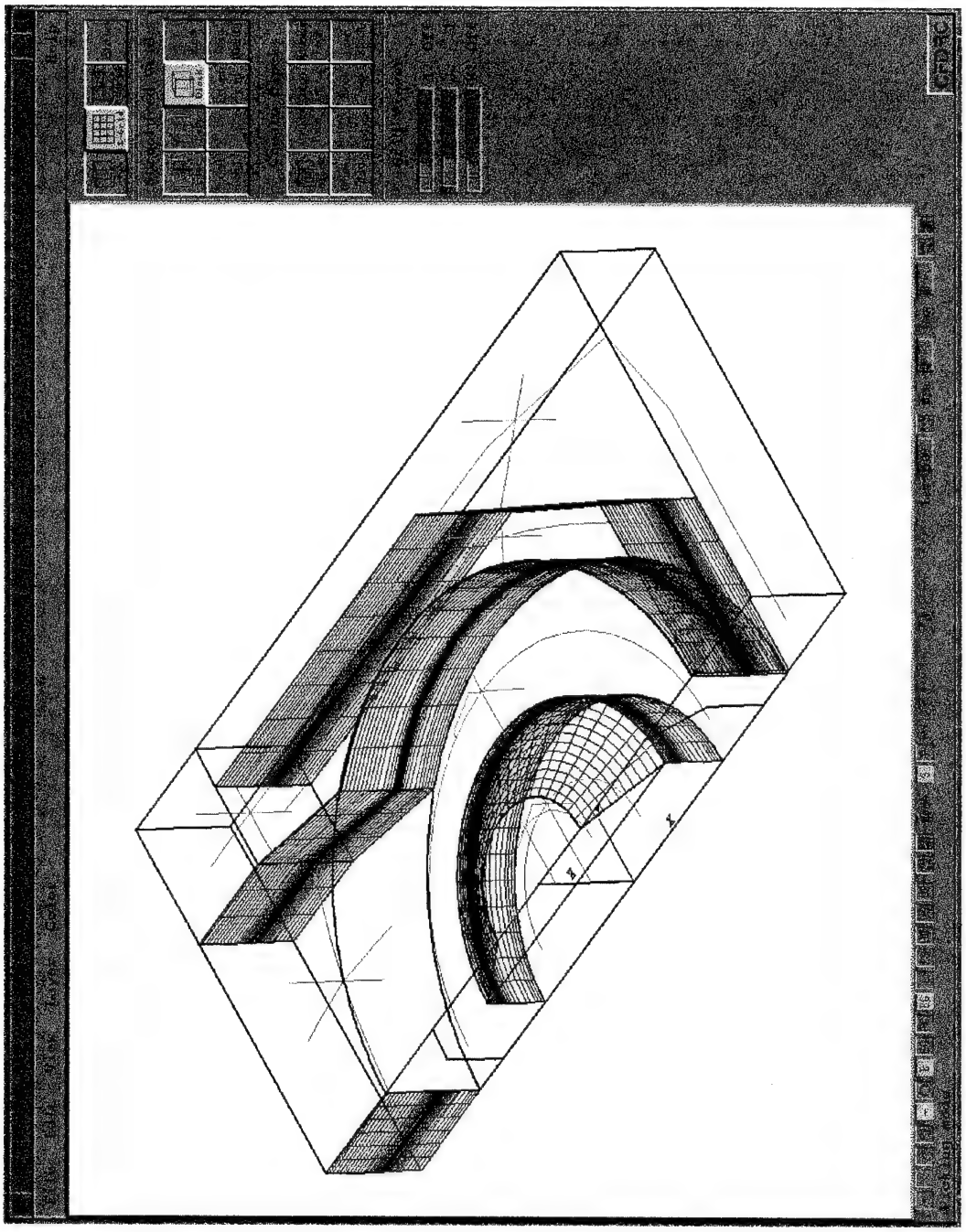

Figure 4-10. Geometry of Reactor Visualized in CFD-GEOM

For the first two flow simulations, which do not model the radiative heat transport, the bottom of the reactor is fixed at 600°K. For case 1 the wafer temperature is set to 800°K and for case 2 it is set to 923°K. All remaining walls are assumed to be 300°K. When radiation is modeled, the fixed bottom wall temperature of 600°K is replaced by an intensity boundary condition. The wafer temperature is not specified but determined as part of the solution. The results of these cases are discussed below.

Computational Results: The model predicts the temperatures, flow, mixing, and surface deposition in the Jipelec reactor. Figure 4-11 shows a 3-D cut away view of a set of sample results. (Only half the reactor is modeled, but the results can be reflected in CFD-VIEW to recapture the full geometry.) The figure indicates the position of the inlet and exit, as well as the general flow pattern over the wafer, under the wafer holder, and out the exit. Some flow also leaks through the gap between the top of the wafer holder and the reactor lid (partially displayed).

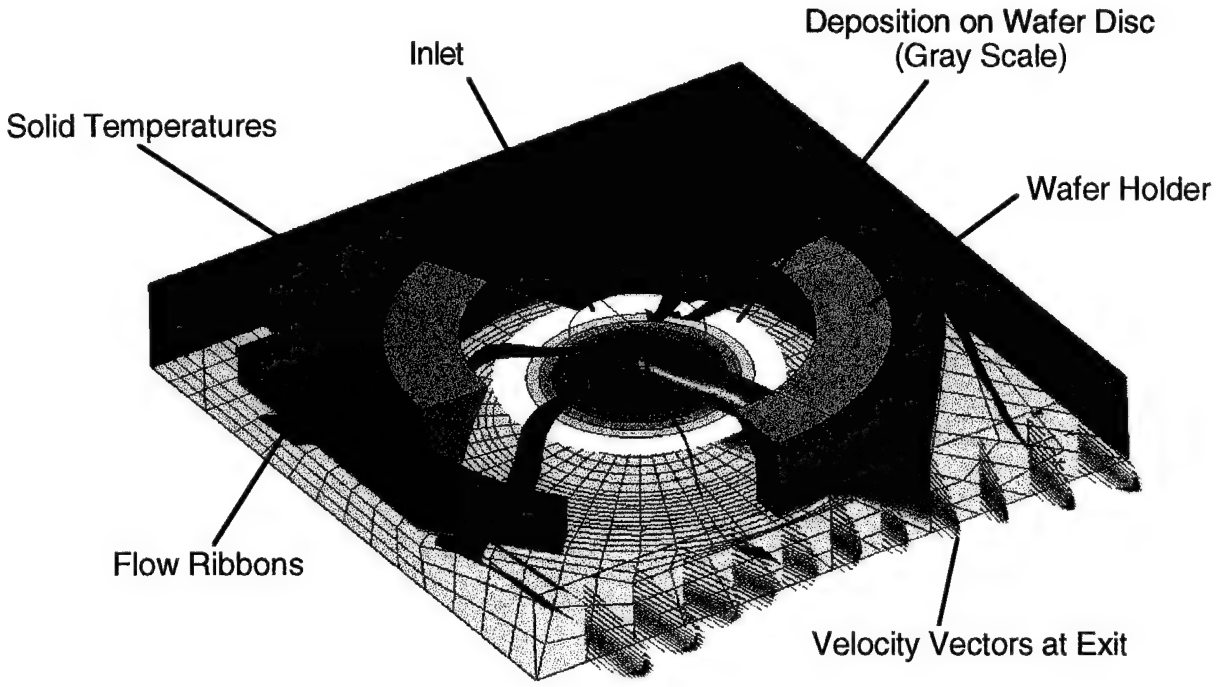

Figure 4-11. Jipelec Reactor

As a first case, a simulation was run without radiation and with the wafer set to 800°, as discussed above. A close-up of the predicted results in the context of CFD-VIEW is shown in Figure 4-12. Again, a cutaway view is presented. Two graphical cutting planes display the mass fraction of silane at the x = 0 midplane and at the exit. Similarly, the temperature is displayed at the plane of symmetry (y = 0) and on the bottom of the reactor. The effect of the fixed wafer temperature of 800°K on the general temperature field is also evident. On the surface of the wafer, the deposition of silicon is relatively uniform, at an average rate of 4.2 kg/m^2 -sec.

In order to determine the effect of temperature on deposition, a second case was run with an elevated fixed wafer temperature of 923°K. The results for this case are shown in Figure 4-12b. Again, the deposition on the wafer is axisymmetric and relatively uniform, but the rate has approximately doubled, as compared with the 800°K case.

The above cases provide insight into the effect of temperature on deposition rates, but by fixing the wafer temperature and neglecting radiation, they oversimplify the physics. In order to create a more realistic simulation, the model was extended to include radiation. The bottom quartz wall boundary condition of a fixed temperature was upgraded to a radiation flux boundary, and the wafer temperature was determined as part of the simulation. The results for this case are shown in Figure 4-13. The most striking feature of the prediction is that the deposition rate on the wafer is no longer uniform, nor even axisymmetric. Apparently, the non-axisymmetric feature of the external chamber of the reactor influences the temperature field in the inner chamber. The maximum temperature of the wafer is 955°K (similar to Case 2) but varies sufficiently across the wafer to cause a variation in deposition from 5e-6 kg/m^2-sec to 8.5e-6 kg/m^2-sec.

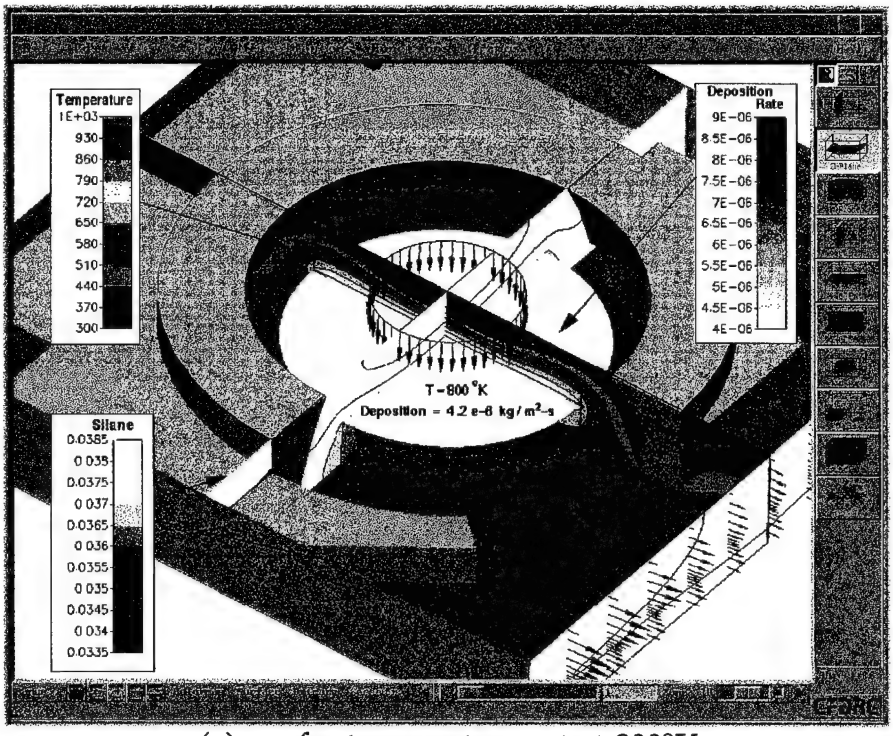

(a) wafer temperature set at 800°K

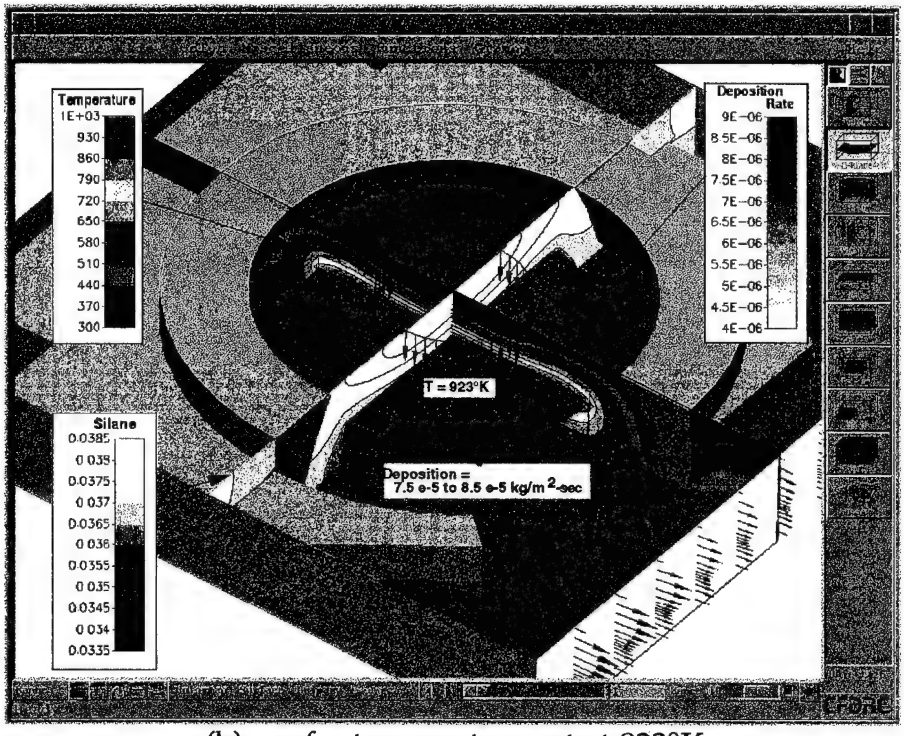

(b) wafer temperature set at 923°K

Figure 4-12. Jipelec Reactor Simulations (No Radiation)

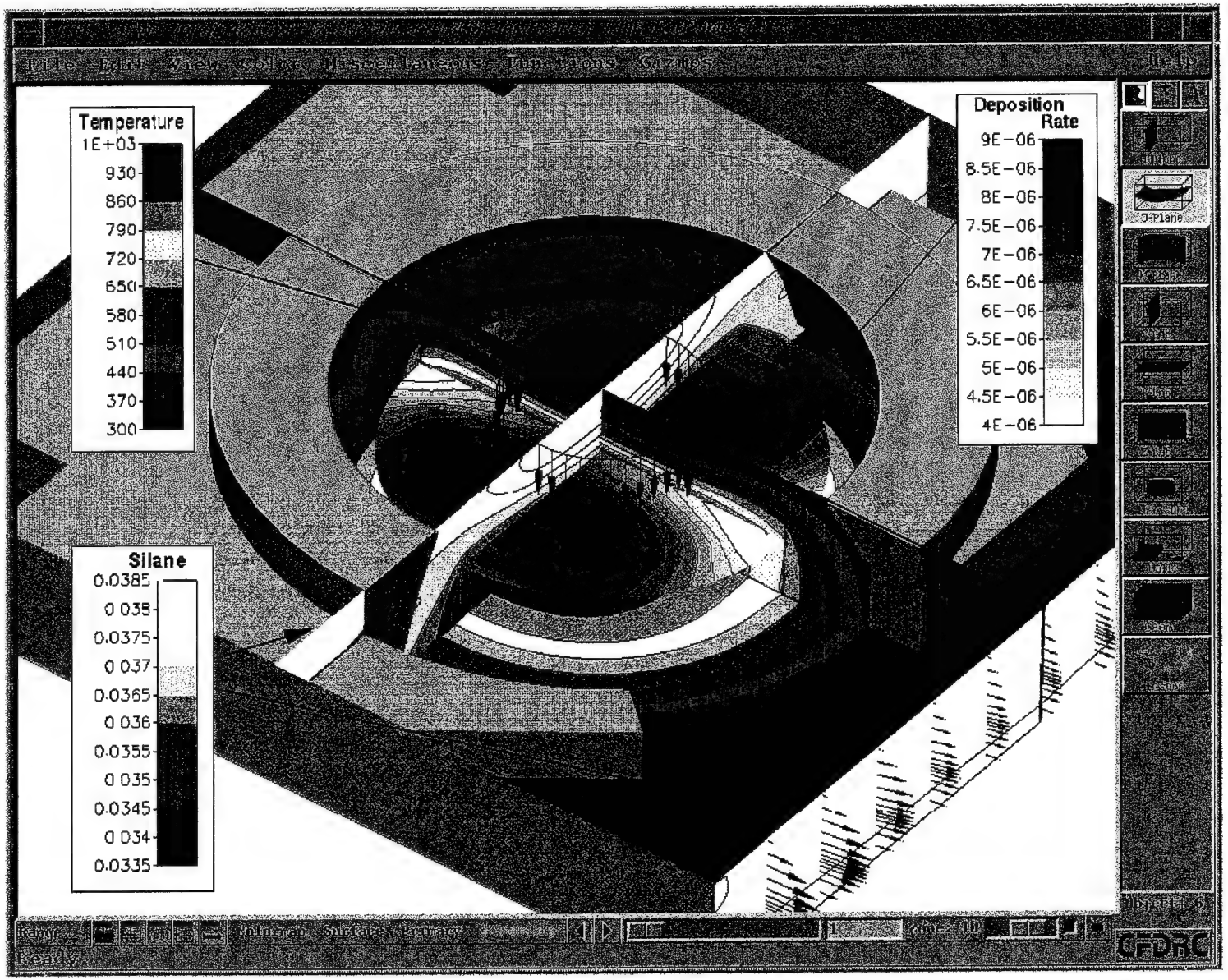

Figure 4-13. Jipelec Reactor Simulation (With Radiation)

4.3 Planetary Reactor

A schematic of the Planetary reactor is shown in Figure 4-14. The reactor consists of seven 2" wafers arranged circumferentially on a circular table. The table is rotated at a fixed angular velocity. The wafers on the table top are also given a rotation about their axes thus creating a planetary effect. This system is built by Aixtron GmbH (Aachen, Germany) and Laboratories d'Electronique Philips (Limeil-Brevannes, France) as a part of an EEC Espirit project (5003 PLANET). The reactor is currently designed for Metal Organic CVD (MOCVD) processes[9].

The key issues in this reactor are the flow and concentration uniformity along the surface of the wafer table. Since the reactants (TMG and arsine) are not premixed, diffusion mixing of the streams is crucial in determining the deposition uniformity.

Operating Conditions: A mixture of hydrogen and arsine (50% arsine and 50% hydrogen) is pumped through the central tube into the chamber immediately above the wafer table. A mixture of trimethyl gallium (TMG) and hydrogen (80% hydrogen and 20% TMG) is pumped through the annulus around the central tube to enter the chamber above the arsine/H2 stream. The reactant inlet temperature is 300°K and the reactor pressure is atmospheric. A constant heat flux condition (of Q=3000 W/sq.m) is imposed on the wafer surfaces. This simulates the heating of the wafer through the base by the lamps. The reactor exit is located circumferentially at the outer radius of the chamber. The deposition of GaAs is modeled through a single surface reaction of the form:

$$Ga(CH_3)_3 + AsH_3 \rightarrow GaAs + 3CH_4$$

The reaction rate is assumed to be high enough that the deposition of GaAs is limited by the diffusion of TMG to the wafer surface. Therefore, the concentration of TMG on the wafer surface is set to zero.

Parametric Study: For this study, the wafer table is assumed to be stationary. Two cases were simulated with wafer rotational speeds of 190 and 380 rpm respectively.

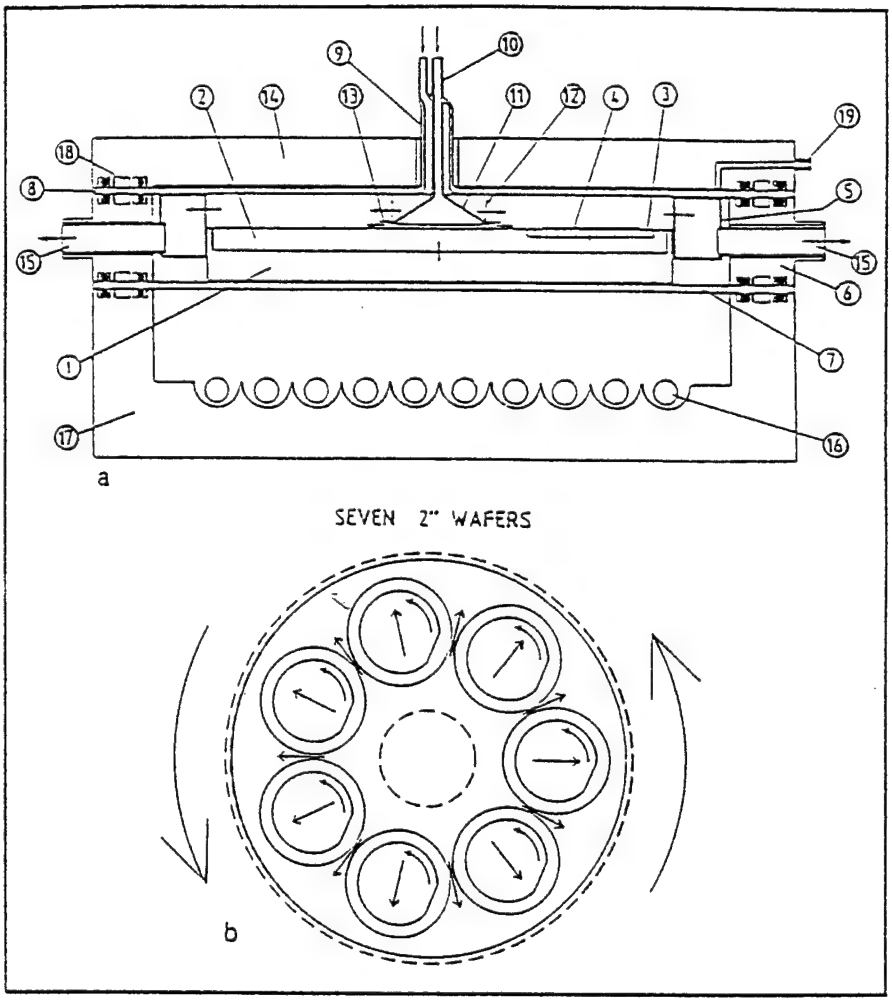

Figure 4-14. (a) Cross-section of the reaction chamber through the main axis. The reactive gas flow is indicated by arrows: (1) stationary part of graphite substrate holder; (2) main rotating disk; (3) satellite disk; (4) 2 inch wafer; (5) molybdenum exhaust gas collector; (6) water cooled stainless steel ring; (7) bottom quartz disk; (8) ceiling quartz disk; (9) outer entrance for main H2 carrier flow; group III precursors and dopants; 910) inner entrance for second H2 carrier flow and group V precursors; (11) cone; (12) cylindrical entrance grating; (13) deflector ring; (14) water cooled aluminum top plate; (15) gas exits; (16) 2 kW infrared lamp; (17) water cooled elliptic mirror; (18) vacuum ring; (19) inlet Ar/H2 mixture for ceiling temperature control. (b) Top view of the substrate holder. The directions of rotation and the flow of the reactor atmosphere are indicated.

Computational Geometry and Grid: The planetary reactor is a cyclic problem comprised of seven "pie" sectors. Due to its symmetry, only one seventh of the reactor needs to be simulated, provided cyclic boundary conditions are imposed between sectors. Figure 4-15 shows the planetary geometry as created in CFD-GEOM. The geometry was first constructed using multiple domains then subsequently composited into two domains. The use of two domains is necessitated by the notch at the inner radius of the slice. This notch corresponds to the diverter shirt separating the flow of hydrogen and trimethyl gallium at the top, from the inflow of hydrogen and arsine at the bottom. Included in the figure are grid planes at grid index j=2 and k=14. The total number of grid cells for this problem is 3380.

The planetary reactor model geometry and grid are more easily visualized in CFD-VIEW, as shown in Figure 4-16. The gray walls in the figure represent solid surfaces. The green disk is the rotating wafer disk. The inlets and exit are the non-gray planes of constant radii, as marked. This grid is passed to the CFD-ACE GUI for incorporation into the Planetary Reactor Model.

Model Setup: The first step in the CFD-ACE GUI was to scale the grid produced by CFD-GEOM. This is required because the geometry was created in inches (as per the drawings) but the analysis code expects SI units. Accordingly, a one-time scaling factor of 0.0254 m/in was applied to convert from inches to meters.

The next step was to specify the type of problem being analyzed. In this case, code options selected solve the heat transfer, chemical vapor deposition, and species mixing for an incompressible flow. Two fluid mixtures are defined corresponding to composition of the two inlet streams: (1) 0.8 H_2 + 0.2 $Ga(CH_3)_3$ and (2) 0.5 H_2 + 0.5 AsH_3. The activation of the multi-component diffusion option instructs the code to solve for the diffusive transport of all four species. The density of the mixtures is computed based on the perfect gas law and the viscosity and conductivity are computed based on kinetic theory. The specific heat is calculated from JANNAF data.

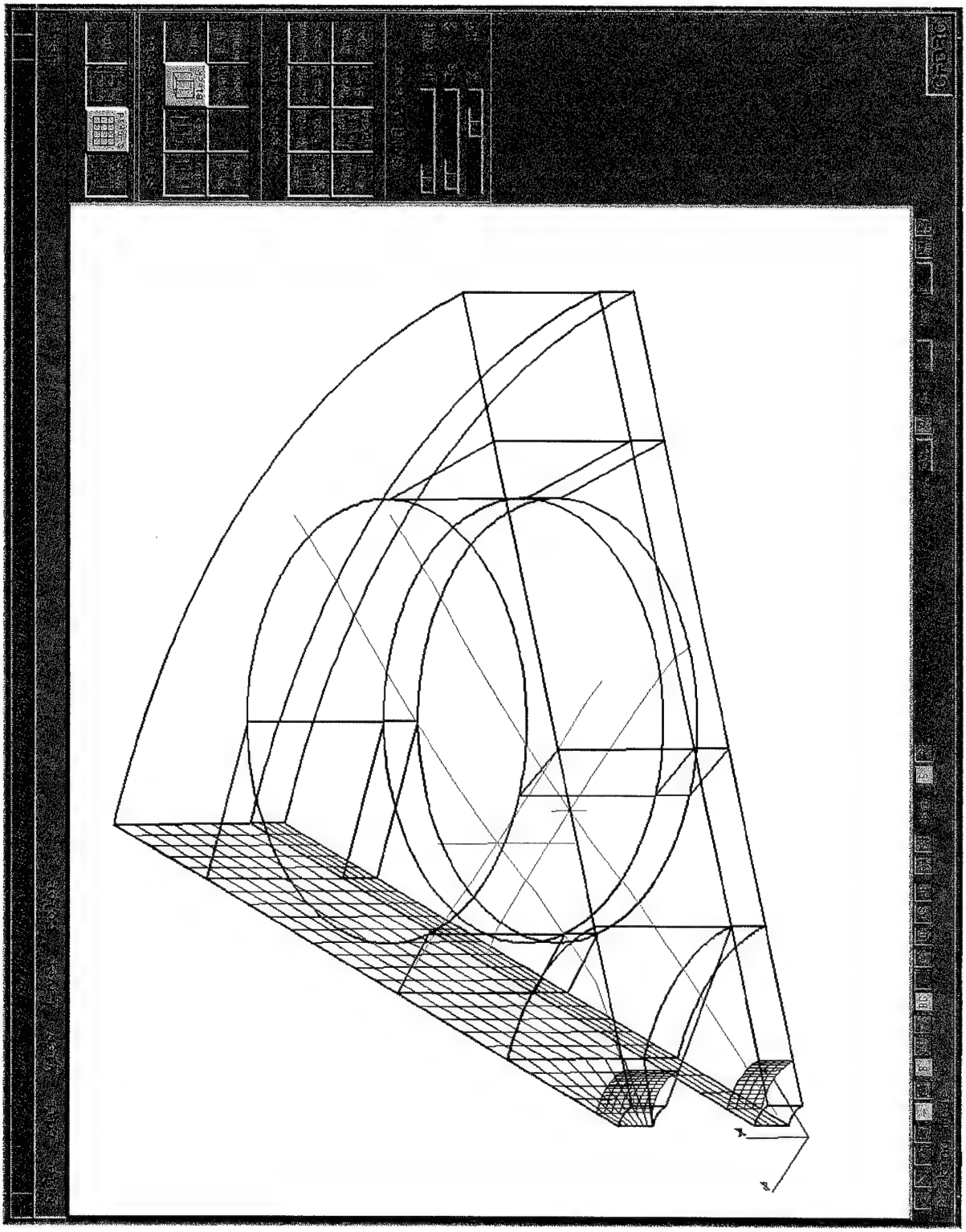

Figure 4-15. Geometry of Planetary Reactor in CFD-GEOM

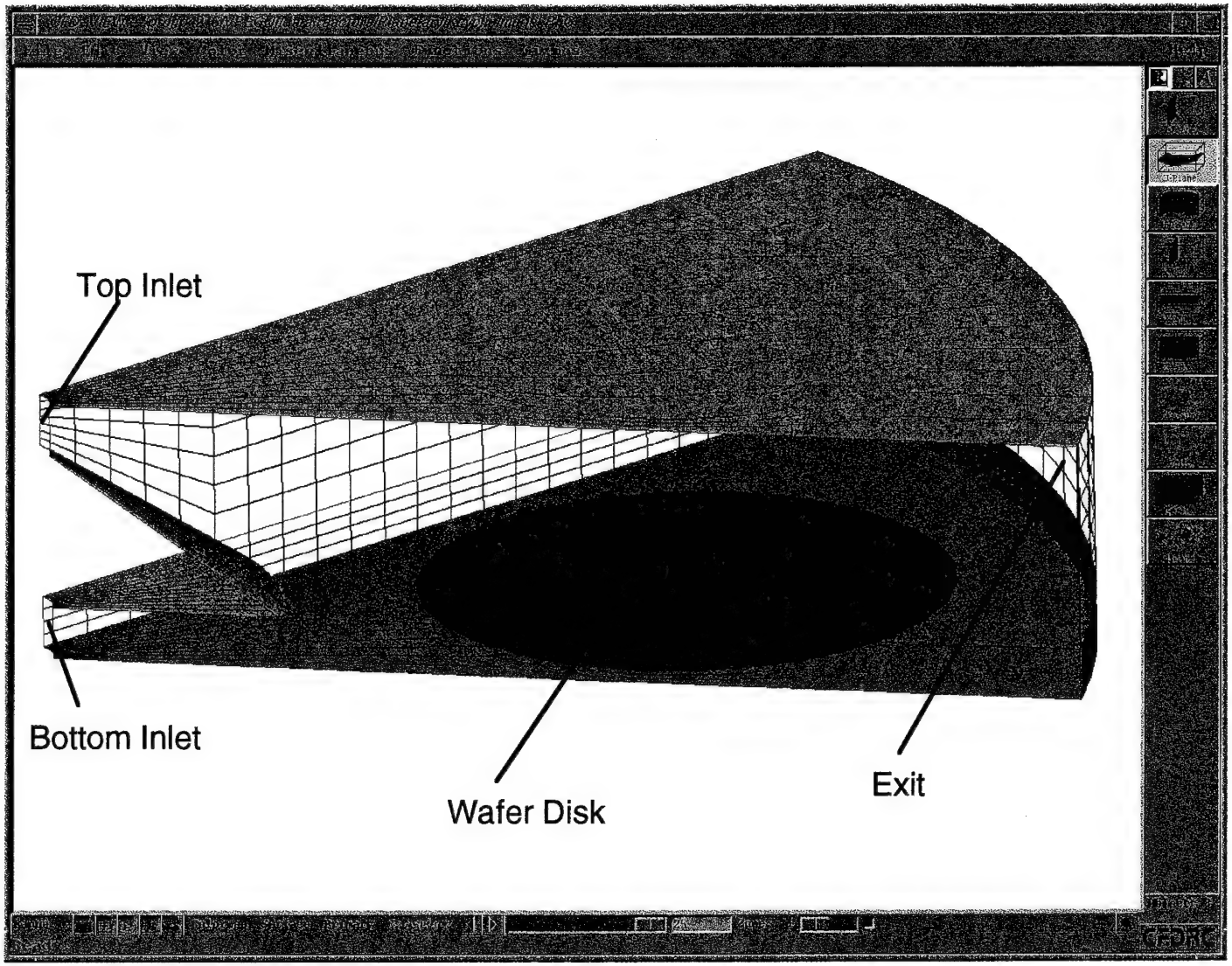

Figure 4-16. Visualization of the Planetary Reactor in CFD-VIEW

The final step in the model setup is to specify the particular boundary condition for a given simulation. Figure 4-17 shows the "boundary condition" window in CFD-ACE with the rotating wafer boundary selected. The column at the right displays the current conditions for that boundary. In the example displayed, the wafer is designated as a rotating wall, rotating about $\langle x_c, y_c, z_c \rangle = \langle 0, 0.066, 0 \rangle$ at an ω (radians/sec) of $\langle x_r, y_r, z_r \rangle = \langle 20, 0, 0 \rangle$, or 191 rpm. The selection of Reaction: "First" at the bottom of the column activates reaction on the disk. The selection of Heat Flux along with the value of Q = 3000 designates the wall as a constant heat flux boundary with 3000 (watts/m^2) of energy. These conditions were used for the baseline (Planet1) simulation. A subsequent parametric study used the same inputs except with the wafer rotation speed doubled. The results of these simulations are compared below.

Computational Results: Two parametric simulations for the boundary reactor were performed, one with the wafers rotating at 190 rpm and the other at 380 rpm. All other boundary conditions were identical, as discussed above. The model solved the velocities, species transport, temperatures and deposition rates for the reactor. Figure 4-18 shows a side-by-side comparison of the predictions. The top of the reactor is partially cut away to reveal the reactor interior. Temperatures are indicated by the color contours, the deposition by the gray scale. Velocity vectors are displayed on the disk. It is observed that the deposition rate is significantly enhanced by increasing the rotational speed. This is to be expected since the process is limited by diffusion transport and increasing the rotation rate results in enhanced diffusion to the wafer.

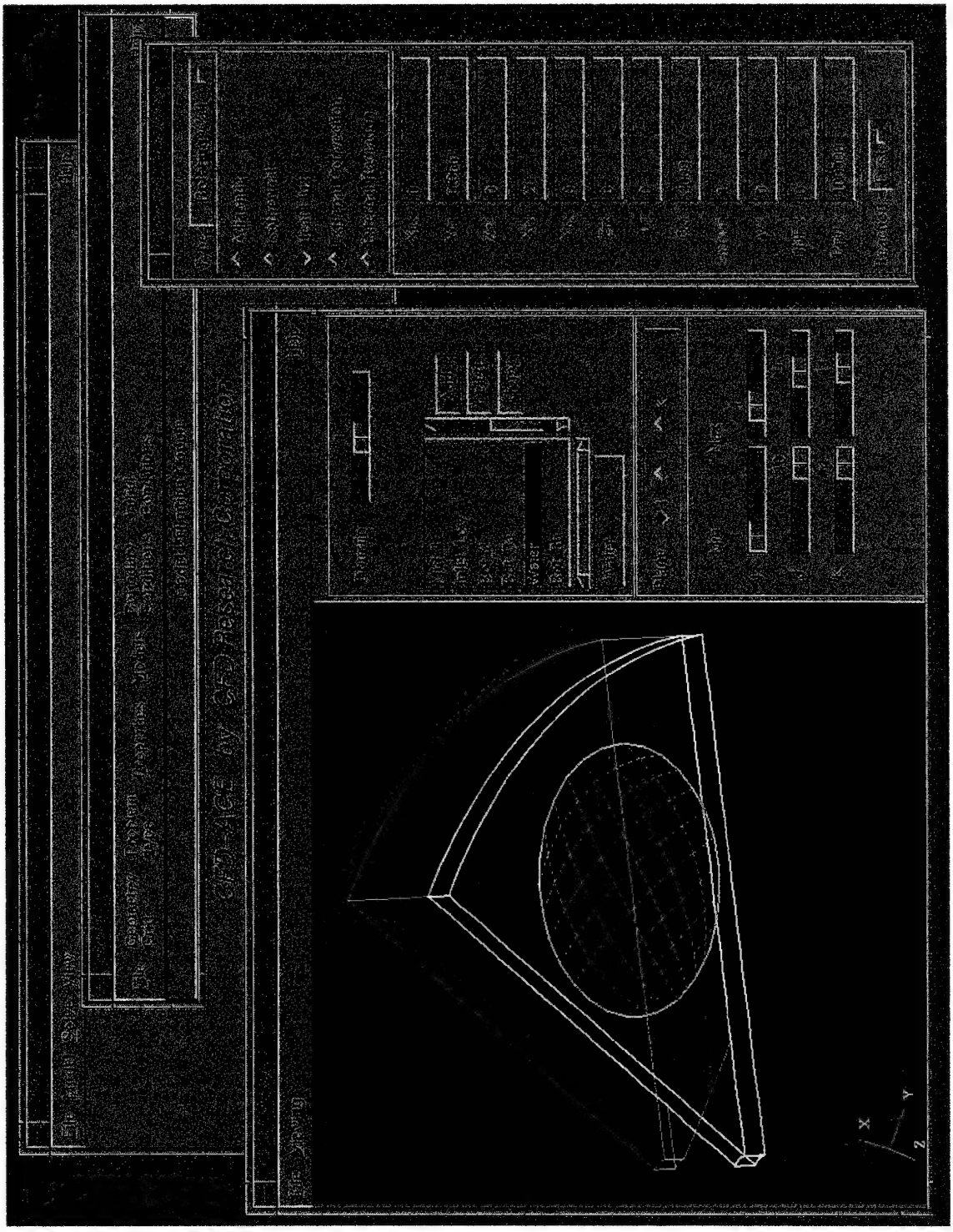

Figure 4-17. Boundary Condition Specification in the CFD-ACE GUI

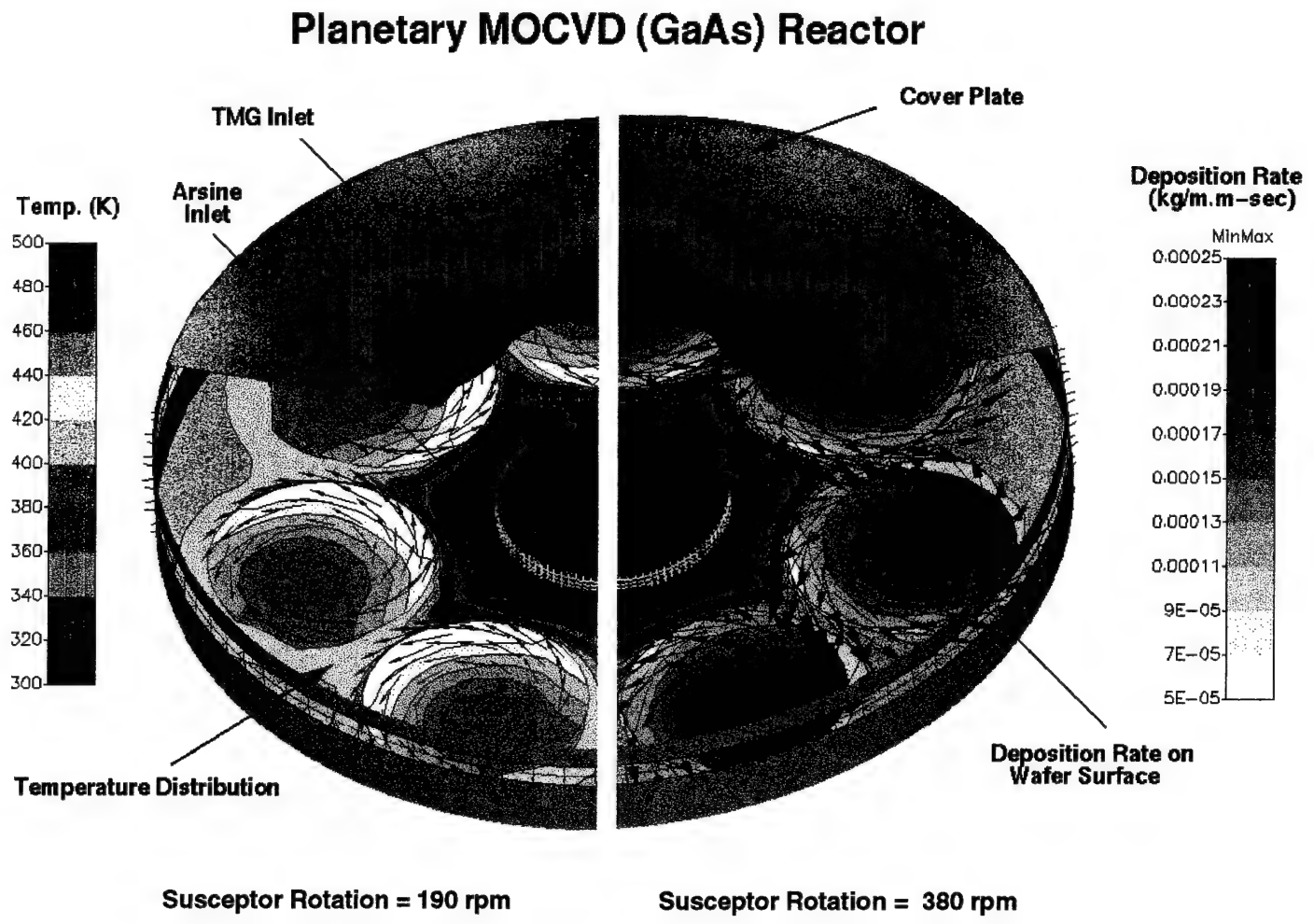

Figure 4-18. Results from the Planetary Reactor Simulations

4.4 Wedge Reactor

Figure 4-19 illustrates the basic design of the wedge reactor. This system is currently in use at the Micro-Electro-Mechanical Systems (MEMS) laboratory in Case Western Reserve University (CWRU) for the fabrication of MEMS components. The reactant flow enters the reactor at the top and flows around the wedge shaped susceptor to the outlet located at the bottom. The susceptor is heated by induction coils located outside the reactor.

One of the concerns in the design of this reactor is the flow uniformity around the susceptor. Since the flow occurs in a narrow passage between the susceptor and the outer walls of the reactor, it is expected that the flow will be fully developed and the boundary layer profiles will be uniform.

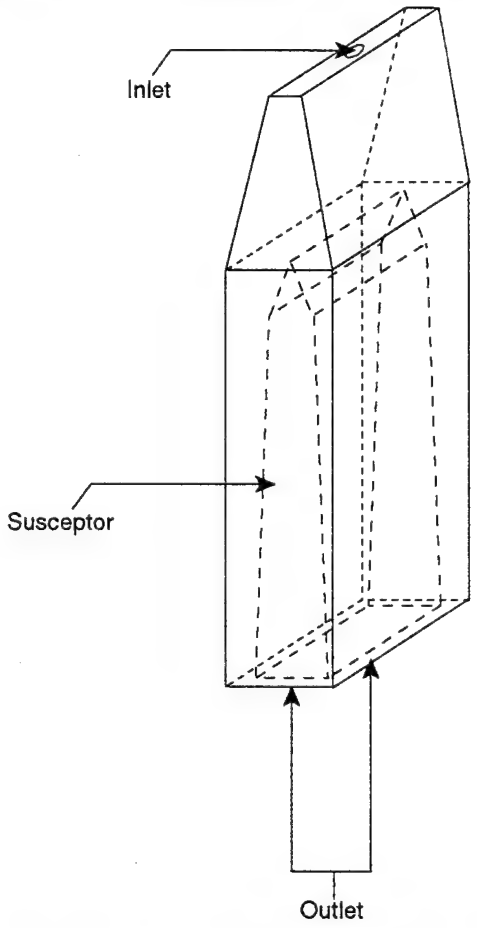

Figure 4-19. Schematic of the Wedge Reactor

Operating Conditions The reactant mixture at the inlet consists of 18% silane, 74% hydrogen and 8% argon by mass. The inlet temperature is 300°K. The susceptor is maintained at a constant temperature of 1623°K. The top and bottom walls of the reactor are set to a fixed temperature of 773°K. The side walls are assumed adiabatic. The inlet velocity is 2.56 meters/sec. The other walls are treated as adiabatic. The surface chemistry is as follows[10]:

$$SiH_4\,(g) \xrightarrow{\gamma_1} Si(s) + 2H_2$$

$$\gamma_1 = 0.0537 \exp(-9400/T)$$

Parametric Study: The reactor pressure is treated as a parameter in this study. Two cases were simulated with reactor pressures of 1 atm and 0.1 atm respectively. The effect of reactor pressure on the deposition process was quantified.

Computational Geometry and Grid: The wedge reactor has two planes of symmetry, one at the "x" = zero plane and the other at "y" = zero. Accordingly, one quarter of the geometry is modelled and the results reflected to recreate the entire domain. The geometry was created in CFD-GEOM, as displayed in Figure 4-20. Three domains are used around the wedge shaped susceptor. Unlike the Bell Jar model, the wedge susceptor is not included in the problem domain, but is instead modelled as an exterior boundary of prescribed temperature. The grid at the k=1 index is shown for each of the three domains. A total of 22,125 grid cells is used.

Figure 4-21 gives a cut-away three dimensional view of the complete geometry. The gray walls and the bottom grid represent solid surfaces. The top wall and near side wall have been partially removed to reveal the wedge substrate. The inlet is a square hole at the front of the reactor, and the exit spans the entire back wall.

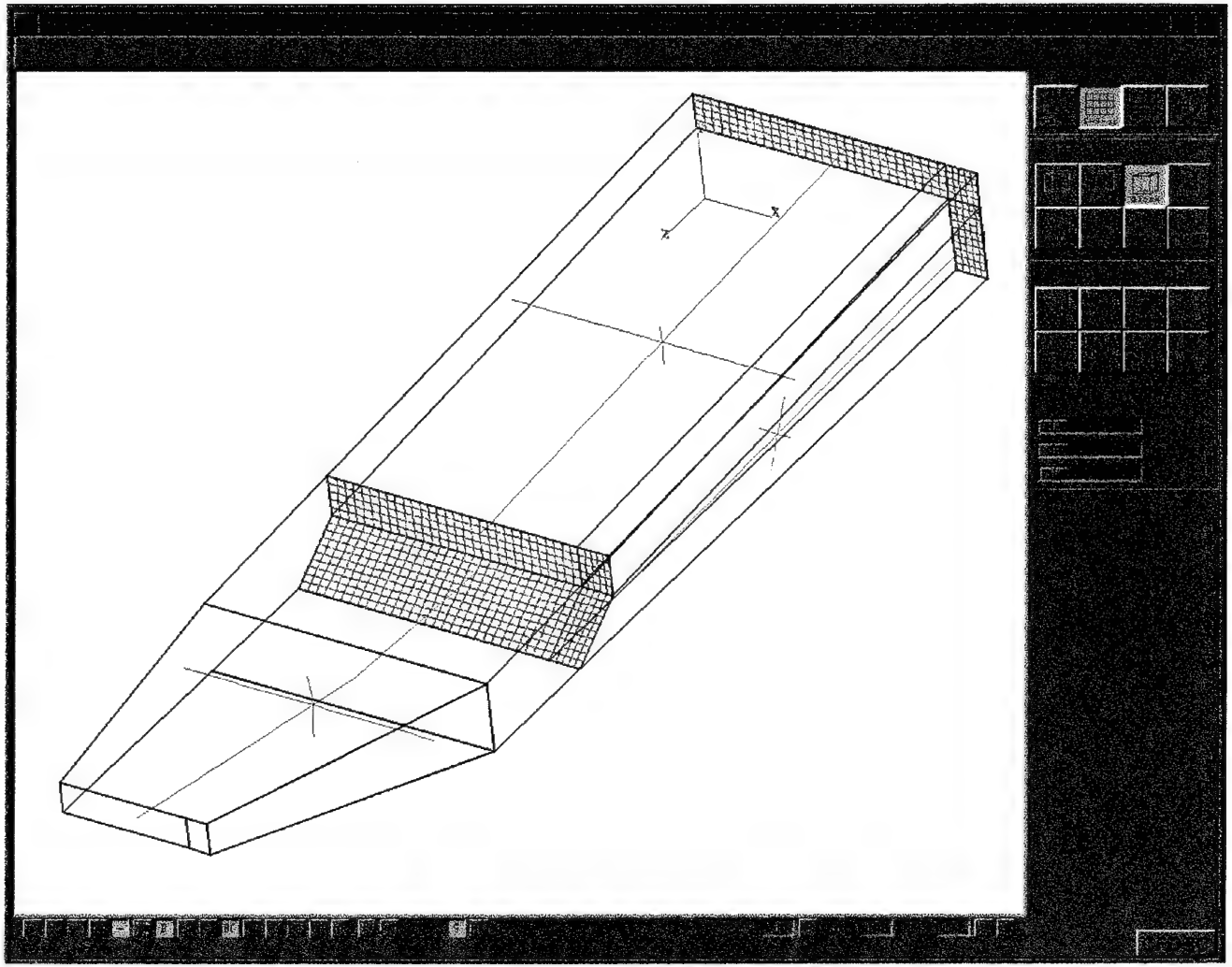

Figure 4-20. Geometry of the Wedge Reactor Visualized in CFD-GEOM

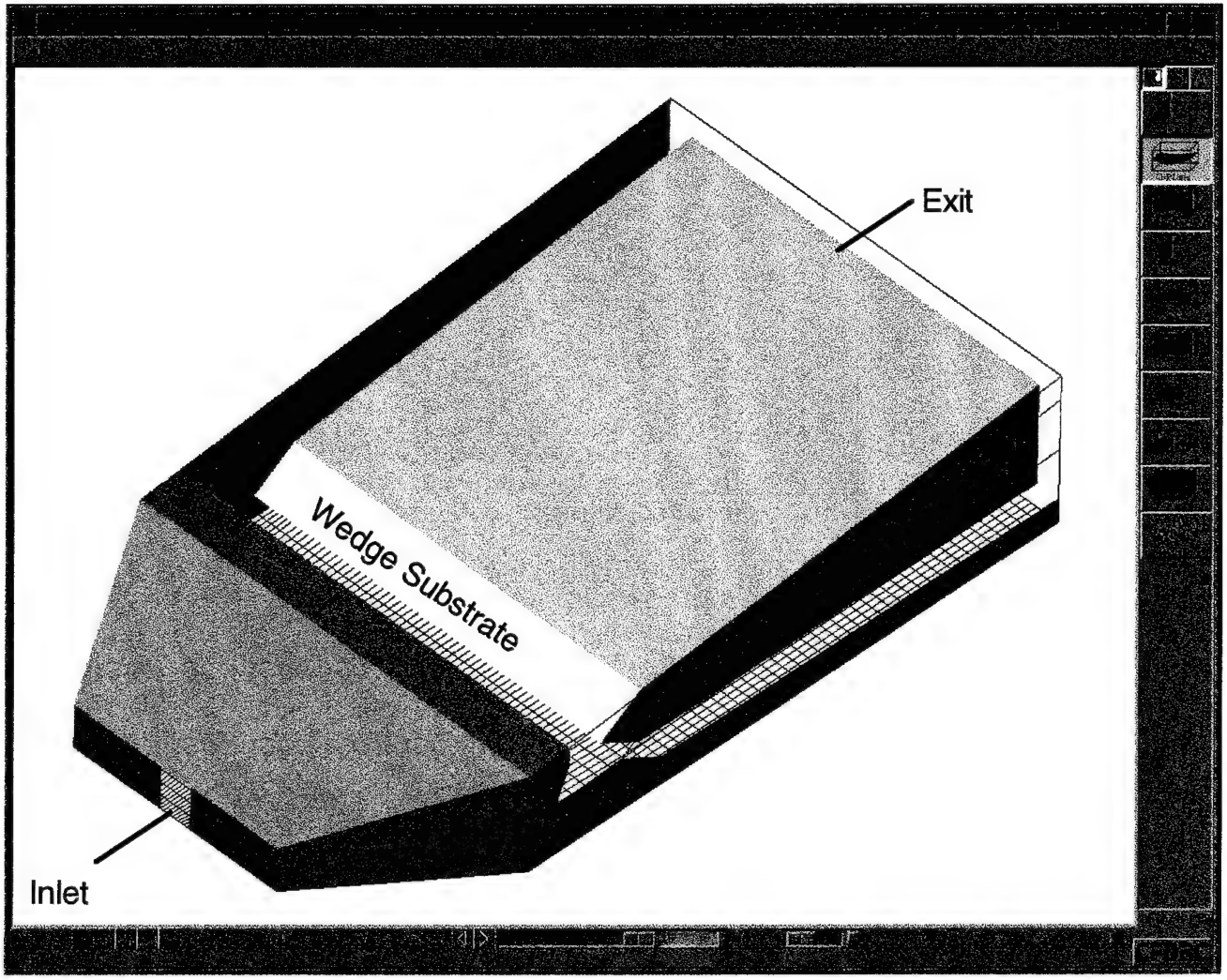

Figure 4-21. Reactor and Substrate Geometry Visualized in CFD-VIEW

Model Setup: The grid created in CFD-GEOM is in meters and can be incorporated directly into CFD-ACE without any scaling. In the CFD-ACE GUI, the problem type is specified as an incompressible flow problem, with mixing and heat transfer. One composition was specified at an inlet mixture of 0.18 SiH_4, 0.74 H_2, and 0.08 Argon. The selection of the multicomponent diffusion option in the properties section instructs the code to solve diffusive transport of all three species in the mixture independently. The density of the mixture is computed based on the perfect gas law, and viscosity and conductivity are computed based on kinetic theory. The specific heat is, again, calculated from JANNAF data.

Computational Results: Simulations were performed for the wedge reactor for pressures of one atmosphere and one tenth atmosphere. These results are compared in Figure 4-22. The gray scale corresponds to the deposition rate with contour lines of constant deposition rates spaced at intervals of 0.4e-5 kg/m^2-sec. The temperature field is indicated by the colored cutting planes and is similar for both. The maximum predicted deposition for the one tenth atmosphere case is 1.4e-5 kg/m^2-sec. At one atmosphere, the depostion rate increases approximately an order of magnitude to a maximum of 12.8e-5 kg/m^2-sec.

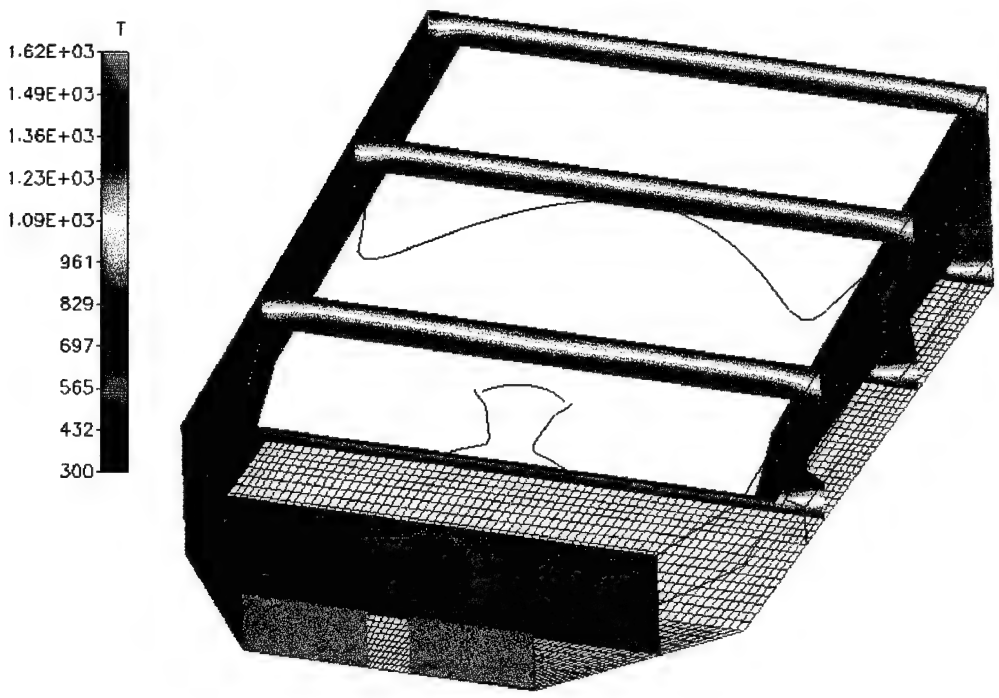

Figure 4-22a. Results for Reactor Pressure of 0.1 atm.

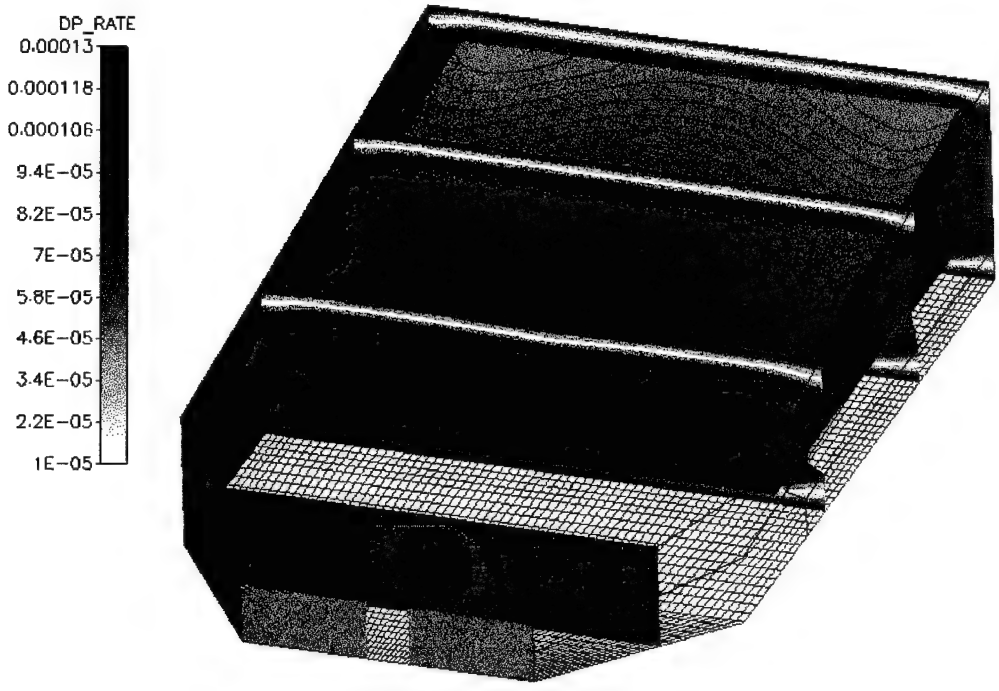

Figure 4-22b. Results for Reactor Pressure of 1 atm.

4.5 Batch Reactor

A schematic of a multi-wafer batch reactor is shown in Figure 4-23. This system is being produced by companies such as Silicon Valley Group (SVG) Thermco and Semitool Inc. The wafers are heated radiatively from a circumferentially located heating element outside the quartz wall of the reactor. The reactant flow is injected radially inward between the wafers from three posts located 120° apart on the circumference. The fluid leaves the reactor axially through the outlet (annulus) located at the bottom.

Radial uniformity of temperature and species distributions are key concerns in the design of this system. Since the edges of the wafers are closer to the heating element, the temperature at the edge is higher than the wafer center temperature. Also, the nature of the reactant injection is such that there is a stagnation point at the center of the reactor. This will affect the uniformity of the flow and species distributions above the wafer.

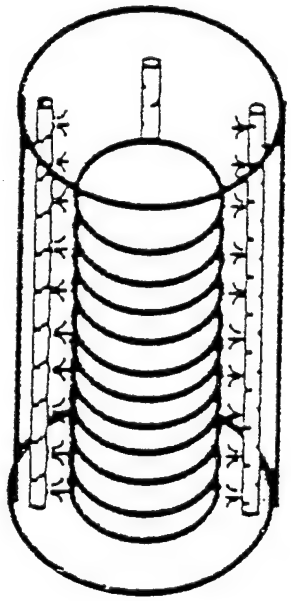

Figure 4-23. Schematic of the Batch Reactor

Operating Conditions: The radiator is maintained at a temperature of 1200°K. The reactor pressure is 10 Torr. A mixture of silane and argon (3.8% silane and 96.2% argon by mass) is injected radially between the wafers from the inlets located on the

posts. The inlet temperature is 300°K. The quartz wall is assumed to be a semi-transparent, absorbing medium. Conjugate heat transfer through the wafer material is considered. The surface reaction is assumed to be the same as that of the Jipelec reactor described in Section 4.2.

Parametric Study: The number of wafers in the reactor was treated as a parameter in this study. Reducing the number of wafers in the batch increases the pitch size. There is evidence to the fact that higher pitch sizes lead to better temperature uniformity in the wafers. Two pitch sizes of 0.3" and 0.6" were modeled. The effect of pitch size on temperature uniformity and the deposition process was quantified.

Computational Geometry and Grid: The batch reactor is axisymmetic with the exception of three injector posts spaced around the circumference at intervals of 120 degrees. The presence of these post necessitates modeling the batch reactor as a cyclic three-dimensional problem with radial symmetry planes bisecting each post. By taking advantage of these cyclic and symmetry boundaries, only one sixth of the domain needs to be modeled. Figure 4-24 shows the partial geometry as created in CFD-GEOM. The geometry includes the bisected post, along with a 60 degree slice of the wafers, the quartz outer wall, and the external radiator.

The blue points and connecting black edges displayed in Figure 4-24 define the geometry of the batch reactor explicitly. Simple modification to the geometry, such as changing the thickness and/or radius of the disks, can be accomplished by moving the points. The grid will readjust accordingly. The grid used in the simulation was a relatively fine grid of 63,308 cells, as shown in Figure 4-25.

CFD-GEOM was also used to define the disk locations as well as the location and type of external boundaries, such as inlets and exits. Figure 4-26 shows the boundary types as specified in CFD-GEOM. The dark blue lines correspond to the symmetry planes. The green highlights the outlets. The light blue lines are wall boundaries such as at the top and bottom of the quartz. Yellow indicates the inlets, including the 10 jets and the external cooling flow. This information is stored in the file model.IBC and is automatically incorporated by the CFD-ACE-GUI for model setup.

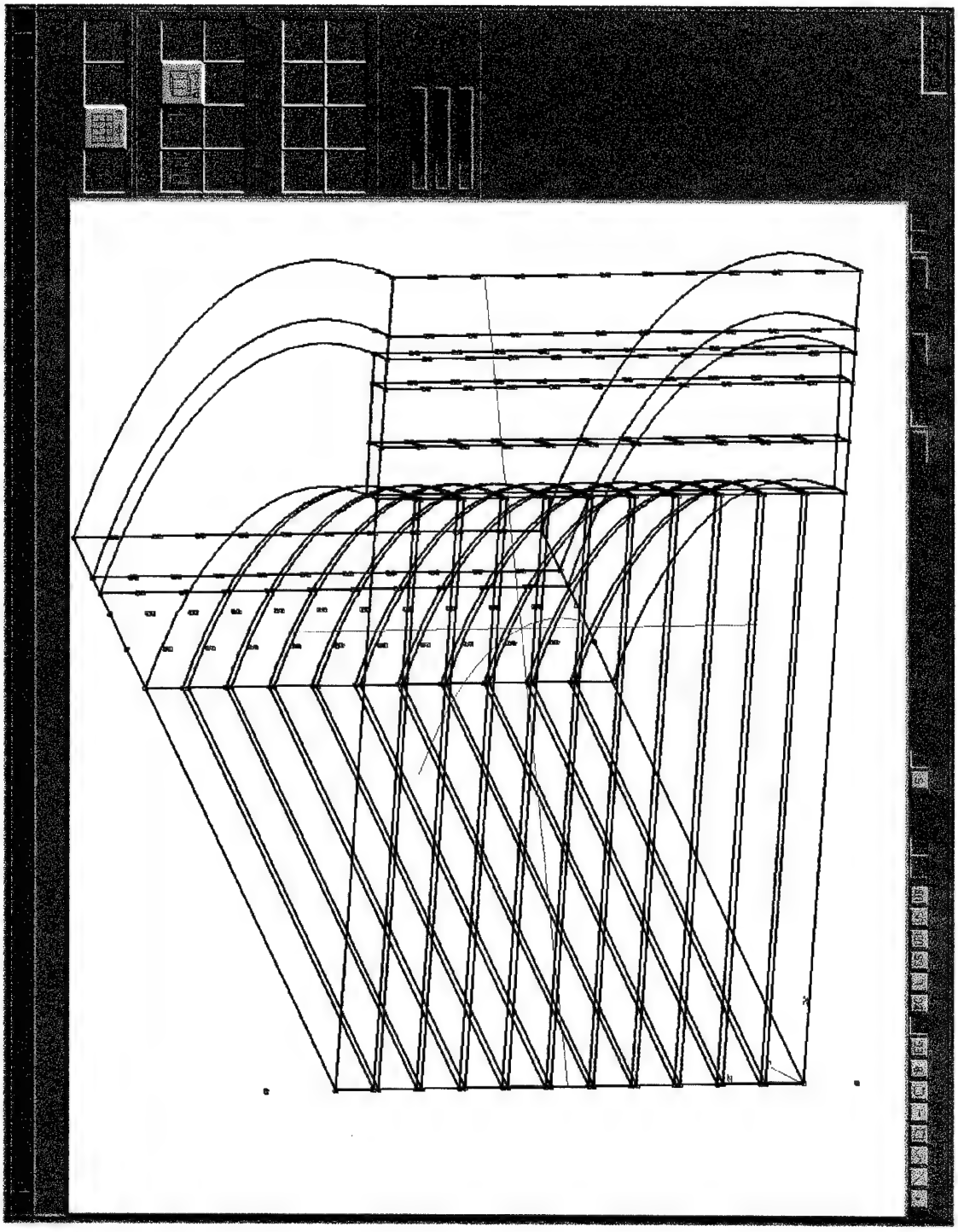

Figure 4-24. Geometry of the Batch Reactor Visualized in CFD-GEOM

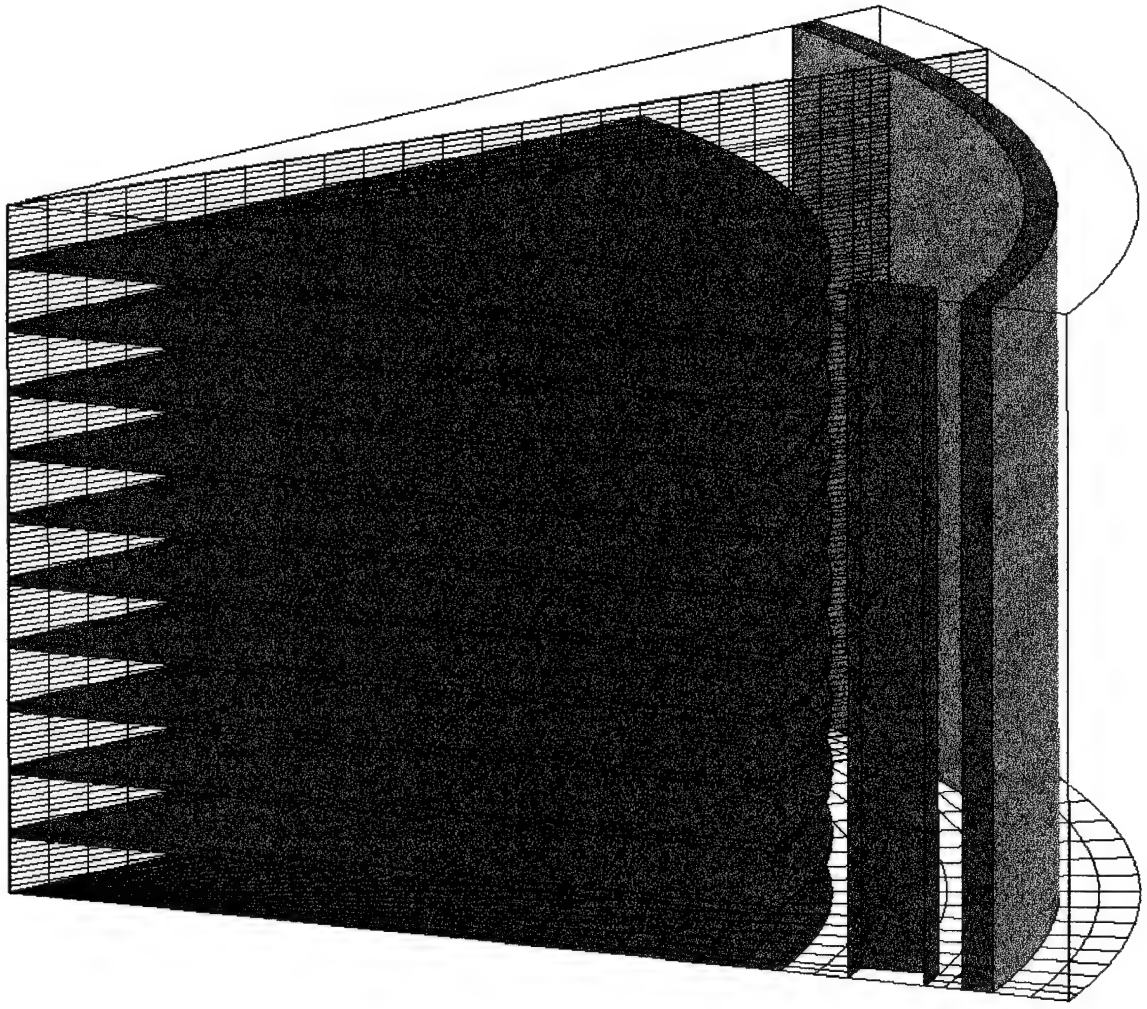

Figure 4-25. Computational Grid for the Batch Reactor

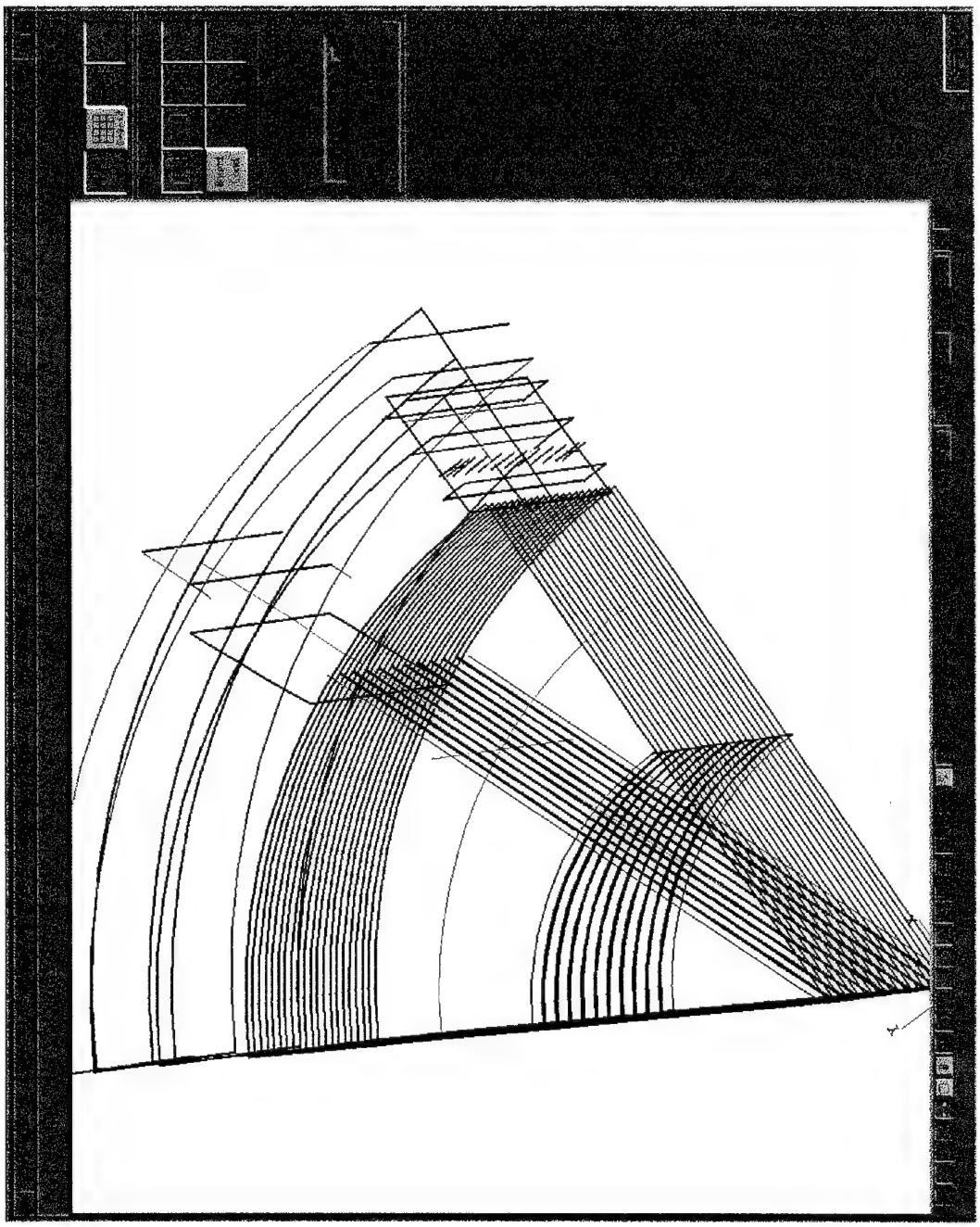

Figure 4-26. Boundary Condition Specification in CFD-GEOM

Model Setup: In the CFD-ACE GUI, the problem type is specified as an incompressible flow problem, with mixing and heat transfer with radiation.

The code solves for the convective transport of a mixture of Silane, Hydrogen, Argon, and Silicon. The selection of the multicomponent diffusion option in the properties section instructs the code to solve diffusive transport of all four species in the mixture independently. The fluid density is computed as a function of the inverse of temperature, and viscosity and conductivity are computed based on kinetic theory. The specific heat is computed based on JANNAF data.

In addition to the fluid material, two solid materials are defined in the model. The first is the disk material which is specified as silicon with constant specific heat, constant density, and temperature dependent conductivity. The second solid is the quartz wall which is modelled as a semi-transparent material with constant density, specific heat and conductivity. Surface reactions are specified on the top surfaces of each disk. Both the internal and surface temperature of the disk are computed as part of the solution. The top and bottom walls of the reactor are assumed adiabatic with emissivities of 1.0. There are ten inlet jets on each post. These inlets spray a mixture of 0.0385 SiH_4 and 0.9615 Argon in between the disks at a velocity of 0.1 meters/sec and a temperature of 300°K. The flow exits at the bottom of the reactor. Outside the quartz wall, there is a cooling flow of gas between the exterior wall and the radiator. The radiator is modelled as cylindrical wall at 1200°K with an emissivity of 0.3.

Computational Results: A ten wafer configuration was run as a baseline case. The results are shown in the 3-D cutaway view in Figure 4-27a. The color flooding indicates temperature and the gray scale indicates deposition rate in kg/m^2-s. As displayed on the fifth disk, the deposition rate is not axisymmetric but instead is strongly influenced by the position of the injectors. Deposition is also a strong function of radial location. For the ten wafer case, the maximum deposition is predicted as 5.6 e-6 kg/m^2-s. When the wafer pitch size is doubled (see Figure 4-27b) the maximum deposition rate increases to 6.1 kg/m^2-s. However, the temperature and deposition rate distributions do not appear to be affected significantly by the change in pitch size.

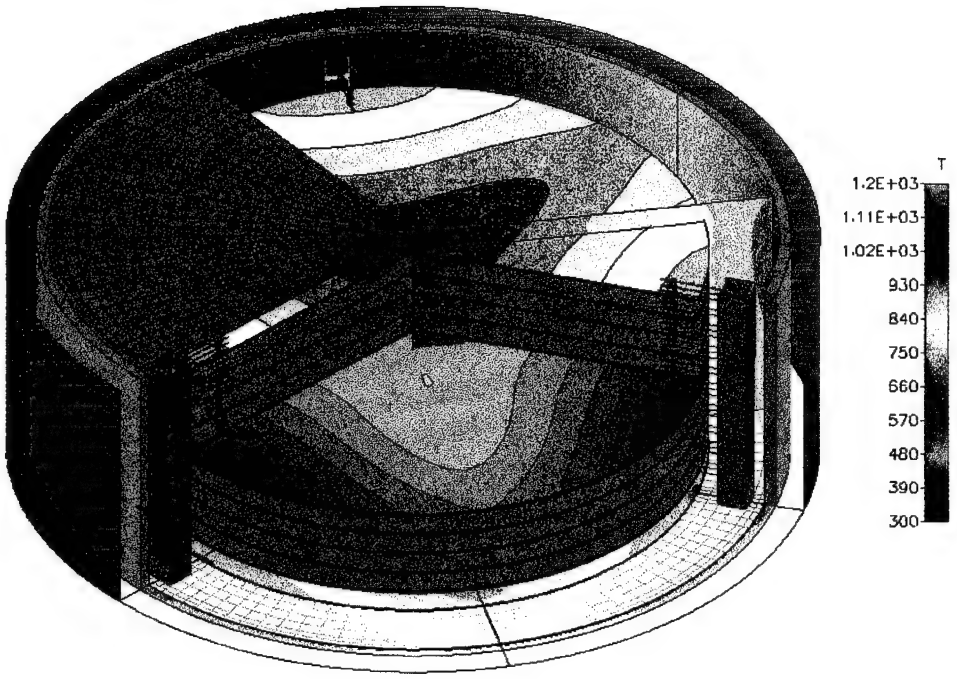

Figure 4-27a. Results for Pitch Size of 0.3"

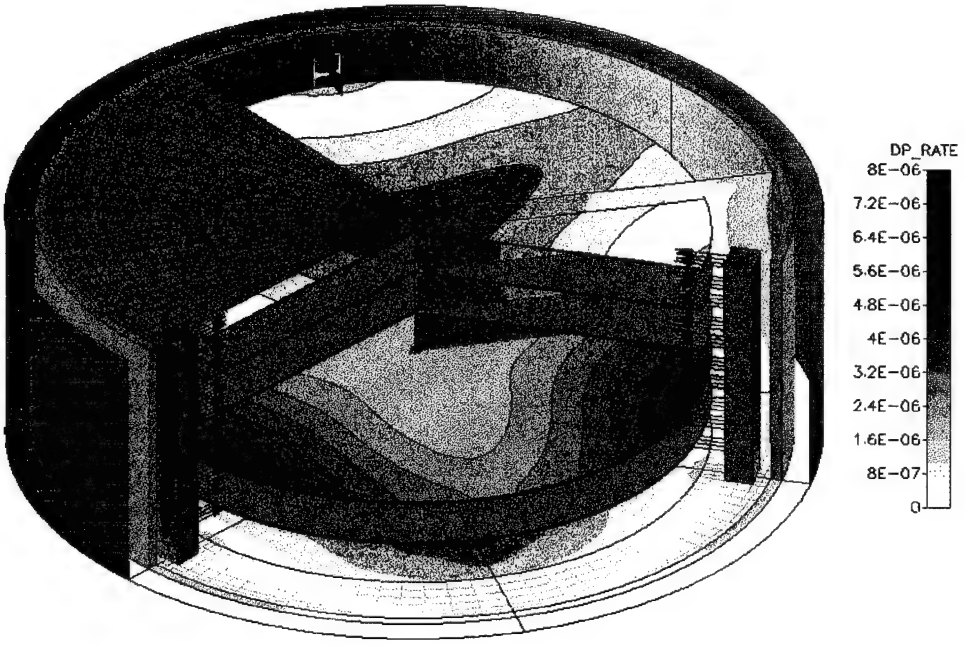

Figure 4-27b. Results for Pitch Size of 0.6"

4.6 Interface with TCAD

Many commercial TCAD models have been developed to simulate steps involved in manufacturing semiconductor devices. The most widely used software (such as SUPREM-3, DEPICT-2, *etc.*) are those marketed by Technology Modeling Associates (TMA), Inc. of Palo Alto, CA. The critical issues addressed by these TCAD models are impurity concentrations, oxidant pressure, oxidation of silicon and polysilicon, effects of ambient gasses, *etc.* Currently the boundary conditions to these CAD models are either approximated or estimated through simple models. However, the conditions that are encountered in actual fabrication equipment are highly three-dimensional and too complex to be understood through simple models. It is therefore necessary to interface sophisticated equipment models to existing TCAD models in order to correlate device performance with equipment design.

An important aspect of interfacing CFD models with TCAD models is the difference in grid types. Most TCAD models use Finite Element (FE) analysis in their simulations, while the VPE uses structured grids. Interfaces need to be developed which interpolate and transfer the information on primary variables from the structured grids to the unstructured grid models for TCAD analysis. The main vehicle for data transfer within the TCAD environment are the SWR (Semiconductor Wafer Representation) and the SPR (Semiconductor Process Representation) object oriented data interface standards. The development of SPR and SWR (by TMA Inc. and Dawn Technologies, respectively) occurred during the same time interval as the current Phase II study. This precluded the development of an interface with SPR and SWR since mature and well tested versions were not available.

However, in order to show proof of concept, a direct interface was created between CFD-ACE and Suprem-3. Suprem-3 is a one-dimensional simulation code from Technology Modeling Associates (TMA). It can take quantities such as temperature or gas pressure as inputs and produce oxide thickness, junction depths, sheet resistance, etc. as output. Since only the Suprem-3 executable is available at CFDRC, the interface between CFD-ACE and Suprem-3 is realized through file exchange. A special interface program has been created which reads all necessary process information such as temperature, pressure, or species concentration from a PLOT3D

file generated by CFD-ACE. The interface program then creates Suprem-3 input files for each grid location on a substrate and executes the Suprem-3 code. After all points are processed by Suprem-3, the interface program generates a PLOT3D file from the Suprem-3 output files. This file can be visualized by the CFD-VIEW visualization package. Sample results are shown in Figure 4-28.

4.7 Demonstration of Particle Transport Model

Figure 4-29 shows the results from the application of the particle transport model to a High-Velocity Oxygen Flame (HVOF) Thermal Spray Torch. Copper particles are injected at the center of a nozzle along with premixed propylene and oxygen and accelerated through a throat to supersonic speeds before impingement on the substrate. The heat release from the fuel-oxygen reaction causes the particles to melt. The results for particle temperatures and velocity agreed reasonably well with data obtained at General Motors for the HVOF system.

4.8 Demonstration of Plasma Chemistry Model

Figure 4-30 shows the results obtained from the plasma chemistry model for a multi-wafer CVD system[11]. The susceptors are also the electrodes in this reactor that are used to generate and sustain the plasma. The plasma enhanced dissociation results in the generation of active radicals in the region between the electrodes.

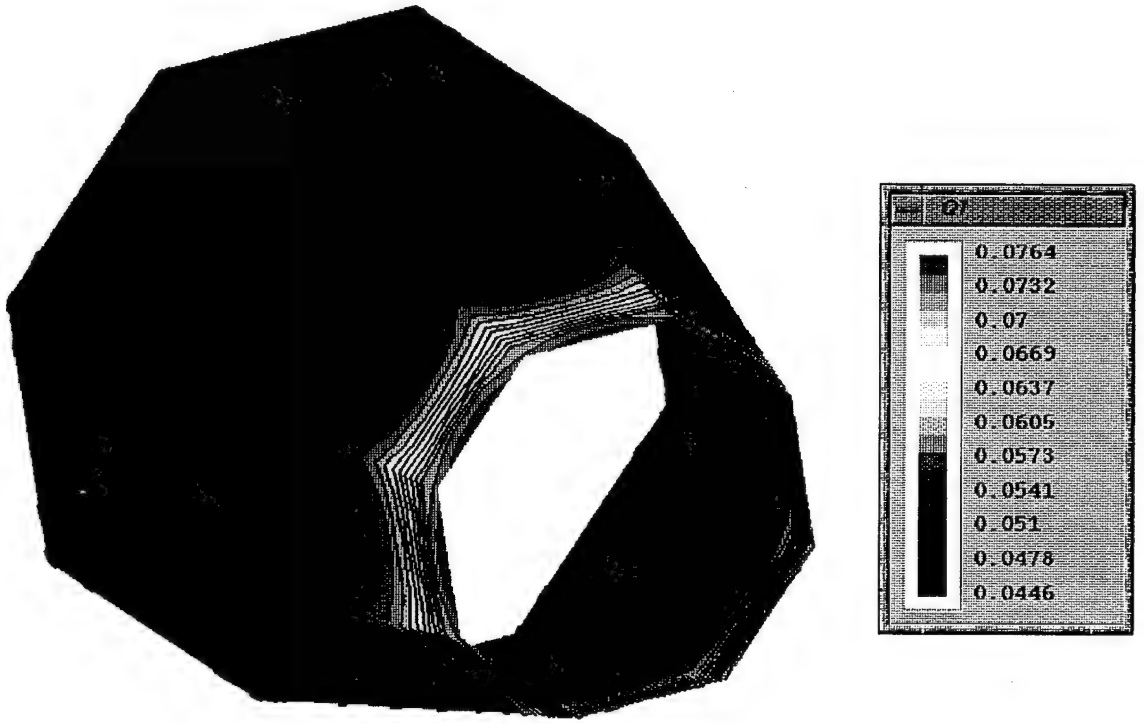

Figure 4-28. Predictions of Oxide Thickness Using TMA-SUPREM (with data from CFD-ACE)

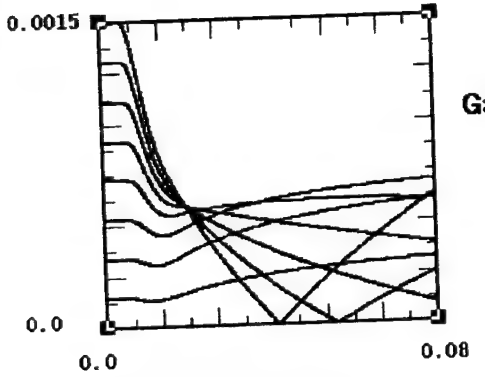

Particle Trajectories
(Not to Scale)

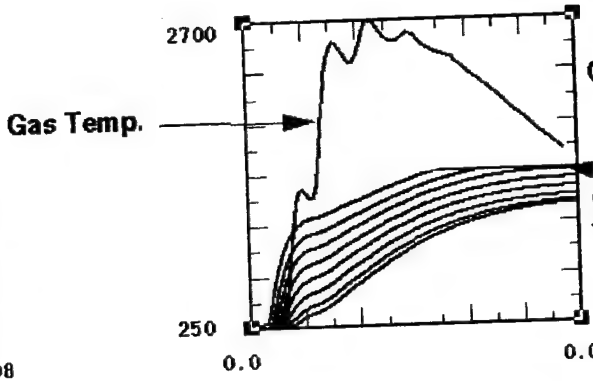

Particle and Gas Temperatures (deg K)

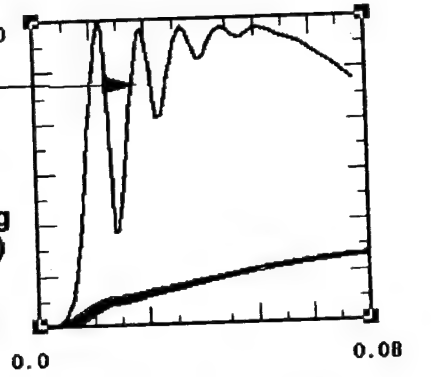

Particle and Gas Velocities (m/s)

83

Copper Particles are injected on the centerline in 8 streams

Premixed Fuel and Oxygen is fed through an annulus

Coolinng Air is injected along the wall of torch

Gas Temperatures in deg K

Analysis Of a High Velocity Oxygen–Fuel (HVOF) Thermal Spray Torch

Figure 4-29. Analysis of a High Velocity Oxygen-Fuel (HVOF) Thermal Spray Torch

4216/4

Computational Results for the Multi-Wafer CVD Reactor

(Susceptor Temperature = 900 K, Mean Plasma Rate Constant = 6.0/sec)

CONTOUR LEVELS
0.06500
0.06752
0.07003
0.07255
0.07506
0.07758
0.08009
0.08261
0.08512
0.08764
0.09015
0.09270
0.10021
0.10273
0.10524
0.10776
0.11027
0.11279
0.11530

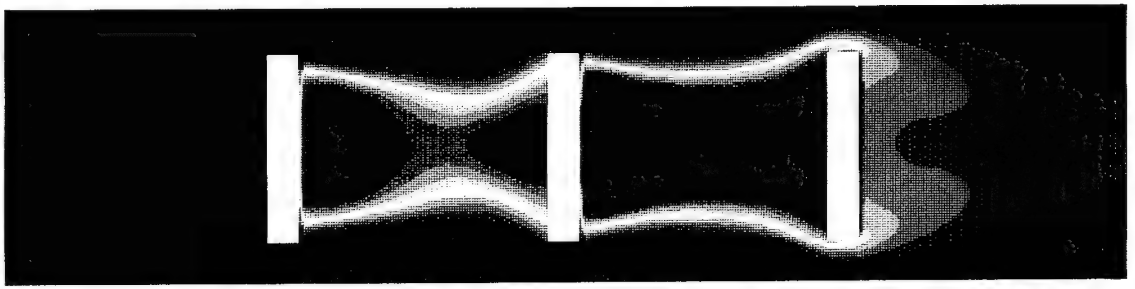

Silane Mass Fraction Distribution

CONTOUR LEVELS
0.00000
0.00152
0.00304
0.00456
0.00608
0.00760
0.00912
0.01064
0.01216
0.01368
0.01520
0.01976
0.02128
0.02280
0.02432
0.02584
0.02736
0.02888
0.03040

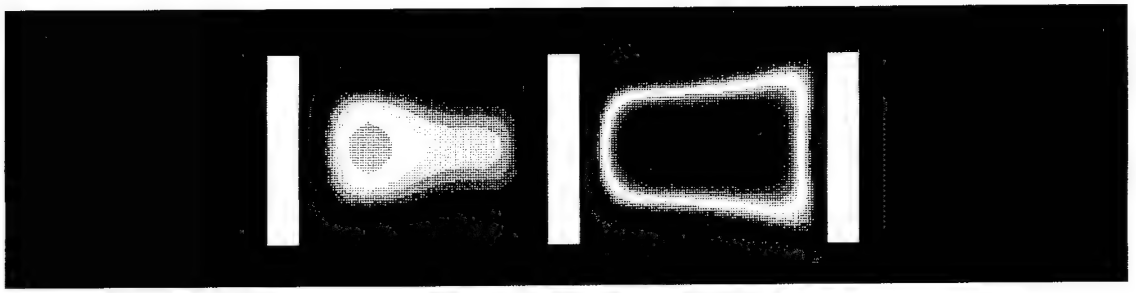

Silene Mass Fraction Distribution

Figure 4-30. Plasma Enhanced Chemistry in a Multi-Wafer CVD Reactor

5. COMMERCIAL APPLICATIONS

The code, CFD-ACE, is currently in use at several leading engineering organizations. Since the incorporation of advanced models for materials processing phenomena (under the current Phase II program), the code has been used for design studies of equipment at the following organizations:

a. **FSI International:** CFD-ACE was used to model FSI's Excalibur wafer cleaning reactor. The simulations were used to optimize process time which resulted in an increased yield for FSI of $ 150,000 per reactor per year.

b. **Silicon Valley Group (SVG) Thermco:** Radiative heating in SVG's vertical reactors was modeled using CFD-ACE. These studies were used to identify design modifications that will best improve temperature uniformity in the wafers during processing. SVG is currently testing many of these design changes. SVG is also licensing CFD-ACE for design studies of equipment.

c. **LAM Research Corporation:** CFD-ACE was used to model the flow and pressure distribution in LAM's etching reactors at pressures as low as 5.0 millitorr. The low pressure transport models developed under the Phase II program were used for these simulations. The predictions of the model compared well with measurements obtained by LAM. CFD-ACE has been officially licensed by LAM Research Corporation and is currently being used for design studies of LAM's equipment.

d. **Motorola:** Motorola is licensing CFD-ACE to perform analysis of oxynitridation processing equipment. The chemistry of the process is highly complex involving 40 reaction steps and 16 species. The Jacobian linearization method developed under the current Phase II program was used to successfully resolve the stiffness of the system.

e. **SemiTool:** SemiTool is licensing the code to perform analysis of radiatively heated batch reactors. The results will be used to optimize

temperature uniformity during processing. SemiTool is also planning to use the results in developing a model based on-line control system for the equipment.

f. **Lawrence Livermore National Laboratories (LLNL):** LLNL is licensing CFD-ACE to couple it with in-house transport models for low pressure non-equilibrium plasmas. CFD-ACE will be used to predict neutral flow patterns, temperature and local composition and the plasma model will predict local concentrations of ions and electrons, the electric field and the local dissociation of species.

g. **Applied Materials:** The flow patterns resulting from the showerhead in Applied's plasma reactor was modeled using CFD-ACE. Applied Materials is currently evaluating the possibility of using CFD-ACE for further detailed simulations of the processing system.

h. **SEMATECH:** CFD-ACE has been delivered to SEMATECH for potential application on Rapid Thermal Processing (RTP) systems. The analysis of RTP systems requires the use of radiation models. CFD-ACE is unique in its capability to model radiation coupled with fluid flow, heat/mass transfer and chemistry for the analysis of complex 3-dimensional systems. The advanced capabilities of CFD-ACE makes it well suited for applications involving RTP systems. SEMATECH is also planning to use CFD-ACE for analysis of problems involving multi-step, finite rate chemistry.

i. **Sandia National Laboratories:** Sandia is currently licensing CFD-ACE for the analysis of a number of problems encountered in CRADA projects. In one particular instance, the code was used to model flow, heat transfer, chemistry and particle transport in a High Velocity Oxygen Flame (HVOF) spray torch. The trajectory of copper particles were calculated and the mass fraction of molten metal was estimated from the calculations. These values compared well with experimental measurements.

Finally, CFDRC has also used the models developed under the current Phase II study to analyze problems for the following organizations:

a. **Case Western Reserve University:** The SiC reactor at Case Western (for the manufacture of MEMS components) was analyzed using CFD-ACE in order to assess the flow and temperature uniformity in the vicinity of the substrate.

b. **Materials and Technologies Corporation:** A novel prototype SiC reactor (under development by MTC for ARPA) was analyzed using CFD-ACE. The model was used to predict the flow field, temperature and concentration distributions in the reactor.

c. **Research Triangle Institute:** CFD-ACE was used to simulate RTI's prototype diamond deposition system. Predicted distributions of diamond film growth compared remarkably well with experimental measurements.

d. **NASA Marshall Space Flight Center:** CFD-ACE is currently being used by NASA-MSFC to analyze problems involving Physical Vapor Transport (PVT) growth of crystals in low gravity environments.

Much of the development during the Phase II study was done in close collaboration with SEMATECH and its member companies. Every effort was made to address the modeling needs identified by SEMATECH and the SIA roadmap.

All journal and conference publications arising from the Phase II study are listed in Appendix B. CFD-ACE and other software developed in this study have been advertised in engineering journals and magazines (such as Solid State Technology and Mechanical Engineering) and through annual brochures released by CFDRC (see Appendix C). In addition, the software has been exhibited at the MRS Meeting (April 1994), I-THERM Meeting (May 1994), a SEMATECH Workshop (June 1994) and through demonstrations to selected equipment companies.

6. PLANS FOR FUTURE WORK

This project was successful in developing and demonstrating an integrated virtual prototyping environment for semiconductor fabrication processes and equipment. The VPE will facilitate the user to develop a design concept into a virtual prototype of the system or process. The early commercial success of this tool demonstrates that there is a significant need for such modeling capabilities in the microelectronic community. The code has also been benchmarked successfully at SEMATECH for RTP applications. A benchmark report on the code is schedule to be released in October 1995.

6.1 Phase III Plans

CFDRC will use its existing client base in the microelectronic community to further expand the applications of the VPE. Specifically, CFDRC will work with the industry to:

a. demonstrate the value of the VPE in reducing design cycle times and costs;
b. develop reduced models for model-based on-line control systems; and
c. apply the VPE to study extendibility of existing equipment to 300 mm wafer processing.

CFDRC will continue to advertise the VPE aggressively. Sample advertisements are shown in Appendix C. The VPE will be exhibited at SEMICON Southwest (October 1995), GOMAC (March 1996), and SEMICON West (July 1996). In addition, CFDRC will arrange private demonstrations to targeted equipment companies.

6.2 Future Development

The current phase II program has laid the foundation for the following projects that CFDRC is currently working on:

a. **Development of Models for Low Pressure, Non-Equilibrium Plasmas:** CFDRC is currently performing this work under an ARPA SBIR

program. The transport of electrons, ions and electron energy in the presence of electric and magnetic fields is being solved to obtain local dissociation constants in non-equilibrium plasmas. The plasma model will be incorporated into the VPE to facilitate the coupled solution of fluid flow and plasma effects.

b. **Development of Models for Particulate/Contaminant Formation and Transport in Reactors:** This work is being performed under an ARPA STTR contract in collaboration with the University of Minnesota and University of Illinois, Urbana-Champaign. The issue of particle formation and transport is an important one for the microelectronic industry since it results in reduced yields amounting to millions of dollars in losses each year. Models are currently being formulated to compute local growth rates, particle sizes, and particle trajectories in processing systems. These models will be linked to the VPE to facilitate the coupled analysis of fluid flow, plasma transport and particle generation in processing reactors.

c. **Development of Microscopic Models for Film Growth:** This work is being done under an ongoing SBIR contract with NASA-LeRC. Although macroscopic transport models have been used to analyze deposition rates and uniformity in vapor phase systems, these models have been unable to predict film morphology and composition at the microscopic level. Under this contract, Monte Carlo models have been developed to model microscopic surface phenomena such as adsorption, diffusion, coalescence, reaction and desorption of growth units on growing films. The microscopic models will be linked to the VPE to quantify the influence of macroscopic operating conditions on microscopic features of film growth.

CFDRC will integrate all of the above models into the framework of the VPE. Furthermore, CFDRC is anticipating future development in the following areas:

a. **Non-Gray Radiation Model:** Inclusion of wavelength dependent optical properties is crucial in order to resolve radiative heat transfer in

practical systems. This will require the development of a banded radiation model with discrete wavelength bands for energy transfer. Additional features that will be incorporated into the model are specular reflection, luminous radiation, etc.

b. **Feature Scale Models:** Microelectronic fabrication processes attempt to maximize morphological and compositional uniformity on the feature scale. Therefore it is important to couple microscopic models for surface phenomena (such as impingement, adsorption, diffusion, coalescence, reaction and desorption) with macroscopic reactor models. Future development in this area will involve plasma-surface interactions, ion impingement, etc.

c. **Visual Computing Environment (VCE):** CFDRC is currently planning the development of a VCE to facilitate Parallel Computational Materials Processing (PCMP). This will involve parallel computations in conjunction with:

(i) Domain Decomposition: The computational domain will be decomposed into several subdomains for concurrent execution;

(ii) Scale Decomposition: The model will be split according to the scale of the processes; i.e., macroscale consisting of reactor model and microscale consisting of film growth and morphology, plasma-substrate interaction, etc. The models will be run simultaneously with appropriate exchange of information through the VCE.

(iii) Model Decomposition: The global model will be decomposed into several submodels that will run concurrently with periodic information exchange between all models. Examples are transport model, radiation model, chemistry model, plasma model, etc.

CFDRC will collaborate with industry, academia, and national laboratories in the development of the VCE.

During the course of this Phase II study, CFDRC was able to successfully demonstrate the utility of modeling tools to the microelectronic industry. Although models for microelectronic fabrication processes have been in use, this study focused on the use of advanced models as design tools. To this end, the study has resulted in a virtual prototyping environment consisting of geometry modeling tools, grid generators, process models, visualization tools, database management software, virtual parts libraries, properties databases, etc. The integration of these components under a single environment has made the design and analysis process considerably easier.

7. REFERENCES

1. Bird, R.B., Stewart, W.E. and Ligthtfoot, E.N., Transport Phenomena, New York: Wiley and Sons, 1960
2. Reid, R.C., Prausnitsz, J.M. and Poling, B.E., The Properties of Gases & Liquids, 4th ed., New York: McGraw-Hill, 1987.
3. Hirschfelder, J.O., Curtiss, C.F. and Bird, R.B., Molecular Theory of Gases and Liquids, New York: Wiley and Sons, 1954.
4. Giridharan, M., Lowry, S., and Krishnan, A., "A Multi-Block, BFC Radiation Model for Complex Geometries," Presented at the 26th AIAA Fluid Dynamics Conference, San Diego, CA, June 19-22, 1995.
5. Zhou, N., Krishnan, A., and Przekwas, A.J., "A Numerical Method for Reacting Flows with Multi-Step Stiff Chemical Kinetics," Presented at the 31st AIAA/ASME/SAE/ASEE Joint Propulsion Conference, San Diego, CA, July 10-12, 1995.
6. Bell, A.T., Techniques and Applications of Plasma Chemistry, ed. J.R. Hollohan and A.T. Bell, pp. 1-55, NewYork: Wiley and Sons, 1974.
7. Sherman, A., Chemical Vapor Deposition for Microelectronics, Noyes Publications, 1984.
8. SEMATECH Technology Transfer Report, "Benchmarking Computational Fluid Dynamics (CFD) for Rapid Thermal Processing (RTP) Applications: Volume II - Definition of Models," 94012174A-XFR, 1994.
9. Frijlink, P.M., *J. Crystal Growth*, vol. 93, pp. 207-215, 1988.
10. Moffat, H.K. and Jensen, K.F., *J. Electrochem. Soc.*, vol. 135, no. 10, pp. 459-470, 1988.
11. Krishnan, A., and Przekwas, A.J., "Mathematical Modeling of PECVD Reactors," presented at Annual AIChE Meeting, Los Angeles, CA, Nov. 1991.

APPENDIX A

SEMATECH BENCHMARK CASES

APPENDIX A

SEMATECH BENCHMARK CASES

A. RESULTS FOR SEMATECH BENCHMARK CASES

This section describes the results obtained from the application of the VPE to the benchmark cases specified by SEMATECH. A more detailed description of these cases is available in Reference 8.

A.1 Model 1

Problem Type: Two-dimensional, axisymmetric, steady state analysis of fluid flow and convective heat transfer.

Geometry: The geometry for this case is shown in Figure 4-9a.

Computational Grid: A (30x50) non-orthogonal, body fitted coordinates (BFC) grid was used (see Figure A-1).

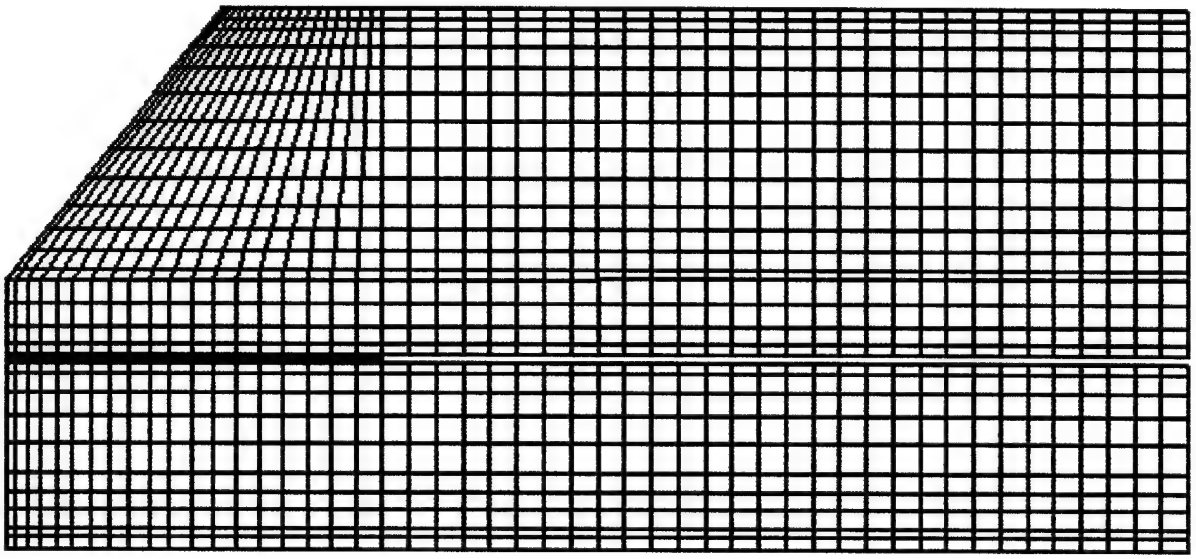

Figure A-1. Computational Grid for Models 1 through 7

Physical Models: A multi-component transport model was used with polynomial fits in temperature for the viscosity, thermal conductivity and specific heat for silane and argon. The coefficients are given below:

Viscosity (kg/m-s)

Silane: $A_0 = -4.79 \times 10^{-7}$, $A_1 = 4.65 \times 10^{-8}$, $A_2 = -2.08 \times 10^{-11}$, $A_3 = 5.52 \times 10^{-15}$

Argon: $A_0 = 5.285 \times 10^{-6}$, $A_1 = 6.34 \times 10^{-8}$, $A_2 = -1.48 \times 10^{-11}$

Thermal Conductivity (W/m-K)

Silane: $B_0 = -5.32 \times 10^{-3}$, $B_1 = 7.02 \times 10^{-5}$, $B_2 = 5.15 \times 10^{-8}$, $B_3 = -2.47 \times 10^{-11}$

Argon: $B_0 = 3.24 \times 10^{-3}$, $B_1 = 5.22 \times 10^{-5}$, $B_2 = -1.17 \times 10^{-8}$

Specific Heat (J/kg-K)

Silane: $C_0 = 474.0$, $C_1 = 3.26$, $C_2 = -1.08 \times 10^{-3}$

Argon: $C_0 = 520.0$

The mixture properties are evaluated according to Equations (2.16) and (2.20).

Boundary Conditions: The inlet flow rates are 2000 sccm of argon and 100 sccm of silane at a temperature of 300°K. The wafer temperature is umiform at 923°K, the quartz window temperature is 600°K and the side walls are maintained at 300°K. The following two cases are considered:

(a) Chamber pressure of 10 torr, and
(b) Chamber pressure of 100 torr.

Results: The results for cases (a) and (b) are shown in Figures A-2 and A-3, respectively. At 10 torr, the flow field is uniform and the maximum temperature of 923°K occurs on the wafer surface. At 100 torr, however, the effect of natural convection becomes obvious in the form of two large recirculation zones in the chamber. The 100 torr case was harder to converge numerically.

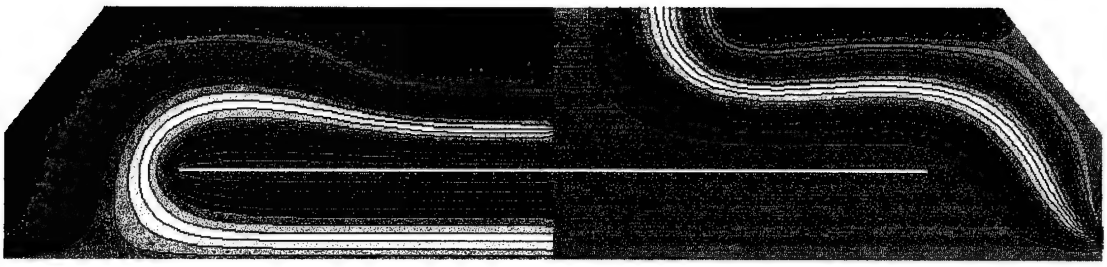

Temperature Streamlines

T_{min} = 300°K
T_{max} = 923°K

Figure A-2. Temperature and Streamlines in Reactor for p = 10 torr

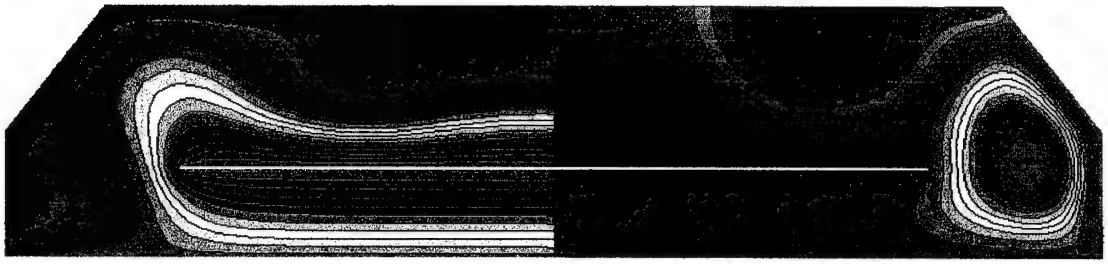

Temperature Streamlines

T_{min} = 300°K
T_{max} = 923°K

Figure A-3. Temperature and Streamlines for p = 100 torr

A.2 Model 2

Problem Type: Same as Model 1 except for the following differences,

(i) a uniform heat flux (to be determined by trial and error) is applied to the front surface of the wafer such that the area averaged temperature of the wafer surface is 923°K,
(ii) heat conduction inside the wafer is considered, and
(iii) radiative heat loss from the wafer edge is modeled.

Geometry and Computational Grid: Same as Model 1.

Physical Models: Same as model 1 with the addition of a conjugate heat transfer model to compute the temperature distribution inside the solid wafer. The wafer conductivity is given as:

$$\lambda_w = 156\left[1.0 - 0.938\left(\frac{T-300}{T}\right)^{0.42}\right]$$

Radiative heat loss from the wafer edge is modeled as a sink term in the energy equation. The wafer emissivity is taken to be 0.65.

Boundary Conditions: Same as Model 1 except for the following:

(i) no boundary conditions are specified on the wafer surface. The wafer temperature is calculated using the conjugate heat transfer model.

(ii) only a chamber pressure of 10 torr is considered.

Results: The results for Model 2 are shown in Figure A-4. A uniform heat flux of 2360 W/sq.m was required to heat up the wafer surface to a mean temperature of 923°K. The model results are qualitatively similar to those of Model 1.

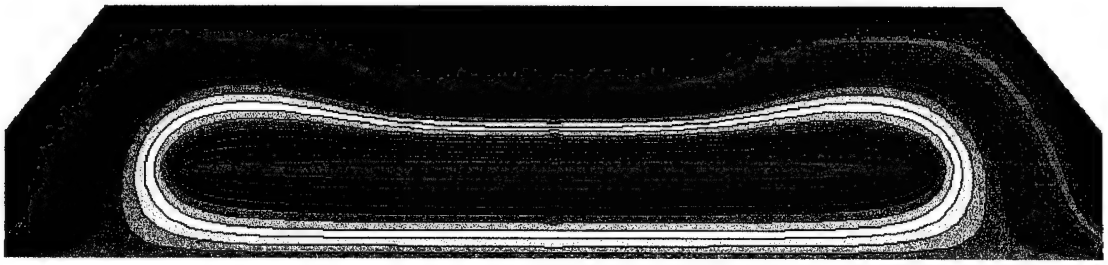

T_{min} = 300°K
T_{max} = 939°K

Figure A-4. Temperature Distribution in Reactor for Case 2

A.3 Model 3

Problem Type: Same as Model 2 except for the following differences,

(i) a single surface reaction is considered,
(ii) kinetic theory of gases is used to compute the multi-component transport coefficients, and
(iii) two wafer temperatures are considered.

Geometry: Same as Model 1.

Computational Grid: The following grid densities are considered :

(i) a 30x50 grid (same as Model 1), and
(ii) a 60x100 grid

Physical Models: A simple surface reaction with the following stoichiometry is considered:

$$SiH_4(g) \rightarrow Si(s) + 2H_2(g)$$

The reaction occurs on all interior surfaces of the chamber. The rate expression for this reaction is given as:

$$R = \gamma \sqrt{\frac{RT}{2\pi M_{SiH_4}}}\, \rho Y_{SiH_4}$$

and the reaction rate probability, γ, is defined as:

$$\gamma = 4.017 \times 10^{-2} \exp\left(\frac{-5021}{T}\right)$$

The multi-component transport coefficients for viscosity, conductivity and the diffusivities are computed from the kinetic theory as described in Section 2.

Boundary Conditions: Same as Model 2, except that two wafer temperatures of 923°K and 1273°K are considered. The heat flux at the wafer surface (to attain the

specified temperature) is determined by trial and error. The wafer temperature of 1273°K is simulated with the 30x50 grid only.

Results: For a wafer temperature of 923°K, the heating rate for the coarse and fine grid is 2360 W/sq.m. The coarse grid results (Figure A-5) and the fine grid results (Figure A-6) are qualitatively similar. The fine grid however predicts a higher concentration of silane on the side walls of the reactor. The heating rate for a mean wafer temperature of 1273°K was found to be 5270 W/sq.m. Results (Figure A-7) indicate a higher rate of consumption of silane due to the higher temperature levels in the chamber.

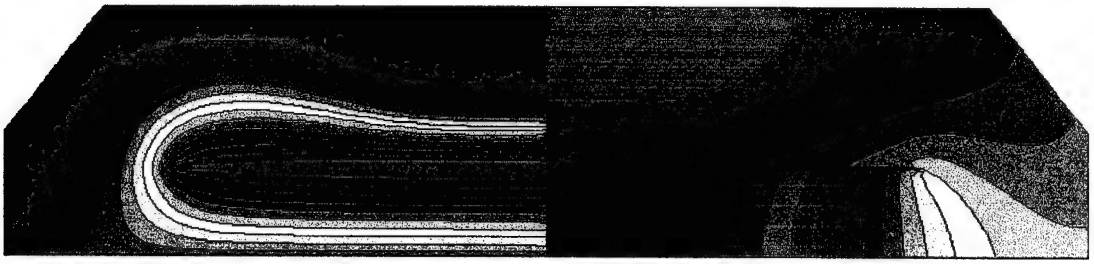

$T_{min} = 300°K$
$T_{max} = 932°K$

$Y_{min} = 0.0199$
$Y_{max} = 0.0385$

Figure A-5. Temperature and Silane Distribution for Coarse Grid

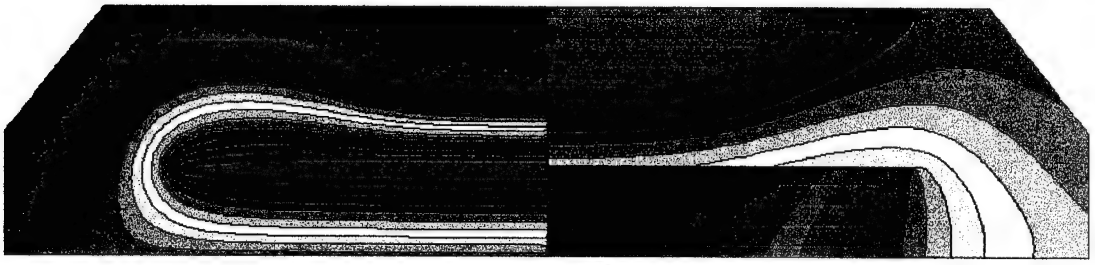

$T_{min} = 300°K$
$T_{max} = 939°K$

$Y_{min} = 0.0299$
$Y_{max} = 0.0385$

Figure A-6. Temperature and Silane Distribution for Fine Grid

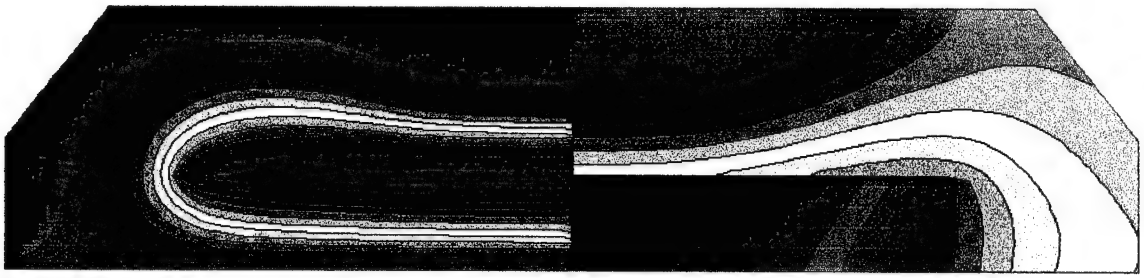

T_{min} = 300°K
T_{max} = 1290°K

Y_{min} = 0.0171
Y_{max} = 0.0385

Figure A-7. Temperature and Silane Distribution for T_s = 1273°K

A.4 Model 4

Problem Type: Same as Model 3 except that the transient heating of the wafer is considered.

Geometry and Computational Grid: Same as Model 1.

Physical Model: A transient model is used to compute the flow and temperature distribution in the field.

Boundary Conditions: Same as Model 3 except that a transient heat-up process is initiated by applying a heat flux of 60000 W/sq.m to the wafer surface (initially at 300°K) at time=0. The heat flux is applied for a time period of 11.8 secs following which the heat flux value from Model 3 (for 923 K) is used. The simulation is continued till 20 seconds.

Results: The temperature and silane distribution in the chamber are shown at four different time instants of t=5, 10, 11.8 and 15 secs (see Figures A-8 through A-11). At t=5 secs, it is observed that the wafer has just started heating up and much of the silane does not uncergo decomposition at the wafer surface. At t=10 secs, the heating process is well underway and significant amounts of silane is undergoing decomposition on the wafer surface. The wafer temperature reaches a value of 923°K at t=11.8 secs and the silane distribution is similar to that predicted by the

steady state model (Model 3). At t=15 secs, the results for the temperature and silne distributions are exactly the same as those predicted by Model 3.

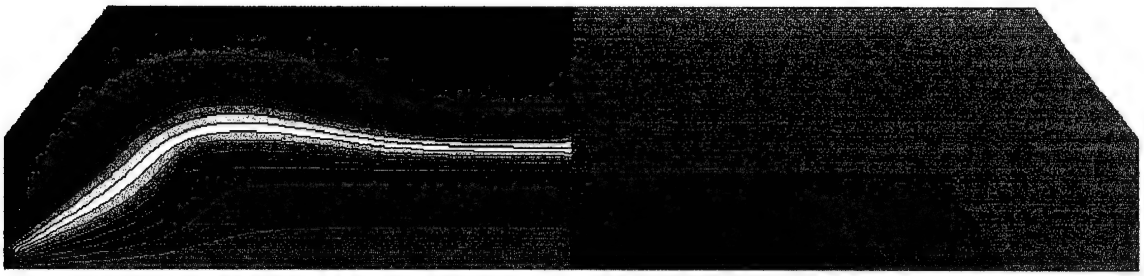

Temperature

$T_{min} = 300°K$

$T_{max} = 600°K$

Silane

$Y_{min} = 0.036$

$Y_{max} = 0.0385$

Figure 4-8. Results at t = 5 secs

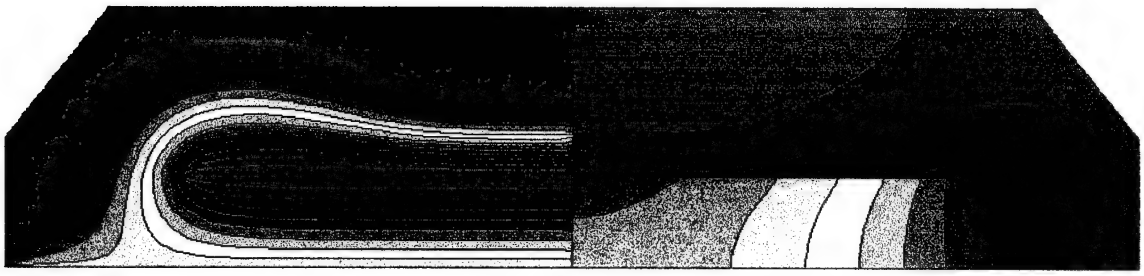

Temperature

$T_{min} = 300°K$

$T_{max} = 833°K$

Silane

$Y_{min} = 0.028$

$Y_{max} = 0.0385$

Figure A-9. Results at t = 10 secs

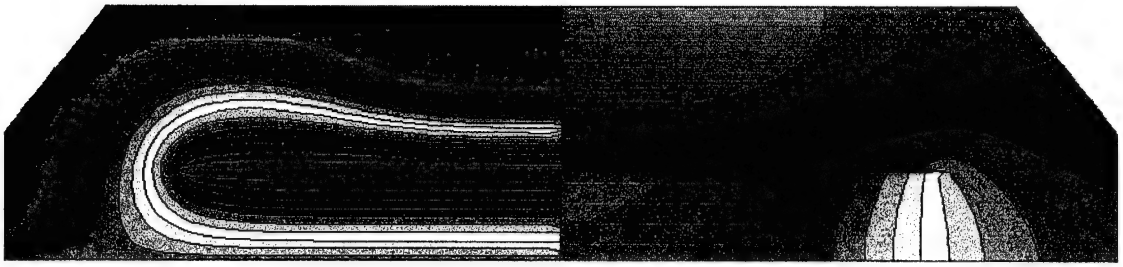

Temperature

$T_{min} = 300°K$
$T_{max} = 927°K$

Silane

$Y_{min} = 0.023$
$Y_{max} = 0.0385$

Figure A-10. Results at t = 11.8 secs

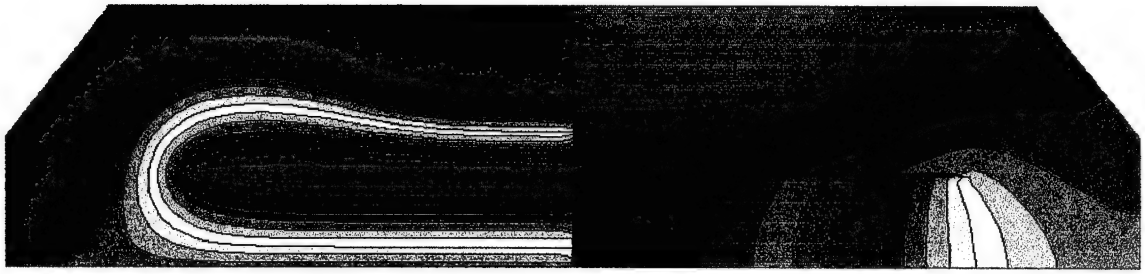

Temperature

$T_{min} = 300°K$
$T_{max} = 928°K$

Silane

$Y_{min} = 0.0199$
$Y_{max} = 0.0385$

Figure A-11. Results at t = 15 secs

A.5 Model 5

Problem Type: Same as Model 3 except that gray radiation between surfaces is considered.

Geometry and Computational Grid: Same as Model 1.

Physical Model: A discrete ordinate gray radiation model is used to solve this problem. The gas is assumed to be optically thin and does not absorb energy

through radiation.

Boundary Conditions: Same as Model 3 except for the following:

a. The window is divided into two zones. The inner zone, out to a radius of 9 cm, is at 1030°K with an emissivity of 1.0. The outer zone between 9 cm and 11 cm is at a temperature of 600°K with an emissivity of 0.92. The emissivity of the wafer surface is 0.65. The outlets are considered black with an emissivity of 1.0. The inlets have an emissivity of 0.15. All the remaining walls are considered to have an emissivity of 0.15.

b. The temperature in the rate expression for the surface reaction occuring at the inner zone of the window will be explicitly taken as 600°K.

Results: Figure A-12 shows the temperature and silane distributions in the chamber.

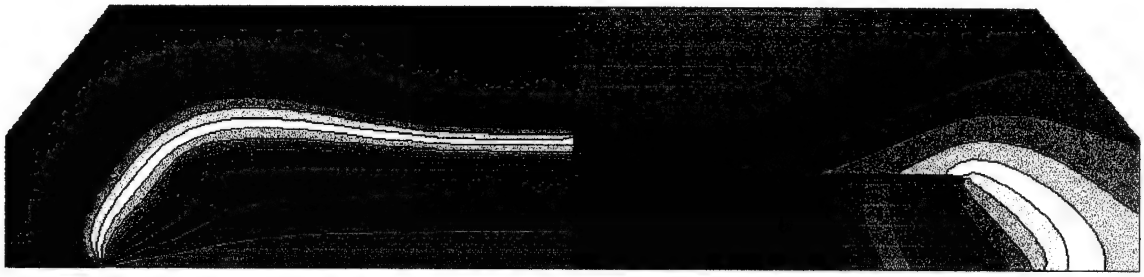

Temperature

$T_{min} = 300°K$
$T_{max} = 1030°K$

Silane

$Y_{min} = 0.0227$
$Y_{max} = 0.0385$

Figure A-12. Temperature and Silane Distribution for Case 5

A.6 Model 6

Problem Type: Same as Model 6 except that non-gray effects are considered.

This case was simulated due to the lack of availability of a non-gray radiation model in CFD-ACE.

A.7 Model 7

Problem Type: Same as Model 3 except that additional gas phase and surface reactions are considered.

Geometry and Computational Grid: Same as Model 1.

Physical Model: Same as Model 3 except that the following gas phase reactions are considered:

$$SiH_4(g) \underset{k_{1f}}{} SiH_2(g) + H_2(g)\,;\, k_{1f} = 2.438 \times 10^{10} \exp\left(\frac{-24705}{T}\right)$$

$$SiH_2(g) + H_2(g) \underset{k_{1r}}{} SiH_4(g)\,;\, k_{1r} = 1.809 \times 10^{5} \exp\left(\frac{3042}{T}\right)$$

$$Si_2H_6(g) \underset{k_{2f}}{} SiH_4(g) + SiH_2(g)\,;\, k_{2f} = 1.584 \times 10^{12} \exp\left(\frac{-20063}{T}\right)$$

$$SiH_4(g) + SiH_2(g) \underset{k_{2r}}{} Si_2H_6(g)\,;\, k_{2r} = 7.771 \times 10^{7} \exp\left(\frac{5120}{T}\right)$$

It is observed that two additional species silylene (SiH_2) and disilane (Si_2H_6) get produced as a result of the gas phase reactions.

Boundary Conditions: Same as Model 3 with a mean wafer temperature of 923°K. The following additional surface reactions are considered:

$$SiH_4(g) \xrightarrow{\gamma_1} Si(s) + 2H_2(g)\,;\, \gamma_1 = 1.08 \times 10^{8} (T)^{-0.8822} \exp\left(\frac{-19052}{T}\right)$$

$$Si_2H_6(g) \gamma_2 2Si(s) + 3H_2(g) ; \gamma_2 = 4.96 \times 10^{16} (T)^{-3.253} \exp\left(\frac{-20219}{T}\right)$$

$$SiH_2(g) \gamma_3 Si(s) + H_2(g) ; \gamma_3 = 1.0$$

Results: Figure A-13 shows the temperature and silane distribution in the reactor. The distributions are very similar to the results of Model 3. Figure A-14 shows the silylene and disilane concentrations in the reactor. It is observed that silylene is present only in the vicinity of the hot wafer surface. Disilane has maximum concentrations above the wafer as well as in the region beneath the wafer.

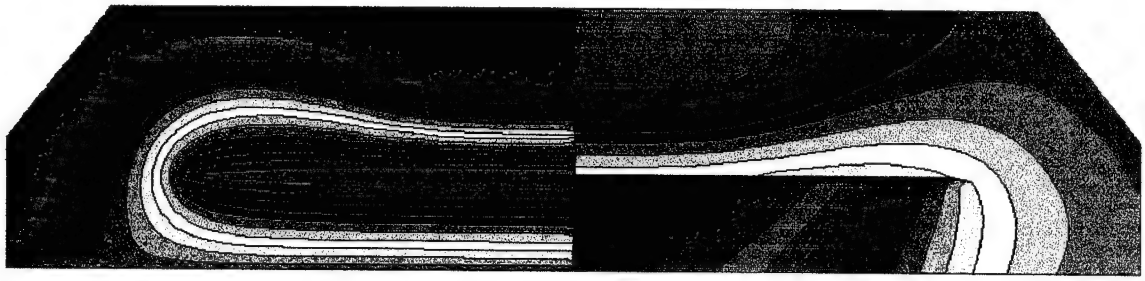

Temperature

$T_{min} = 300°K$

$T_{max} = 940°K$

Silane

$Y_{min} = 0.0274$

$Y_{max} = 0.0385$

Figure A-13. Temperature and Silane Distribution for Case 7

Silylene

$Y_{min} = 0.0$

$Y_{max} = 1.35 \times 10^{-5}$

Disilane

$Y_{min} = 0.0$

$Y_{max} = 3.05 \times 10^{-8}$

Figure A-14. Silylene and Disilane Distribution for Case 7

A.8 Model 8

Problem Type: Same as Model 5 except for the following:

a. The radiation is from a set of lamps located below a quartz window.
b. The model considers the radiation and conjugate heat transfer through a cavity containing argon and the quartz window itself.

Geometry: The geometry for Models 8 and 9 is shown in Figure 4-9b. For Model 8, the water layer is ignored and the entire thickness is treated as quartz.

Computational Grid: A 60x60 non-orthogonal BFC grid for this case is shown in Figure A-15.

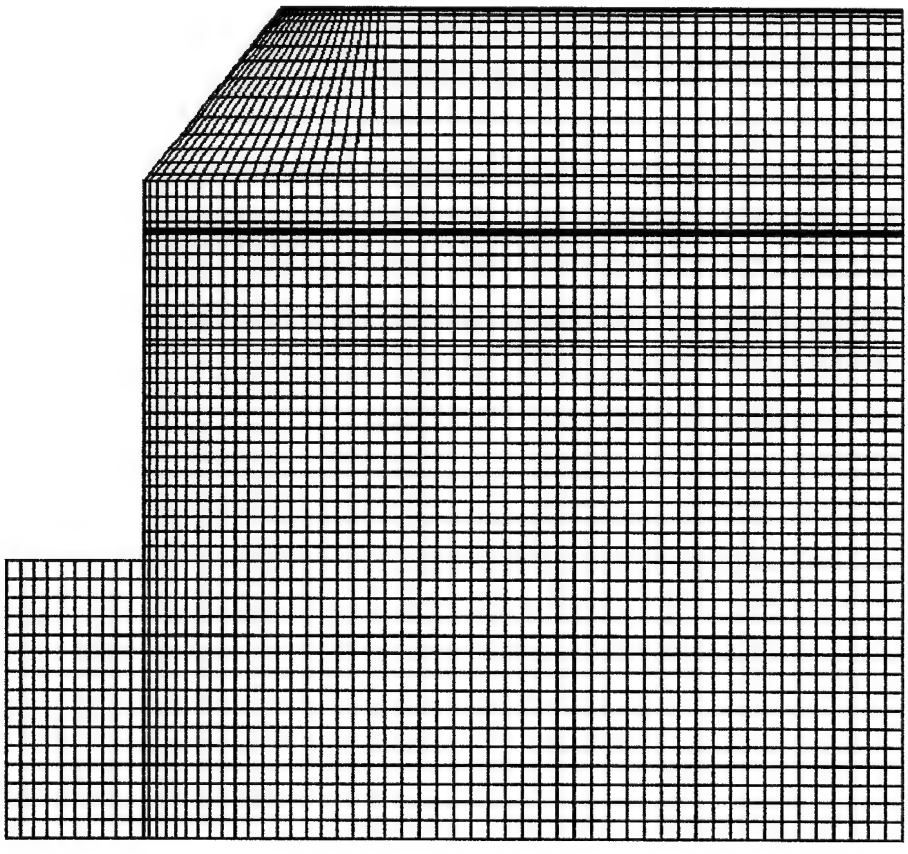

Figure A-15. Computational Grid for Cases 8 and 9

Physical Models: Same as Model 5 except that the radiation through the semi-transparent quartz window is taken into account.

Boundary Conditions: All side walls are at 300°K. The lamp heating zone temperature is adjusted in order to obtain a mean wafer temperature of 923°K. The emissivity of the heating zone is 0.3. The absorption coefficient and thermal conductivity for quartz are 19.6 /cm and 1.9 W/m-K respectively.

Results: A heating zone temperature of 1850°K was required to bring the mean temperature of the wafer to 923°K. Figure A-16 shows the temperature and silane distribution in the chamber. It is observed that the temperature decreases monotonically from the lamp zone to the wafer. The energy is transported to the wafer surface through radiation as well as conduction.

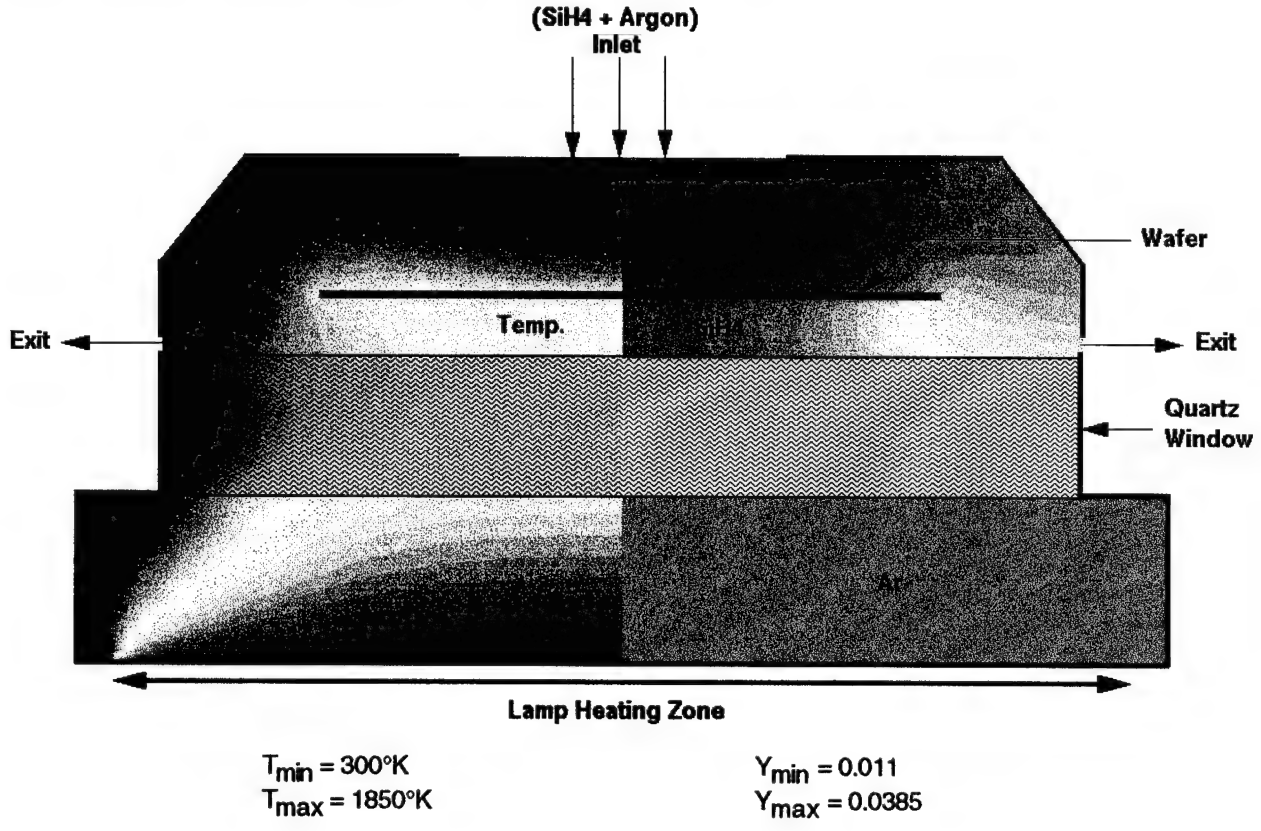

Figure A-16. Temperature and Silane Distribution for Case 8

A.9 Model 9

Problem Type: Same as Model 8 except for the following:

a. The inlet gas is a mixture of dichlorosilane (DCS) and hydrogen.
b. A semi-transparent water layer is included in the quartz window.

Geometry and Computational Grid: Same as Model 8 except for the consideration of the water layer.

Physical Model: Same as Model 8 except for the following:

a. The surface reaction for the DCS-H_2 system is as follows:

$$SiH_2Cl_2(g) \rightarrow Si(s) + 2HCl(g)$$

and the reaction rate is given as:

$$R = 2.86 \times 10^{11} \exp\left(\frac{-29700}{T}\right) \rho Y_{DCS}$$

b. Thermal radiation through a semi-transparent layer of water is considered.

Boundary Conditions: Same as Model 8 except for the following:

a. the inlet flow rates of DCS and hydrogen are 50 sccm and 6000 sccm respectively at a temperature of 300°K.
b. the reactor pressure is 2 torr.
c. the temperature of the water layer is assumed to be maintained at 300°K in order to simulate heat transfer to a channel with large mass flow rate.
d. the absorption coefficient for water is 51.7 /m.
e. the lamp heating zone temperature is adjusted to obtain a mean wafer temperature of 1023°K.

Results: Figure A-17 shows the temperature and HCl distribution in the chamber. It is observed that the water layer acts as a heat sink in the quartz window, i.e., heat is conducted from the chamber as well as the lamp into the water layer. Therefore, the wafer is being heated solely by radiation from the lamps. A lamp temperature of 2060°K was required to bring the mean wafer temperature to 1023°K.

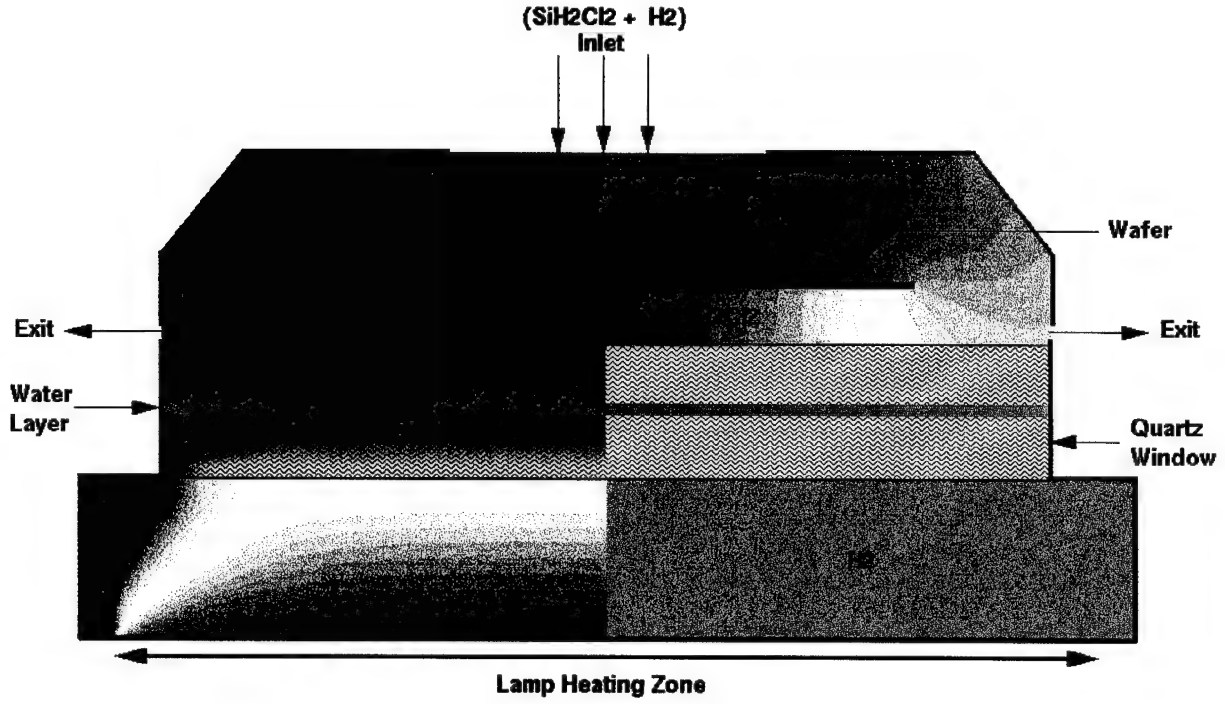

Figure A-17. Temperature and HCl Distributions for Case 9

A.10 Model 10

Problem Type: 3-dimensional solution of fluid flow, heat transfer and surface reaction in the chamber.

Geometry: The geometry of the reactor is shown in Figure 4-8.

Computational Grid: A multi-block computational grid was generated for this problem (see Figure 4-10).

Physical Model: Same as Model 3 except for the following:

a. A complete 3-dimensional model was used in the simulations.
b. The wafer surface temperature was maintained at 923°K.
c. Conjugate Heat Transfer through the wafer holds is considered.

Boundary Conditions: All external boundaries of the reactor with the exception of the bottom window surface are maintained at 300°K. The window is maintained at 600°K.

Results: The results for Model 10 are shown in Figure 4-12. It is observed that the temperature and silane concentration distributions are similar to what was obtained for the 2-d case in Model 3. However, a more comprehensive simulation (Figure 4-13) with radiation shows the three-dimensional effects may influence the deposition at the wafer surface.

APPENDIX B

PUBLICATIONS AND EXHIBITIONS RESULTING FROM THE CURRENT PROJECT

APPENDIX B

PUBLICATIONS AND EXHIBITIONS RESULTING FROM THE CURRENT PROJECT

B.1 Publications and Presentations

(1) M. Giridharan, S. Lowry and A. Krishnan, "Coupled Conductive-Convective-Radiative Conjugate Heat Transfer Model for Complex Applications," To be presented at the International Mechanical Engineering Congress and Exposition, San Francisco, CA, November, 1995.

(2) V. Singh, A. Krishnan and B. Berney, "Designing Low Pressure Systems with Continuum Models," To be presented at the 42nd National Symposium of the AVS, Minneapolis, MN, October 16-20, 1995.

(3) N. Zhou, A. Krishnan and A. J. Przekwas, "A Numerical Method for Reacting Flows with Multi-Step Stiff Chemical Kinetics," Presented at the 31st AIAA/ASME/SAE/ASEE Joint Propulsion Conference, San Diego, CA, July 10-12, 1995.

(4) M. Giridharan, S. Lowry and A. Krishnan, " A Multi-Block, BFC Radiation Model for Complex Geometries," Presented at the 26th AIAA Fluid Dynamics Conference, San Diego, CA, June 19-22, 1995.

(5) A. Krishnan and N. Zhou, "Analysis of Chemical Vapor Deposition in Industrial Reactors," Presented at the Fourth ASME/JSME Thermal Engineering Joint Conference, Hawaii, March 19-24, 1995.

(6) N. Zhou and A. Krishnan, "Numerical Simulation of Crystal Growth by Physical Vapor Transport in Microgravity Environments," Presented at the 33rd Aerospace Sciences Meeting, Reno, NV, January 9-12, 1995.

(7) A. Krishnan, N. Zhou and A.J. Przekwas, "A Computational Model for Chemical Vapor Deposition Processes in Industrial Reactors," Presented at the I-THERM Meeting, Washington, D.C., May 4-7, 1994.

(8) A. Krishnan, N. Zhou, G. Mo and A.J. Przekwas, "Virtual Prototyping of Semiconductor Fabrication Equipment," Presented at the MRS Spring Meeting, San Francisco, April 4-8, 1994.

(9) S. Y. Ho, A. D. Leonard, A. Krishnan, B. Van Eck, J. Baecker and T. Vaughn, "Computational Analysis of the FSI Excalibur II Wafer Cleaning Reactor," Presented at the Microcontamination Conference, San Jose, September 21-23, 1993.

B.2 Exhibitions

(1) To be exhibited Government Microcircuit Applications Conference (GOMAC) 1996, Orlando, FL, March 18-21, 1996

(2) To be exhibited at SEMICON/Southwest, Austin, Texas, October 23-26, 1995.

(3) Exhibited at SEMATECH Workshop, Austin, Texas, June 19-22, 1994.

(4) Exhibited at the I-THERM Meeting, Washington, D.C., May 4-7, 1994.

(5) Exhibited at the MRS Spring Meeting, San Francisco, April 4-8, 1994.

APPENDIX C

JOURNAL ADVERTISEMENTS AND MATERIALS BROCHURE

CFD-ACE 2.0

Industry Leaders Depend on CFD-ACE for Material Processing...

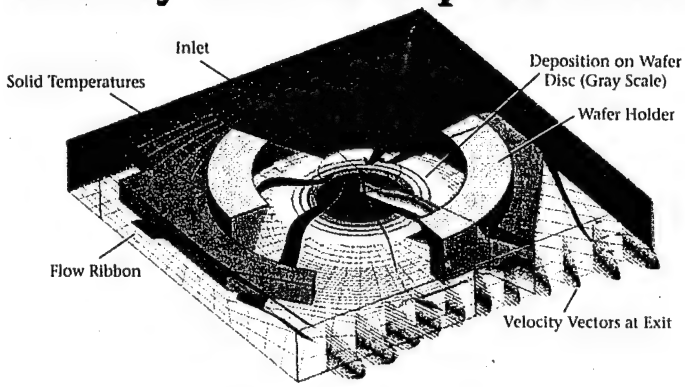

Jipelec CVD Reactor; Velocity, Temperature, and Deposition Rate

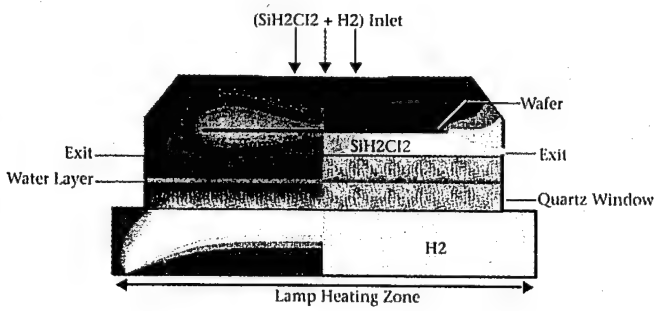

Radiation Heating of Wafer in a Silicon CVD Reactor with Multi-media Conjugate Heat Transfer

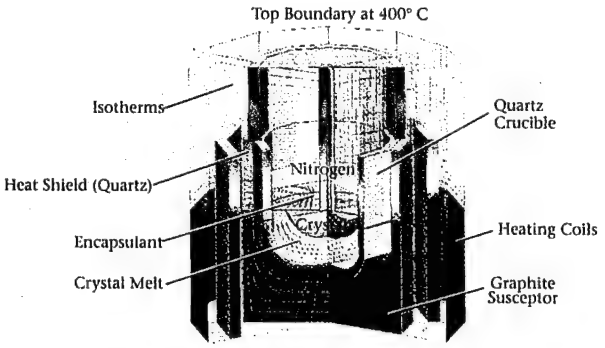

Heat Transfer in LEK Crystal Growth System

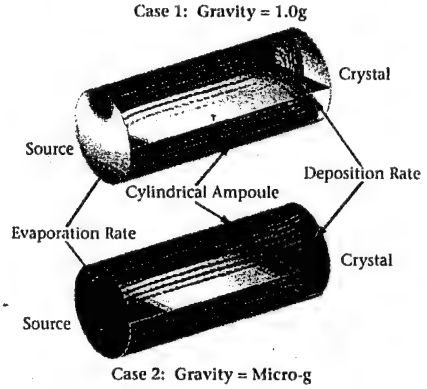

Physical Vapor Transport; Growth of Iodine Crystals

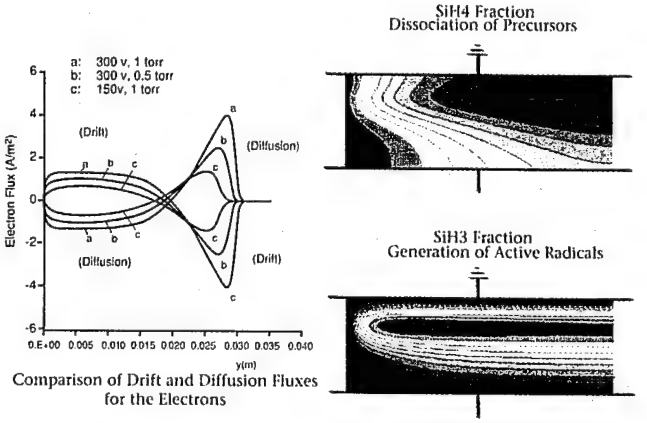

Comparison of Drift and Diffusion Fluxes for the Electrons

Plasma Enhanced CVD of Silicon from Silane

...plus other applications of Lam Research Corp., SVG Thermco, Semitool, Motorola, Intel, IBM, Sandia National Labs, Lawrence Livermore Labs, SEMATECH, ARPA,...and many others.

CFD-ACE Highlights

- **Overnight calculations of large complex 3D problems** on an engineering workstation
- Multi-component species transport model with thermodiffusion (Soret Effect) for low pressure applications (e.g., etching, deposition, etc.)
- Efficient algorithms for highly stiff, multi-step finite rate gas/surface chemistry (50 reactions; 25 species)
- **Discrete Ordinate radiation model** with semi-transparent participating media
- Tightly integrated analysis environment

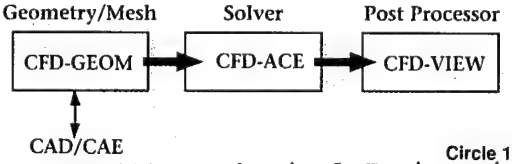

User Support

CFDRC provides software licensees with the highest quality support based on:

- Extensive experience in microelectronic materials processing applications
- **Hundreds of person-years** of experience in CFD development and industrial applications

Design & Analysis Services

CFDRC also offers cost-effective analysis and design support services. Full protection of proprietary data guaranteed.

CFDRC

"On the Leading Edge of CFD Technology"

CFD Research Corporation
3325 Triana Blvd., Huntsville, AL 35805
Telephone: (205) 536-6576 Fax: (205) 536-6590
email: sales@cfdrc.com

Circle 118 on Reader Service Card

1995

MICROELECTRONIC MATERIALS APPLICATIONS AT CFD RESEARCH CORPORATION

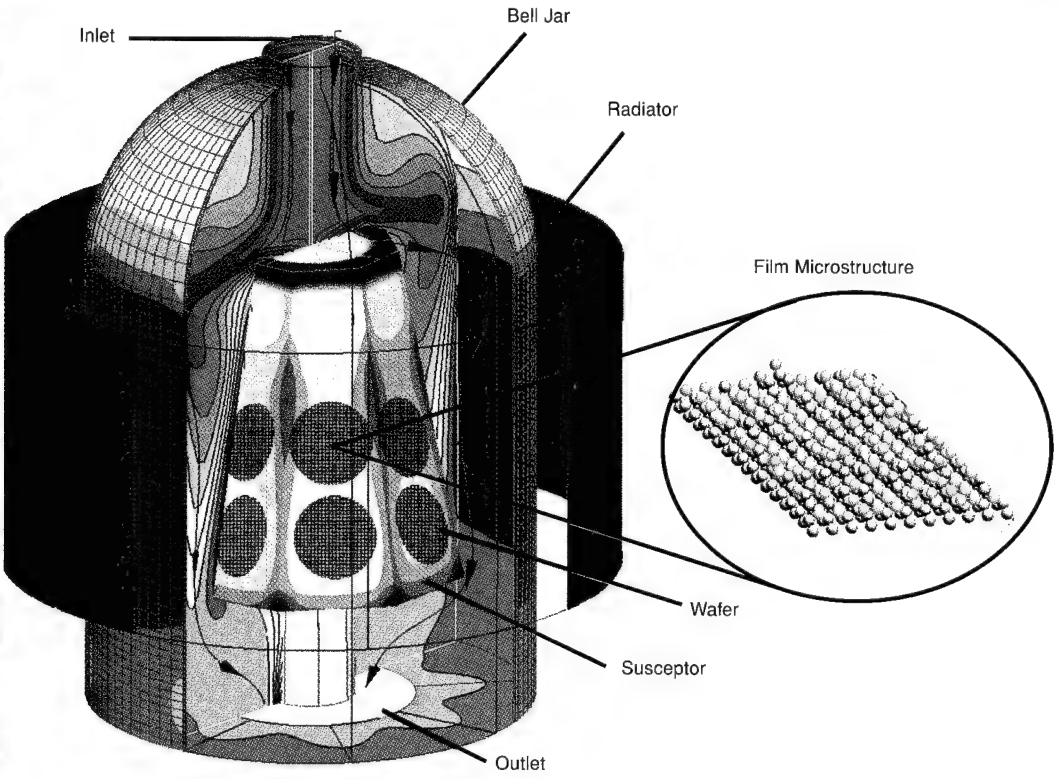

Barrel CVD Reactor

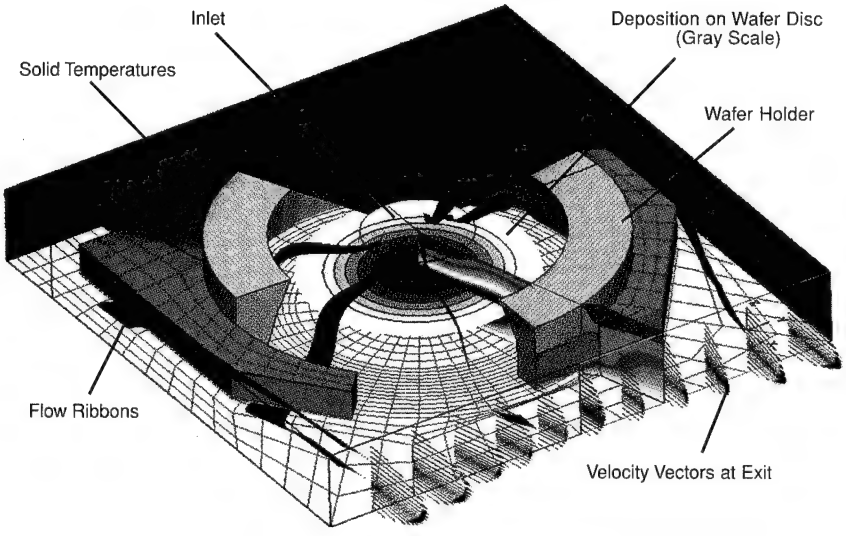

Jipelec CVD Reactor

Advanced Analysis Software and Services for:

- **Virtual Prototyping, and**
- **Design Optimization**

of Microelectronic Fabrication Equipment and Processes

NEED FOR MODELING

The production of high quality microelectronic materials and devices requires efficient manipulation of complex interacting physical phenomena over a range of length/time scales. Advanced computational models of these phenomena are invaluable in providing insights and guidelines for the design of new and improved fabrication processes/systems.

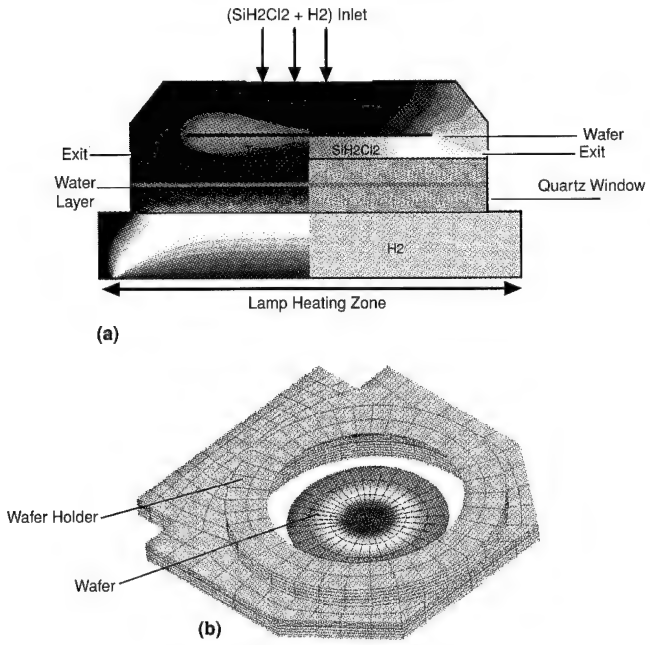

Radiation Heating of Wafer in a Silicon CVD Reactor with Multi-media Conjugate Heat Transfer (a) 2D Slice (b) 3D Geometry

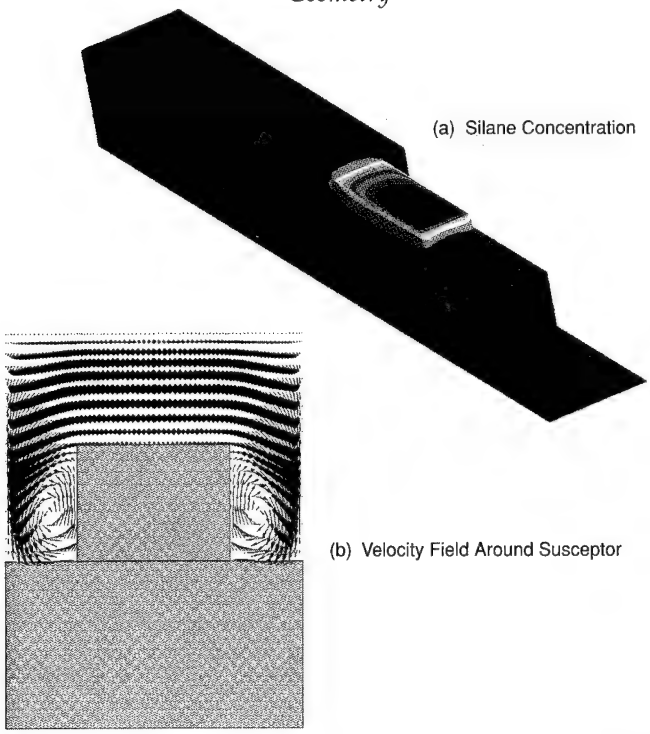

Assessment of Natural Convection Effects in an Inductively Heated Horizontal Reactor

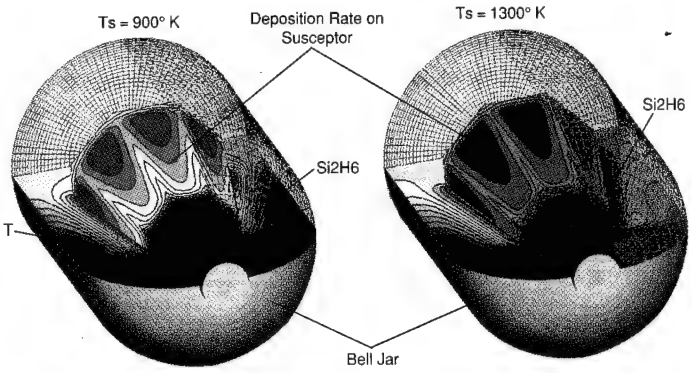

Effect of Substrate Temperature on Silicon Deposition Rate in a Barrel Reactor

MODELING CAPABILITIES

CFD Research Corp. (CFDRC) has developed an advanced general-purpose Computational Fluid Dynamics code, **CFD-ACE**, which is being applied successfully for a variety of industrial applications. CFDRC has also adapted the code for modeling a range of materials processing phenomena. The advanced materials modeling capabilities of **CFD-ACE** include:

△ Multi-component transport model (based on Kinetic Theory of Gases) to compute viscosity, thermal conductivity, thermodiffusion (Soret Effect) and diffusion coefficients as functions of local pressure, temperature and composition.

△ User specified polynomial fits for all transport properties and an extensive library of default values.

△ Multi-step gas phase and surface reaction capability to simulate processes such as Chemical Vapor Deposition (CVD), Physical Vapor Deposition (PVD), Physical Vapor Transport (PVT) and etching. Complete coupling is maintained between the gas phase and surface chemistry. Special algorithms are available to treat highly stiff systems.

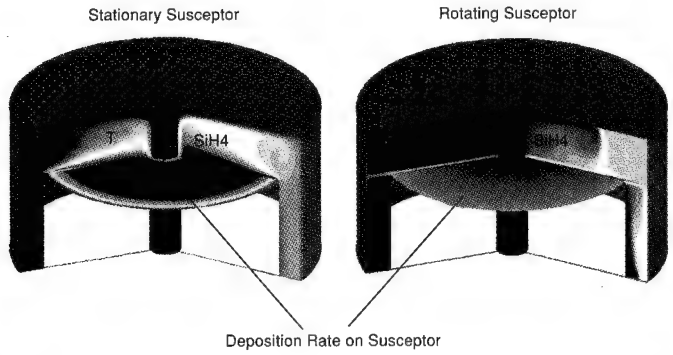

Effect of Susceptor Rotation on CVD of Silicon in a Radial Flow Reactor

MODELING CAPABILITIES, Cont'd.

- △ Multi-media, conjugate heat transfer models with fully implicit formulation.
- △ Discrete-ordinate thermal radiation model for 2D/3D, Cartesian/non-orthogonal geometries with participating semi-transparent media.
- △ Advanced (2-D and 3-D) pressure-based fluid flow solvers utilizing highly conservative formulation with Body-Fitted-Coordinates (BFC) capability for complex flow configurations.
- △ Multi-block formulation to enable optimal use of grid points and improved accuracy for simulation of complex reactor geometries.
- △ Integrated with advanced Interactive 3D Geometry Modeling and Grid Generation software **CFD-GEOM**. Also accepts geometry information from CAD/CAM software.
- △ Integrated with advanced Interactive 3-D Graphics Animation and Flow Visualization software **CFD-VIEW**.
- △ Intuitive, easy-to-use Graphical User Interface (GUI).
- △ Extensive ongoing validation and applications.

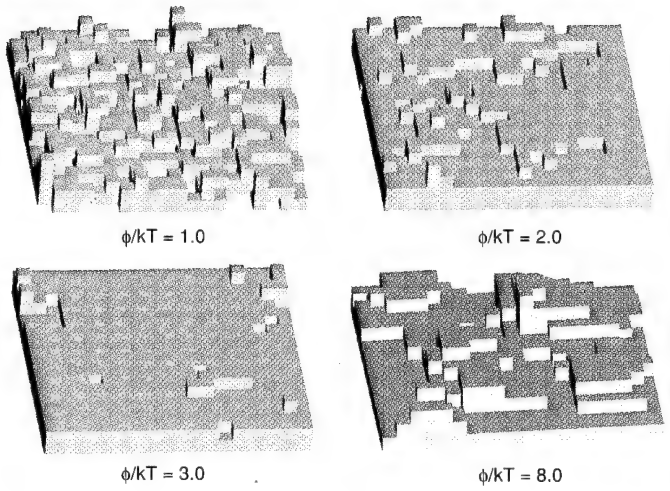

Effect of Growth Temperature on Film Morphology (Monte Carlo Surface Model Developed at CFDRC)

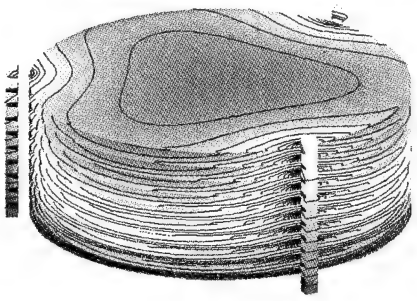

Coupled (Fluid Flow + Radiation + Gas/Surface Chemistry + Multi-media Conjugate Heat Transfer) Analysis of Silicon CVD in a Batch Wafer System (Temperature Distribution Shown)

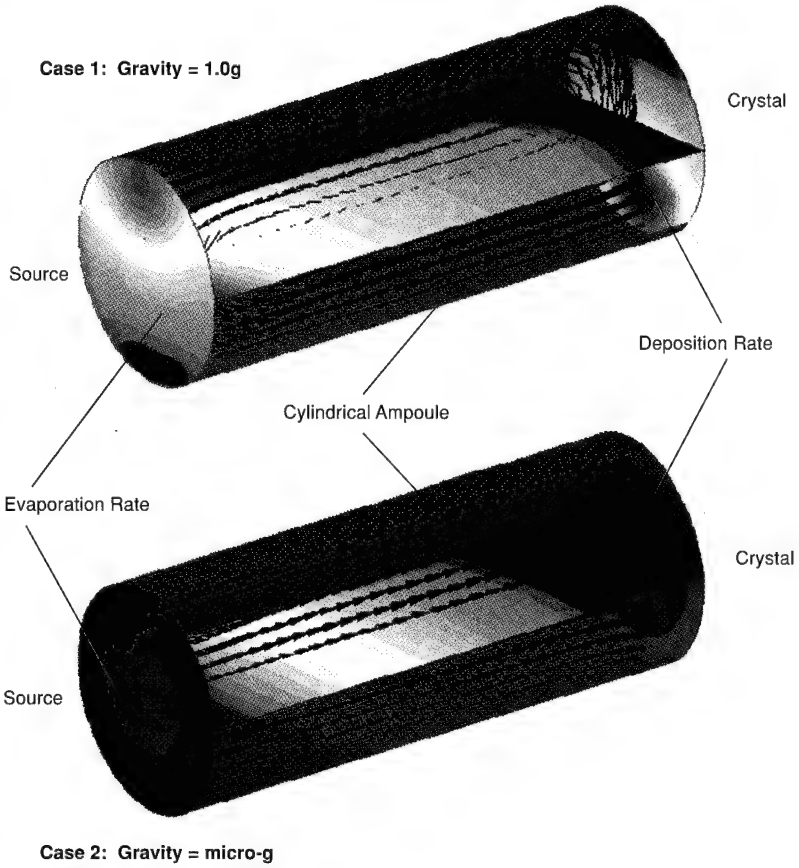

Effect of Gravity on Growth of Iodine Crystals by Physical Vapor Transport

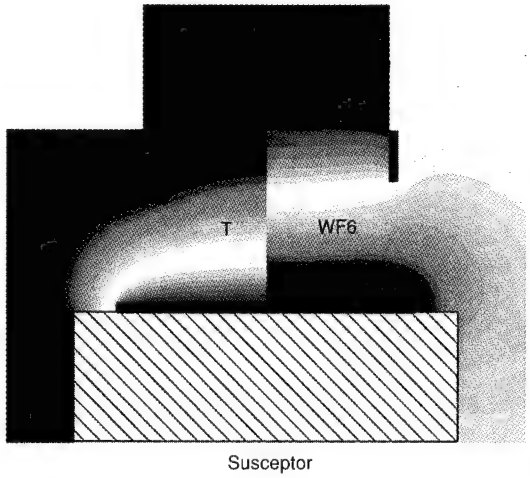

CVD of Tungsten from Tungstenhexafluoride (WF_6)

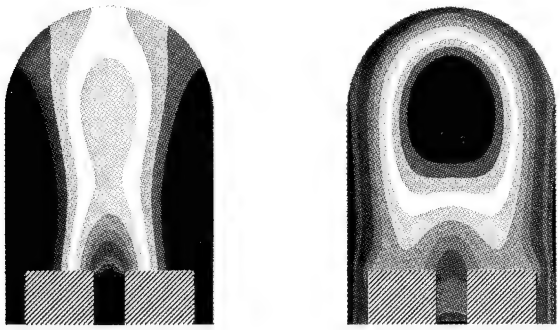

(a) Particle Density Distribution (b) Particle Size Distribution

Nucleation and Transport of Particulate Contaminants in a Fabrication Reactor

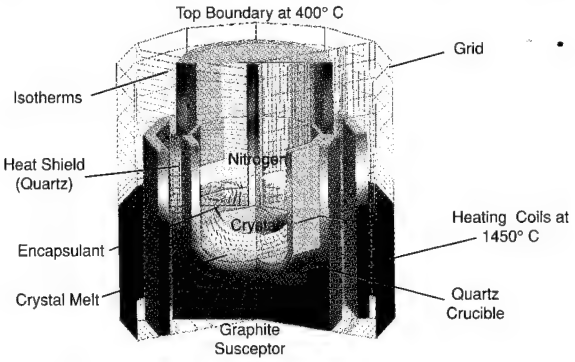

Liquid Encapsulated Kyropolous Crystal Growth Showing Heat Transfer and Convection

APPLICATIONS

Virtual Prototyping: CFDRC is working on an ARPA sponsored initiative to develop virtual design environments for semiconductor fabrication processes/equipment. Software from various disciplines such as Geometry Modeling, Process Modeling, Data Visualization and Database Management are currently being integrated to form the virtual prototyping environment.

Microscopic Surface Phenomena: The properties of thin films are greatly influenced by the film morphology and composition. Monte Carlo models are being developed by CFDRC to simulate surface phenomena such as adsorption, diffusion, coalescence and desorption in vapor deposition systems. The microscopic models are being coupled to macroscale reactor models to elucidate the dependence of film morphology and composition on processing parameters such as the reactor pressure, temperature, flow rates, and reactor geometry.

Plasma Processing: Plasmas are used routinely in fabrication systems to enhance reaction rates at low temperatures. CFDRC is developing models for low pressure plasmas that include the generation and transport of charged species under the influence of the electromagnetic field. The plasma model is being coupled to the existing fluid flow/ transport model to facilitate analysis of practical plasma assisted fabrication systems.

Particulate Contamination: Microcontamination is a serious problem in fabrication reactors that results in defective products, reduced yields and higher costs. CFDRC is currently developing physical models to predict contaminant formation through mechanisms such as homogenous nucleation from the vapor phase, heterogenous nucleation on surfaces and ion-induced nucleation in plasma reactors. Advanced particle transport models also consider effects of gas phase drag, thermophoresis, gravity, electrostatic and ionic drag forces on particle trajectories in the processing system.

Dendritic Solutal Growth: The quality of multicomponent alloys is directly related to the composition distribution and dendritic structure that evolves during the solidification process. CFDRC has a directional dendritic solidification model that is currently being extended to the formation of generic alloys.

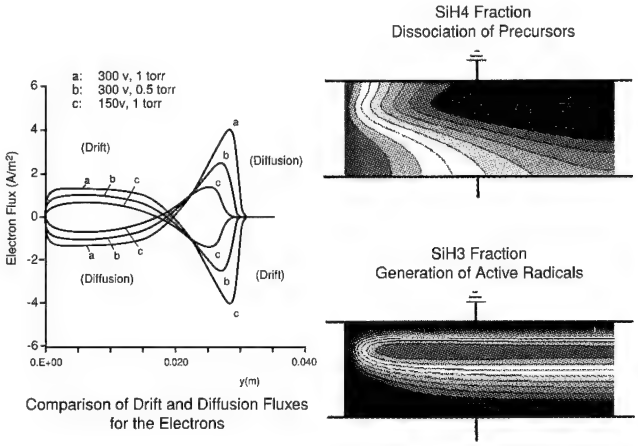

Comparison of Drift and Diffusion Fluxes for the Electrons

Plasma Enhanced Chemical Vapor Deposition of Silicon from Silane in a Capacitively Coupled Parallel Plate System

CFDRC CUSTOMERS FOR MATERIALS APPLICATIONS

- ARPA
- SEMATECH
- Sandia National Labs
- FSI International
- NASA-LeRC
- SVG Thermco
- LAM Research Corp.
- ...and others
- Lawrence Livermore Labs
- Motorola
- IBM
- Semitool
- NASA-MSFC

For further information, contact

CFDRC

"On the Leading Edge of CFD Technology"

CFD Research Corporation
3325 Triana Blvd.
Huntsville, AL 35805
Telephone: (205) 536-6576 Fax: (205) 536-6590
email: sales@cfdrc.com

1994

CFD Research Corporation

CFDRC

MATERIALS PROCESSING

Computational Fluid Dynamics Applications

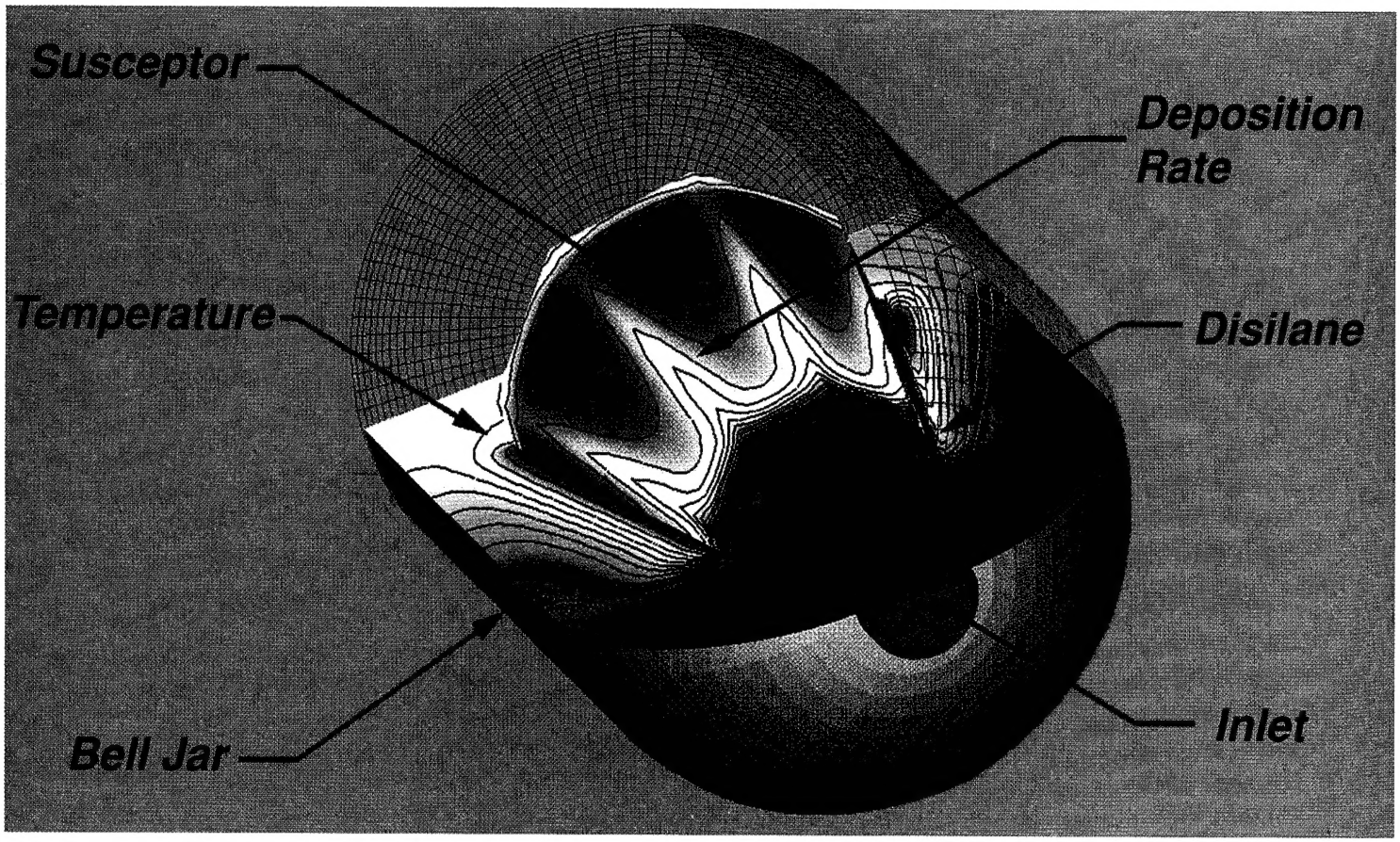

3-D Simulation of a Barrel CVD Reactor (Using CFD-ACE)

NEED FOR MODELING

The traditional field of materials fabrication has included processes such as forging, extrusion and hot-working of raw materials and molding and casting techniques for the production of engineering components. The advent of the microelectronics industry has led to widespread applications of materials processes for the synthesis of advanced integrated devices. Examples of microelectronics fabrication processes are bulk crystal and thin film growth, etching, metallization, lithography, etc.

Materials processing involves the integration of knowledge from a wide range of disciplines. The properties (and hence the technological usefulness) of materials are strongly influenced by the prevailing conditions during processing. Therefore the production of high quality materials and devices requires efficient manipulation of complex interacting physical phenomena over a range of length/time scales. Advanced computational models of these phenomena are invaluable in providing insights and guidelines for the design of new and improved fabrication processes/systems.

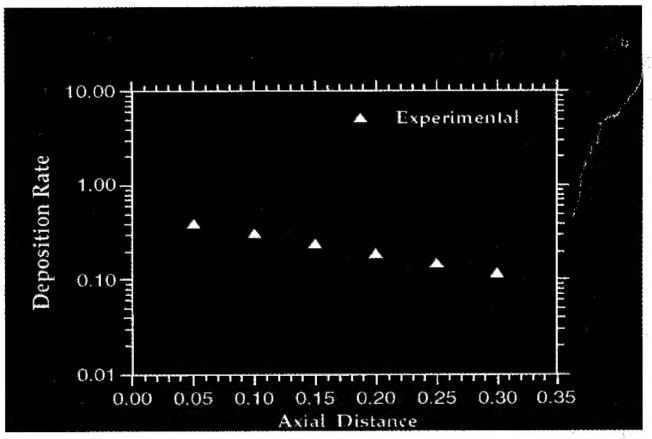

Silicon Deposition Rate Distribution in a Horizontal CVD Reactor (CFD-ACE)

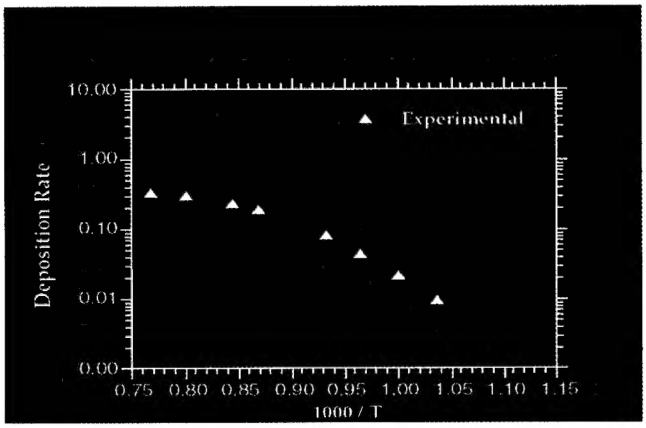

Variation of Silicon Deposition Rate with Substrate Temperature (CFD-ACE)

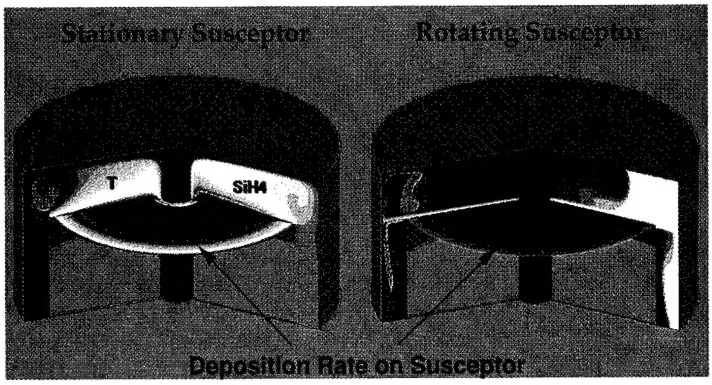

Effect of Susceptor Rotation on CVD of Silicon in a Radial Flow Reactor (CFD-ACE)

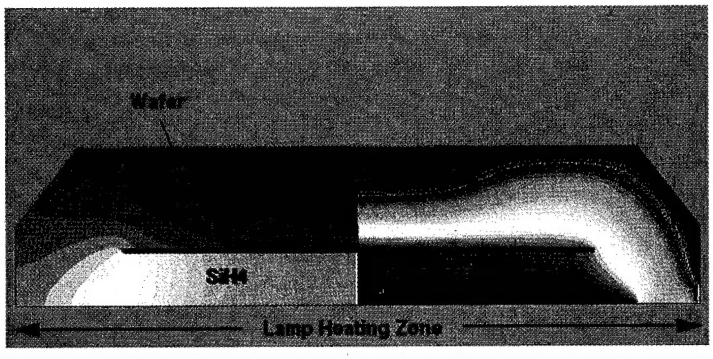

Thermal Radiation, Fluid Flow and Chemistry in a Silicon CVD Reactor

MODELING CAPABILITIES

CFD Research Corp. (CFDRC) has developed a general-purpose advanced Computational Fluid Dynamics code, CFD-ACE, which is being commercialized successfully for a variety of applications. CFDRC has also adapted the code for modeling a range of materials processing phenomena. The advanced materials modeling capabilities of CFD-ACE include:

△ Multi-component transport model (based on Kinetic Theory of Gases) to compute viscosity, thermal conductivity, thermodiffusion (Soret Effect) and diffusion coefficients as functions of local pressure, temperature and composition.

△ User specified polynomial fits for all transport properties.

△ Multi-step gas phase and surface reaction capability to simulate processes such as Chemical Vapor Deposition (CVD), Physical Vapor Deposition (PVD), Physical Vapor Transport (PVT) and etching. Complete coupling is maintained between the gas phase and surface chemistry.

MODELING CAPABILITIES, Cont'd.

- △ Multi-media, conjugate heat transfer models with fully implicit formulation.
- △ Discrete-ordinate thermal radiation model for 2D/3D, Cartesian/non-orthogonal geometries with participating media.
- △ Advanced (2-D and 3-D) pressure-based fluid flow solvers utilizing highly conservative formulation with Body-Fitted-Coordinates (BFC) capability for complex flow configurations.
- △ Multi-block formulation to enable optimal use of grid points and improved accuracy for simulation of complex reactor geometries.
- △ Integrated with advanced Interactive 3D Geometry Modeling and Grid Generation software CFD-GEOM. Also accepts geometry information from CAD/CAM software.
- △ Integrated with advanced Interactive 3-D Graphics Animation and Flow Visualization software CFD-VIEW.
- △ Graphical User Interface (GUI).

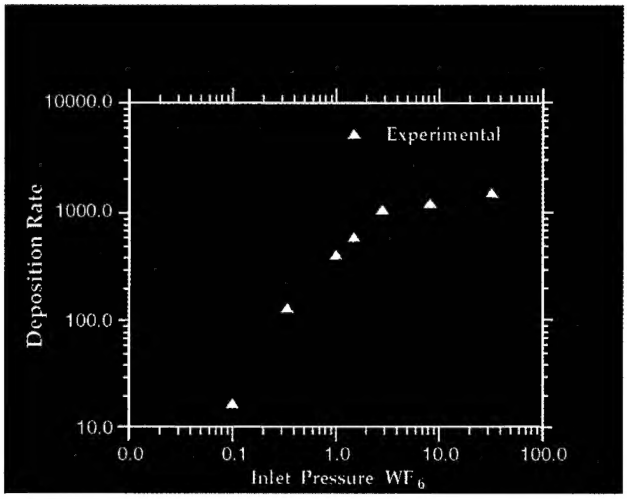

Variation of Tungsten Deposition Rate with Inlet Concentration of Tungstenhexafluoride (WF_6) (CFD-ACE)

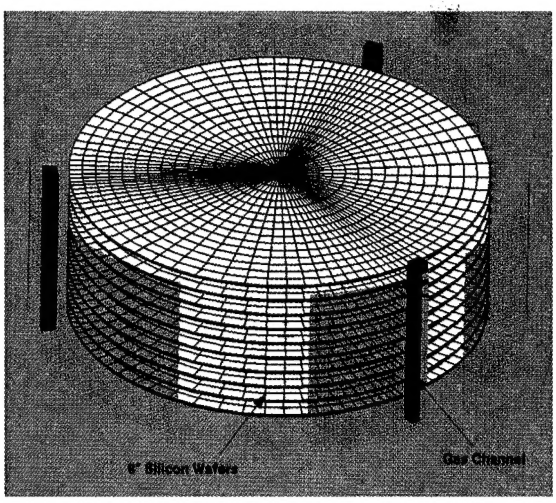

3-D Computational Model of a Mini-Batch Wafer System (CFD-GEOM)

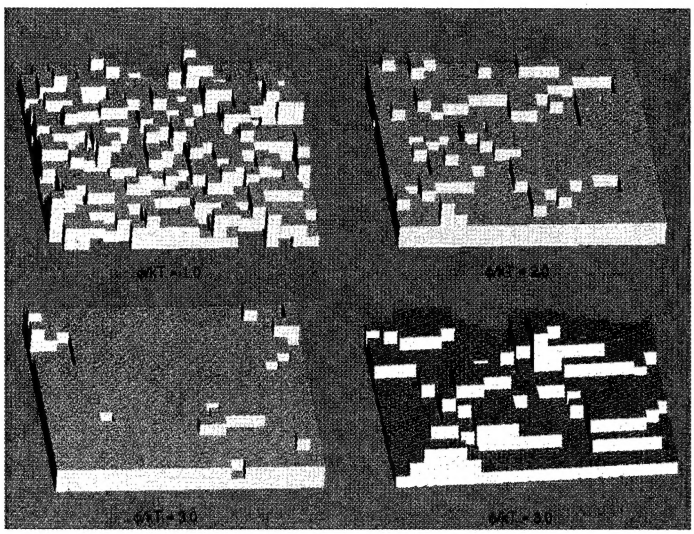

Effect of Growth Temperature on Film Morphology (Monte Carlo Surface Model Developed at CFDRC)

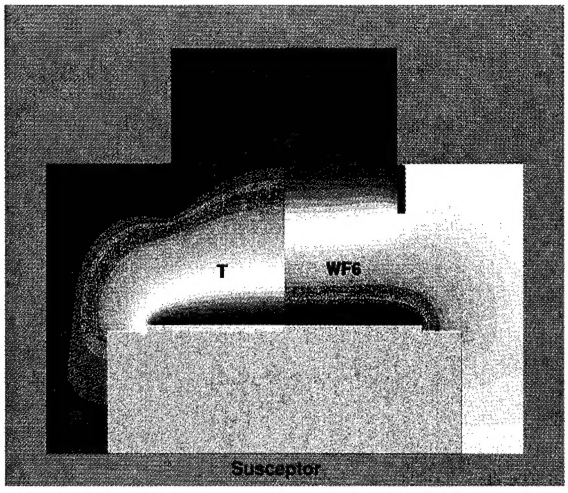

CVD of Tungsten from Tungstenhexafluoride (WF_6) (CFD-ACE)

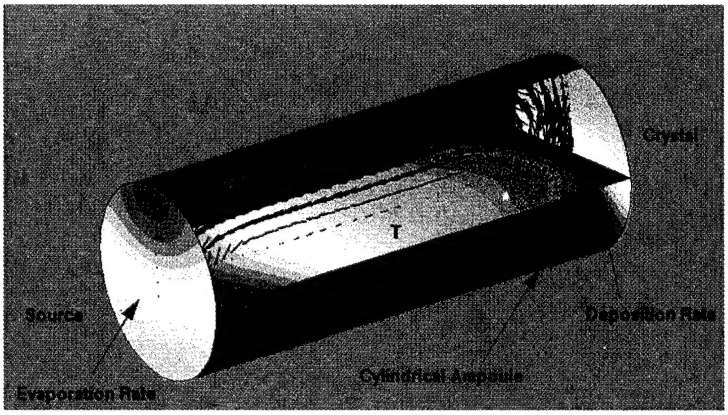

Growth of Iodine Crystals by Physical Vapor Transport (CFD-ACE)

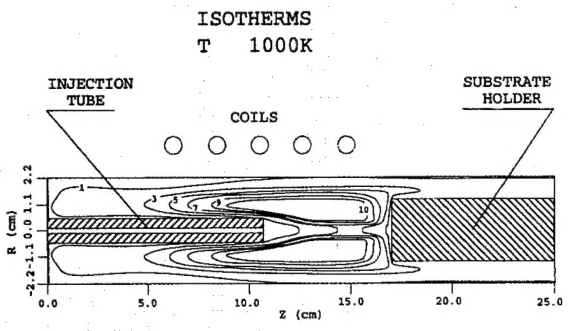

Temperature Distribution in a Diamond CVD Reactor

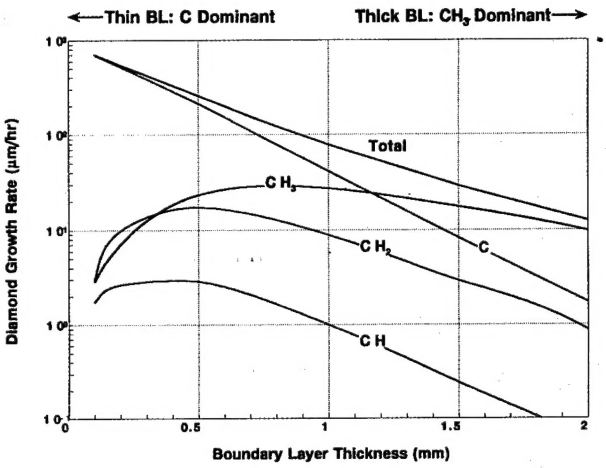

Influence of Boundary Layer Thickness on Diamond Growth

APPLICATIONS

Virtual Prototyping: CFDRC is working on an ARPA sponsored initiative to develop virtual design environments for semiconductor fabrication processes/ equipment. Software from various disciplines such as CAD/CAM, Process Modeling, Data Visualization and Expert Systems are currently being integrated to form the design environment.

Microscopic Surface Phenomena: The properties of thin films are greatly influenced by the film morphology and composition. Monte Carlo models are being developed by CFDRC (under a NASA-LeRC SBIR program) to simulate surface phenomena such as absorption, diffusion, coalescence and desorption in vapor deposition systems. The microscopic models are being coupled to macroscale reactor models to elucidate the dependence of film morphology and composition on processing parameters such as the reactor pressure, temperature, flow rates, and reactor geometry.

Plasma Processing: Plasmas are used routinely in fabrication systems to enhance reaction rates at low temperatures. CFDRC is developing models for low pressure plasmas (under an ARPA SBIR project) that include the generation and transport of charged species under the influence of the electric field. The plasma model is being coupled to the existing fluid flow/ transport model to facilitate analysis of practical plasma assisted fabrication systems.

Diamond CVD: Diamond possesses highly favorable properties such as large thermal conductivity, negligible electrical conductivity and a high degree of lubricity in addition to its hardness. The growth of diamond films at atmospheric pressure has attracted considerable interest in recent years. CFDRC is currently developing models for inductively coupled rf thermal plasmas for diamond deposition.

Dendritic Solutal Growth: The quality of multi-component alloys is directly related to the composition distribution and dendritic structure that evolves during the solidification process. CFDRC has a directional dendritic solidification model that is currently being extended to the formation of generic alloys.

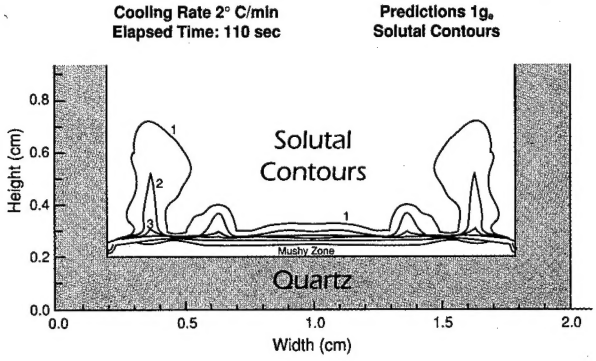

Solutal Distribution in Directional Dendritic Growth

- ARPA
- SEMATECH
- Sandia National Labs
- FSI International
- NASA-LeRC
- SVG, Inc.

FOR FURTHER INFORMATION CONTACT:

Dr. Anantha Krishnan or Dr. Sam Lowry

CFD Research Corporation
3325 Triana Blvd.
Huntsville, AL 35805

Tel. (205) 536-6576 Fax: (205) 536-6590